MODIFIED HYSTERESIS CURRENT CONTROLLER OF HALF BRIDGE BIDIRECTIONAL DC-DC CONVERTER USING CHASSIS DYNAMOMETER FOR ELECTRIC VEHICLE

NURUL AZWA BINTI OTHMAN

Master of Engineering (Electrical)

UNIVERSITI MALAYSIA PAHANG

UNIVERSITI MALAYSIA PAHANG

DECLARATION OF THESIS AND COPYRIGHT

Author's Full Name	: NURUL AZWA BINTI OTHMAN
Date of Birth	: 24 March 1988
Title	: MODIFIED HYSTERESIS CURRENT CONTROLLER OF HALF BRIDGE BIDIRECTIONAL DC-DC CONVERTER USING CHASSIS DYNAMOMETER FOR ELECTRIC VEHICLE
Academic Session	: 2014/2015

I declare that this thesis is classified as:

☐	CONFIDENTIAL	(Contains confidential information under the Official Secret Act 1997)*
☐	RESTRICTED	(Contains restricted information as specified by the organization where research was done)*
☑	OPEN ACCESS	I agree that my thesis to be published as online open access (Full Text)

I acknowledge that Universiti Malaysia Pahang reserves the following rights:

1. The Thesis is the Property of Universiti Malaysia Pahang
2. The Library of Universiti Malaysia Pahang has the right to make copies of the thesis for the purpose of research only.
3. The Library has the right to make copies of the thesis for academic exchange.

Certified by:

_______________________	_______________________
(Student's Signature)	(Supervisor's Signature)
_______________________	_______________________
880324-06-5096	DR. HAMDAN BIN DANIYAL
Date: 15 February 2017	Date: 15 February 2017

NOTE : * If the thesis is CONFIDENTIAL or RESTRICTED, please attach a thesis declaration letter.

SUPERVISOR'S DECLARATION

I hereby declare that I have checked this thesis and in my opinion, this thesis is adequate in terms of scope and quality for the award of the degree of Master of Engineering in Electrical.

____

(Supervisor's Signature)

Full Name : DR. HAMDAN BIN DANIYAL

Position : Senior Lecturer

Date : 15 February 2017

STUDENT'S DECLARATION

I hereby declare that the work in this thesis is based on my original work except for quotations and citations which have been duly acknowledged. I also declare that it has not been previously or concurrently submitted for any other degree at Universiti Malaysia Pahang or any other institutions.

____

(Student's Signature)

Full Name : NURUL AZWA BINTI OTHMAN

ID Number : MEE14003

Date : 15 February 2017

MODIFIED HYSTERESIS CURRENT CONTROLLER OF HALF BRIDGE BIDIRECTIONAL DC-DC CONVERTER USING CHASSIS DYNAMOMETER FOR ELECTRIC VEHICLE

NURUL AZWA BINTI OTHMAN

Thesis submitted in fulfillment of the requirements
for the award of the degree of
Master of Engineering (Electrical)

Faculty of Electrical & Electronics Engineering

UNIVERSITI MALAYSIA PAHANG

FEBRUARY 2017

ACKNOWLEDGEMENTS

Alhamdulillah, thanks to Allah gives me opportunity to do master. I am grateful and would like to express my sincere gratitude to my supervisor Dr. Hamdan Daniyal for his germinal ideas, invaluable guidance, continuous encouragement and constant support in making this research possible. He has always impressed me with his outstanding professional conduct, his strong conviction for engineering, and his belief that a master program is only a start of a life-long learning experience. I appreciate his consistent support from the first day I applied to graduate program to these concluding moments. I am truly grateful for his progressive vision about my training in engineering, his tolerance of my naïve mistakes, and his commitment to my future career.

I also would like to express very special thanks to my committee members: especially Mr Shafie Bakar. I would like to acknowledge their comments and suggestions, which was crucial for the successful completion of this study. I would also like to thanks to the former FKEE members, Tn. Shaikh Nasir for his suggestions and co-operation in the study. I also sincerely thanks for the time spent proofreading and correcting my many mistakes.

My sincere thanks go to all my lab mates and members of SuPER of the Fakulti Kejuruteraan Elektrik & Elektronik, UMP, who helped me in many ways and made my stay at UMP pleasant and unforgettable. Many special thanks go to member group for their excellent co-operation, inspirations and supports during this study.

Importantly, I acknowledge my sincere indebtedness and gratitude with my deepest love to my parents Mr. Othman Bakar and Mrs. Faridah Salleh for their love, dream and sacrifice throughout my life. I appreciate their consistently encouraged me to carry on my higher studies in Malaysia. I am also grateful to my siblings for their sacrifice, patience, and understanding that were inevitable to make this work possible. I cannot find the appropriate words that could properly describe my appreciation for their devotion, support and faith in my ability to attain my goals.

ABSTRAK

Kemajuan dalam bidang penyelidikan dan pembangunan kenderaan elektrik (EV) turut memberi kesan yang sama terhadap kemajuan ujian prestasi dan pengukuran dalam EV. Secara kebiasaanya, casis dinamometer digunakan untuk mengukur kuasa yang dihasilkan dari Kenderaan Dalam Ujian (VUT) biasanya dari kenderaan Engin Pembakaran Dalaman (ICE) yang mendapat tenaga secara satu arah. Terdapat had tertentu dalam pengagihan kuasa secara sehala ini untuk EV yang berkemajuan dalam brek regeneratif, dimana kuasa kinetik dari kenderaan diubah kepada kuasa elektrik. Untuk menguji dan mengukur keupayaan ini, casis dynamometer yang baru dengan penghantaran kuasa secara dwi-arah diperlukan. Dengan itu, kajian ini mencadangkan penggunaan half-bridge pengubah dwiarah DC-DC (HBDC) sebagai Unit Penyerapan dan Pengagihan Tenaga (PADU) untuk dinamometer berasaskan DC mesin. PADU dikawal oleh pengubahsuaian Pengawal Arus Histerisis (HCC) dan pengawal PID. Pengubahsuaian HCC dan PID mewakili kawalan aliran kuasa ke belakang dan sebaliknya semasa ujian. Ujian tersebut melibatkan keadaan normal dan keadaan brek regeneratif. Dalam keadaan biasa, kuasa akan dihantar oleh mesin DC seterusnya untuk keadaan regeneratif brek, bekalan kuasa diserap oleh mesin DC. Beberapa jenis kes ujian telah diambil kira; ujian peningkatan, ujian penurunan, keadaan panduan biasa, keadaan membrek dan keadaan berhenti. Didapati bahawa HBDC berjaya mengawal aliran kuasa dalam kedua-dua keadaan normal dan keadaan brek regeneratif. Berbanding dengan konvensional HBDC, pengubahsuaian HBDC mengurangkan kehilangan dalam pengaliran sebanyak 28.21% pengurangan dan kehilangan dalam pensuisan sebanyak 7.69% pengurangan. Untuk menilai kawalan aliran kuasa, beberapa sudut pengukuran kuasa diambil dalam simulasi dan keputusan menyeluruh dibentangkan. Berdasarkan keputusan ini, ujian untuk EV semasa keadaan normal dan keadaan brek regeneratif dicapai dengan jayanya melaksanakan kawalan aliran kuasa dwiarah dalam casis dinamometer.

ABSTRACT

The advancement of research and development for Electric Vehicle (EV) has pushed a similar advancement in the EV performance test and measurement. Traditionally, chassis dynamometer is used to measuring power delivered from Vehicle Under Test (VUT) typically by Internal Combustion Engine (ICE) vehicle which access power by unidirectional. This one-way power delivery becomes a limitation for advanced EV with the regenerative braking feature, which the kinetic power of the vehicles is converted into electrical power. To test and measure this capability, a new chassis dynamometer is needed where the power delivery must be bidirectional. With that intention, this study proposes the usage of half-bridge bidirectional DC–DC converter (HBDC) as the Power Absorption and Delivery Unit (PADU) for a DC machine based dynamometer. PADU is controlled by modified Hysteresis Current Controller (HCC) and PID controller. The modified HCC and PID control power flow direction; back and forth during testing. The testing includes normal condition and regenerative braking condition. In normal condition, power is delivered by the DC machine whereas in regenerative braking condition, power is absorbed by the DC machine. Several test cases are considered; inclination test, declination test, normal drive condition, brake condition and stop condition. It is found that the HBDC successfully control the power flow in both normal condition and regenerative braking condition. As compared to conventional HBDC, modified HBDC reduces conduction loss with up to 28.21% reduction and switching loss with up to 7.69% reduction. To evaluate the power flow control, several power measurement points are taken in the simulation and comprehensive results are presented. Based on these results, the testing for an EV during normal condition and regenerative braking condition is achieved by successfully implement bidirectional power flow control in chassis dynamometer.

TABLE OF CONTENT

LIST OF TABLES

LIST OF FIGURES

LIST OF SYMBOLS

Ω	OHM
τ	Z source inverter
ω	Speed in rad/s
μ	Permeability
a	Acceleration
C	Capacitance
F_a	Acceleration Force
F_c	Constant Force
F_{car}	Vehicle Force
F_g	Gravitational Force
F_n	Net Force
$F_{propulsion}$	Vehicle Propulsion Force
$F_{roadload}$	Frictional of road load Force
$F_{total(load)}$	Total road load Force
F_v	Velocity Force
F_w	Total force applied on wheels
g	Gravitational
I_a	Actual Current
I_d	Desired Current
I_f	Field Current
I_L	Inductor Current
I_{ref}	Reference Current
$I_{ref\,(-)}$	Lower band reference Current
$I_{ref\,(+)}$	Upper band reference current
L	Inductance
L_a	Armature Inductance
L_f	Field Armature
m_{car}	Vehicle mass
n	Speed in rpm
P	Power
P_{dyno}	Power at Dyno (DC machine)

$P_{dyno(e)}$	Electrical Power at Dyno (DC machine)
$P_{dyno(m)}$	Mechanical Power at Dyno (DC machine)
P_{IN}	Input Power
P_{OUT}	Output Power
P_{PADU}	Power at PADU
$P_{propulsion}$	Power of vehicle propulsion
P_{SS}	Power at Sink/Source (storage)
P_{VUT}	Power at VUT (prime mover)
$P_{VUT(e)}$	Electrical Power at VUT (prime mover)
$P_{VUT(m)}$	Mechanical Power at VUT (prime mover)
R_a	Armature Resistance
R_f	Field Resistance
$S1$	Switch 1
$S2$	Switch 2
v	Velocity
V_{IN}	Input Velocity
V_{OUT}	Output Velocity
V_t	Total Voltage rated

LIST OF ABBREVIATIONS

AC	Alternating Current
APF	Active Pass Filter
BLDC	Brushless Direct Current Motor
DC	Direct Current
CCM	Continuous Conduction Mode
CNG	Compressed Natural Gas
EEV	Energy Efficient Vehicles
EMF	Electromagnetic Field
EV	Electric Vehicles
HBDC	Half-Bridge Bidirectional DC-DC Converter
HCC	Hysteresis Current Controller
HEV	Hybrid Electric Vehicle
HV	High Voltage
LCL	Less Container Load
LPG	L*i*quid Petroleum Gas
LV	Low Voltage
ICE	Internal Combustion Engine
IGBT	Insulated Gate Bipolar Transistor
MAI	Malaysia Automotive Institute
MOSFET	Metal Oxide Semiconductor Field Effect Transistor
NAP	National Automotive Policy
PADU	Power Absorption and Delivery Unit
PSIM	Power SIM
PWM	Pulse Width Modulation
SEPIC	Single Ended Primary Inductor Converter
UPS	Uninterruptible Power Supply
VUT	Vehicle Under Test
ZCS	Zero Current Switching
ZVC	Zero Voltage Switching

CHAPTER 1

INTRODUCTION

1.1 Background

1.1.1 Energy Efficient Vehicles (EEV)

In early 2014, the Malaysian Automotive Institute (MAI) has introduced Energy Efficient Vehicles (EEV) category as a critical part of the National Automotive Policy (NAP) 2014. The focus of NAP is to transform the domestic automotive industry and integrate it into the increasingly competitive regional and global industry network. Hence, develop Malaysia as the regional automotive hub in EEV (NAP, 2014). EEV is defined by MAI as *"vehicles that meet a set of define specification in terms of emission level (g/km) and fuel consumption (l/100km)"*. EEV includes fuel efficient vehicles, hybrid vehicles, Electric Vehicles (EV) and vehicle using alternative fuel such as CNG, LPG, and Biodiesel, ethanol, hydrogen and fuel cell (Mustapa Mohamed, 2014). As stipulated in NAP 2014, all vehicles targeted for EEV category must be tested to ensure that the efficiency of the vehicles is within the predefined range. Typically, this testing is carried out by using dynamometer.

1.1.2 Dynamometer

There are two main categories of dynamometer, which are engine dynamometer and chassis dynamometer. Engine dynamometer measures the performance and the efficiency of an engine alone, without connecting to any other systems. On the other hand, chassis dynamometer, or in short "chassis dyno", measure the performance and the efficiency of the whole vehicle. Chassis dynamometer measures the power delivered to the road surface by emulating the surface using a "drive roller". Both categories of dynamometer calculate input/output power directly by measuring two main components, the torque (Nm) and the speed (rpm). Between the two categories, chassis dynamometer is more suitable for the EEV test because the category set by MAI is for the whole vehicle system and not just its engine evaluation.

Chassis dynamometer is used to simulate driving on a road inside a laboratory in controlled conditions. The working principles of a conventional dynamometer are always about absorbing power and energy from the vehicle and dissipate the absorbed power normally as heat. At the same time, it captures the torque and the speed of the test unit as performance measures. By manipulating the brake, chassis dynamometer emulates the vehicle road load condition according to the intended application. Chassis dynamometer detects the vehicle dynamics, emission targets and fuel consumption of multiple loading conditions through the vehicle by simulating road driving conditions (Mayyas et al., 2013).

There are two types of absorption methods normally used in chassis dynamometer; eddy current brake or generator brake. The main difference between the two is in the principle of energy convention used. As for eddy current brake, it does not generate electricity, but uses the electrical power supply to charge the electromagnetic coils. The brake’s input shaft spins a rotor inside that result in a magnetic field. When current is supplied to the coils, the engine under test becomes more difficult to turn the rotor due to the braking effect of the magnetic field generated around the coils. Eddy current brakes dissipate the power from the vehicle as heat input to the rotor; hence the rotor must be cooled using a fan that is fixed on the rotor. Generator brake, on the other hand, converts the mechanical energy from the vehicle to electrical energy. The energy from the generator is then stored or dissipated as heat using variable load. Bigger loads means more power required from the generator, hence the roller become harder to turn. The main advantage of generator brake over eddy current brake is its’ capability to emulate the dynamic load change, hence test the vehicle dynamic performance. Thus, generator brake is more appropriate for EEV test. Furthermore, generator brake will be able to test the regenerative braking function of some EEV.

1.1.3 Regenerative Braking

Among the types of EEV are electric vehicles (EV) and hybrid electric vehicles (HEV). EV runs fully on battery supply, while HEV combine the power from the battery via electric motor and from the fossil fuel via internal combustion engine (ICE). Both types of vehicles usually are capable of "regenerative braking", a term referred to a brake that converts the inertia of a vehicle into electric power that charges an electrical energy storage device.

Conventional chassis dynamometer will not be able to test regenerative braking because regenerative braking requires a counter-driving power flow; from inertia of the vehicle to the energy storage in the vehicle. To emulate vehicle inertia, a dynamometer will have to roll the wheel of a vehicle during regenerative braking by using external power. This is not designed for in conventional dynamometer as there is no application in traditional vehicle. Hence, this study is an attempt to develop a dynamometer capable of testing the regenerative braking of EV.

1.1.4 Bidirectional DC-DC Converter

Regenerative braking occurs employed by the bidirectional converter application. Bidirectional converter can be applied on DC and AC systems. It is design for transfer energy back and forth thus it can be used for two-way power flow application. The energy transfer then can be stored and reused again if demanded by the other side. Typically, unidirectional power transfer express energy as load or dissipate as heat. There are many types of topologies available for bidirectional converter such as half-bridge, full-bride, push-pull and it is usually performs as isolated or non-isolated bidirectional. The Half-Bridge Bidirectional DC-DC Converter (HBDC) is designed with minimum number of devices. Simultaneously, HBDC implement zero voltage switching (ZVS) on all active switching devices causing minimization in switching losses (Park & Song, 2011). Moreover, HBDC is results from the combination of a boost mode in one direction and buck mode in the opposite direction and it has higher efficiency compared to other topologies (Ribeiro et al., 2014). Therefore, bidirectional converter application is widely used in energy storage, renewable energy, grid lines and also as AC and DC load apparatus.

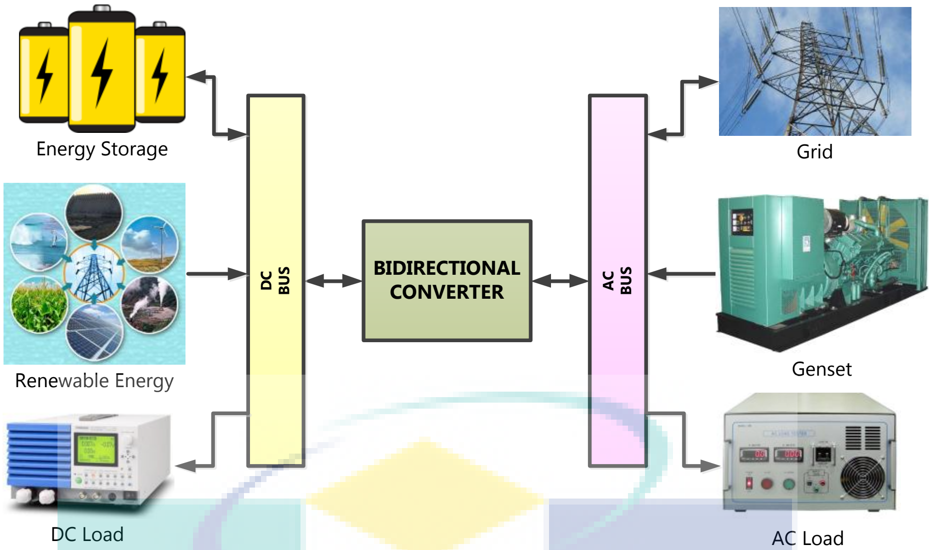

Figure 1.1 Wide spread of bidirectional converter applications

1.2 Problem Statements

Conventional dynamometers have been designed for Internal Combustion Engine (ICE), hence the lack of testing mechanism for regenerative braking in EEV. There is a need to measure the efficiency of an EV, and this requires (1) a test and measurement system for EV power flow and (2) another test and measurement system for regenerative braking. To realize this test, a chassis dynamometer with bidirectional power flow is required. This study will focus on developing a simulation of a bidirectional DC-DC converter for controlling the current and subsequently the power flow in DC machine chassis dynamometer. Being unprecedented, the challenge in developing this converter lies on a suitable topology and control technique for managing bidirectional power flow in EV chassis dynamometer. This is particularly challenging in ensuring accurate power transfer to test the capability of regenerative braking. To implement the new chassis dynamometer, half-bridge bidirectional DC-DC converter topology and PID controller together with modified Hysteresis Current Controller (HCC) control technique is proposed.

1.3 Objective

The proposed research focuses on developing a controller for bidirectional DC-DC converter in chassis dynamometer to allow for the emulation of regenerative braking condition. The specific objectives are;

i) To design a simulation of current control technique in bidirectional DC-DC converter thus reduces switching losses using modified hysteresis current control (HCC) and PID controller.
ii) To design and control a new chassis dynamometer based on a developed half-bridge bidirectional DC-DC converter to carry out the normal road load test and regenerative braking test.
iii) To analyse power and energy transfer of bidirectional chassis dynamometer from (to) a DC machine between (from) a power source (sink) capability.

1.4 Contributions

The main contributions of this proposed research are:

i) A new chassis dynamometer design that integrates a DC machine with a bidirectional DC-DC converter. The DC machine generates power similar to that in storage, and this power represents the regenerative braking in the new chassis dynamometer.
ii) Based on the operation of the bidirectional DC-DC converter, the power flow management is regulated by Hysteresis Current Control (HCC) together with PID controller. When comparing the performance of conventional and modified method of HCC, it is found that the modified HCC has reduced the conduction and switching losses.

1.5 Scopes

This research aims to design a controller for new chassis dynamometer in simulation with the absent of hardware structure. The modified Hysteresis Current Controller and PID controller are applied in half-bridge bidirectional DC-DC converter (HBDC) topology to implement new chassis dynamometer with bidirectional power flow. Simulation of the modified HCC together with PID controller attached with HDBC is known as Power Absorption and Delivery Unit (PADU) is designed in this research.

This research focuses on power transfer of new chassis dynamometer with bidirectional flow and evaluates new current control technique in controlling current of DC Machine. Testing conditions of the new chassis dynamometer are normal condition tests and regenerative braking tests.

1.6 Thesis Overview

This thesis is divided into five chapters which are arranged as follow:

Chapter 1 introduces the proposed research. This chapter provides the background of electric vehicle, chassis dynamometer, regenerative braking and bidirectional DC-DC converter. Also, this chapter states the objectives, methodology and outline of the thesis.

Chapter 2 presents the literature reviews. This chapter discusses the chassis dynamometer application, various types of bidirectional DC-DC converter, and focuses on overall control of bidirectional DC-DC converter.

Chapter 3 provides the operating principles of the proposed bidirectional DC-DC converter. This chapter also details the current and torque control strategy and power flow designs.

Chapter 4 presents the results of proposed method and discusses the validation of the performance results.

Chapter 5 discusses the conclusion and summarizes the contributions of this research, while giving recommendation for future works.

CHAPTER 2

LITERATURE REVIEW

2.1 Introduction

This chapter presents the literature review of Electric Vehicle (EV) operation systems and the characteristics of various types of chassis dynamometer. Hysteresis Current Controller (HCC) is introduced together with PID controller as current control technique. Besides, the various bidirectional DC-DC converter topologies are presented. Furthermore, the capability to tests EV in chassis dynamometer using current control technique for half-bridge bidirectional DC-DC converter will be discussed.

2.2 Chassis Dynamometer

The dynamometer, which acts to determine torque and power required to drive a machine, is a core equipment of various types of test stations, such as a motor performance test station, mechanical drive test station and engine performance test station (Jiaqiang Yang, Jin Huang, 2005). Chassis dynamometer allows testing of vehicle performance in the laboratory by emulates real road load condition, therefore tests can be easily repeated. Recently, the chassis dynamometer has been widely used to compensate road testing on a real track, as tests on real tracks is influenced by weather conditions and thus making it more expensive (Mayyas et al., 2013). Theoretically, a chassis dynamometer measures power delivered to the “drive roller” (drum) by the drive wheels. During testing, the VUT is positioned on the chassis dynamometer with its drive wheels on the rollers. The software then calculates the output torque, based on how fast of vehicle accelerates the roller or via a load cell that measures power absorbed by the rollers, from which the output horsepower is calculated. Previously, a dynamometer roller incapable to test the vehicle’s dynamic braking performance. Therefore, previous finding (Yinding et al., 2011) depicts that; the equivalent moment of inertia test is applicable to applied at the vehicle to tests braking performance. It should be noted that with different mass and speed, the roller brake unit can reflect the vehicle road braking performance. The difference is tested with a car with 4000 kg and motorcycle with 2000 kg. The road braking performance means the load experiences the inertia for both condition tests. As for the mass of both vehicles is difference, chassis dynamometer emulates load road condition with different load measurement rely on produced speed from each vehicles.

Dynamometer can be categorized into passive dynamometer or active dynamometer. Passive dynamometer is known as absorption dynamometer which is developed for driving purposes. On the other hand, active dynamometer has better performance with capability to do either absorb or drive also known as a universal dynamometer. Active dynamometer is used to specifically determine torque and power for machine under test (MUT) to test and evaluate the performance, fuel efficiency and emission of fuel cell hybrid vehicles (Mingjie et al., 2010). There are two types of dynamometer which is engine dynamometer (measures output power directly from the engine) or a chassis dynamometer (measures output power from engine or drivetrain) (Jirawattanasomkul & Koetniyom, 2000). In addition, chassis dynamometer can be used for a variety engine development, including calibration of engine management controller and detailed investigation on the behaviour of combustion.

The conventional method of chassis dynamometer testing is limited to the VUT tests with power absorption only. According Figure 2.1, the installation of conventional chassis dynamometer shows the use of Power Absorption Unit (PAU) to absorb power while supplied torque and speed measurement is used as control purposes. The cross-section of conventional chassis dynamometer with drum attached with PAU is clarified in Figure 2.2. The drum is attached with PAU to absorbing power from rolling drums. Furthermore, the present load gives acceleration and deceleration of the drum and power absorption can be reduces with the inclusion of flywheels (Bennetts, 2002). An addition of load and speed gauges is recording the reaction force of the assembly at the surface of the drums. The disadvantage of conventional chassis dynamometer is that the control of test bed was left to the operator. However, advancement in technology has upgraded the chassis dynamometer to become a development platform for Energy Efficient Vehicle (EEV).

The modern chassis dynamometer aiming at extending a recently commercial available dynamometer as the wheel mounted configuration of the dynamometer. Thus, this type of chassis dynamometer is beneficial used to isolate the tire vibrations in an effort to decouple the vibrations that origins from the drivetrain (Öberg, Nyberg, & Nielsen, 2013). Figure 2.3 define the development of modern chassis dynamometer with electrical drives, power electronics and precision motion control of electrical machines for torque and power. This advancement of modern chassis dynamometer assists in cost reduction and become a versatile setup. Thus, the difference conventional and modern chassis dynamometer is relying on the usage of drum and PAU.

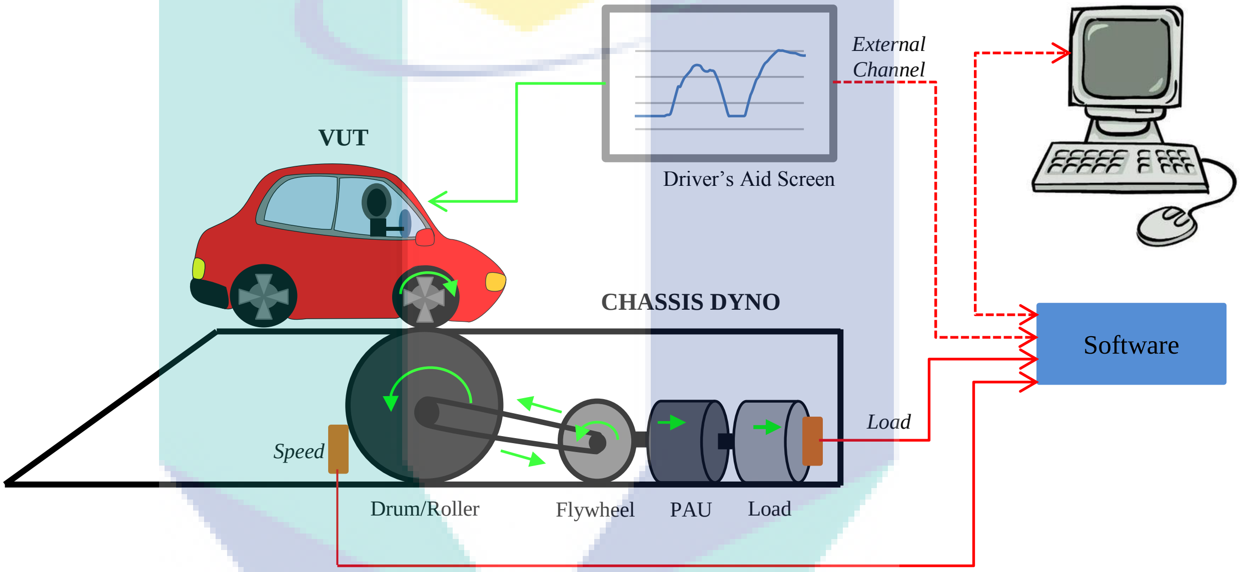

Figure 2.1 The arrangement of conventional chassis dynamometer

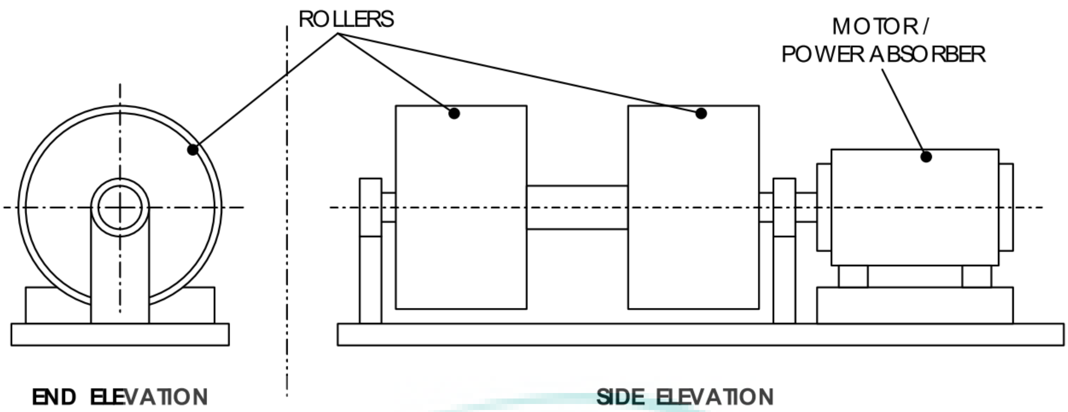

Figure 2.2 The cross-section of conventional chassis dynamometer

Source: Bennetts (2002)

Figure 2.3 A glance of the modern chassis dynamometer configuration. A Golf V with a 1.4 *l* multifuel engine has been mounted to the dynamometer units in a 4WD configuration

Source: Öberg, Nyberg, & Nielsen (2013)

Currently, complete vehicle test mainly consists of road test and chassis dynamometer test. However, the controllability and repeatability of road tests are easily changed by variable factors, such as road conditions and environment. By controlling the variable factors, chassis dynamometer test can accurately simulate vehicles on road load resistance, thus the inaccuracy in performance encountered during testing can be overcome (Maodong, Lei, & Weigao, 2010). Vehicle on road load resistance includes air resistance, rolling resistance, acceleration resistance and driveline friction resistance. The mechanical loss of a chassis dynamometer testing system, such as rolling loss between tires and roller, friction loss in the driveline and chassis dynamometer can be acquired by conducting unloaded coast down test on the dynamometer. Numerous tests can be carried out using the chassis dynamometer; one of the tests is the constant speed test that is measured from the torque produced from the VUT drivetrain (Öberg, Nyberg, & Nielsen, 2013). The test should be conducted by following standard Environment Protection Agency (EPA) test procedures (Kelly et al., 2002). Nonetheless, this testing procedure typically for conventional chassis dynamometer for testing Internal Combustion Engine (ICE) types. It is important concerning to the pollution effects and standardizes the condition of performance with difference capability.

The chassis dynamometer test procedures include the following:

a) FTP-75 (EPA urban emissions certification test procedure)
b) Highway Fuel Economy Test (HWFET)
c) US06 aggressive driving cycle performed at 0°C, 20°C, and 40°C
d) SC03 air conditioning cycle performed at 95OF with and without air conditioning

2.3 Motor Selection for Power Circuit

The motor characteristics influence the performance of PAU in chassis dynamometer, thus motor selection needs to be properly selected for bidirectional chassis dynamometer. The basic performance requirement of a chassis dynamometer to be used for road load condition testing and regenerative braking testing are the capability to perform bidirectional power flow as well as having a high start-up torque. An electrical machine is a device that can convert either mechanical energy to electrical energy (a generator) or electrical energy to mechanical energy (a motor). Electric motors can be categorized as either DC motors or AC motors (Joshi, 2013).

2.3.1 AC Motor - Brushless Direct Current Motor (BLDC)

Brushless Direct Current Motor (BLDC), also known as permanent magnet synchronous motor, is an electronically commutated motor; commutation is based on hall position sensors, instead of carbon brushes. The rotor is a permanent magnet instead of the electrical windings as in a normal DC motor. Therefore, a fixed armature winding eliminates the problem of connecting the current supply to the rotating armature. Compared to the normal DC motor, the efficiency of BLDC is higher; in addition, electronically commutation reduces wear and tear. Thus, BLDC have longer lifetime, while no maintenance is needed because of the absence of the carbon brush that would cause commutation erosion. It also eliminates the ionizing sparks from the commutator. On the other hand, BLDC is more expensive than the DC motor due to the complexity of its electronic control. Also, BLDC has limitation in power rating due to heat generated in the motor.

2.3.2 AC Motor - Induction Motor

AC motor, also called asynchronous motor, is the most preferred motor for use in EV. In AC motor, current is induced by the electromagnetic induction in the rotor winding due to magnetic field of the stator winding. AC motor can be categorized into two types, namely, wound rotor and squirrel cage. The advantages of an induction motor are reliability, low maintenance, rugged and are able to operate in adverse environment. On the other hand, its disadvantages are lower efficiency due to the presence of the windings in the both rotor and stator that increases the copper losses. Also, it has low power factor and low inverter usage.

2.3.3 DC Motor

Typical DC motor has an electrical winding in the rotor, while its stator is composed of permanent magnet or electrical winding that acts as electromagnets. The action of a commutator in a DC motor produces a distribution of current directions in the armature conductors regardless of the rotation of the shaft. The torque of a motor maximum during low speed, which gradually decreases as speed is increased. The main drawback of DC motor is that its power rating is limited by heat produces by the armature; power is affected by heat dissipation in the air gap, which increases the temperature in the air gap (Zhang, 2008). Furthermore, when operated at high speeds, increase in friction between the carbon brush and the commutator will result in decreased torque. Also, the bulky construction with brushed commutation in a DC machine requires periodical maintenance.

After examining the characteristics of the various types of motor, DC motor is selected to be used in this study due to its reliability for bidirectional chassis dynamometer performance. Since the operation for bidirectional chassis dynamometer is for transferring power back and forth, the DC motor is named as DC machine as the motor behaves both as a motor and a generator. DC motor is mainly used in the system of power dynamometer, because of its excellent speed regulation capability and facile control ability (Jiaqiang Yang, Jin Huang, 2005). Moreover from (Duan & Zeng, 2010), they stated that, DC dynamometer is more suitable for speed or torque control and possible to deal with a wide adjustable range. In this study, a bidirectional DC-DC converter is used in conjunction with a DC machine to drive the drum of the chassis dynamometer. In DC motor, there is a direct relationship between torque and rotor current of the motor (Sun & Zhang, 2015).

A dynamometer that consists of a DC motor together with a bidirectional DC-DC converter has been used in a wind turbine system (Caricchi et al, 1994). With the bidirectional converter, the DC machine acts as a motor during motoring mode, and it acts as a generator during regenerative mode. During the operation, in order to achieve speed control of the DC motor, its current and speed feedback are compared with their respective references (Joshi & Samanta, 2013); proportional to the voltage supply, torque is used as reference to control the current and speed of the bidirectional chassis dynamometer, whether in motoring mode or regenerative mode. Recently, DC machine and DC drives are widely used in applications requiring an adjustable speed variation, good speed regulation, and frequent starting, braking and reversing. Some important applications are: rolling mills, paper mills mine winders, hoists, machine tools, traction, printing presses, textile mills, excavators and cranes (Hardy et al., 2011).

2.4 Controller in Control Circuit

2.4.1 Hysteresis Current Controller (HCC)

The important part in designing bidirectional chassis dynamometer is the controller. The controller implemented in this system uses the hysteresis current control technique, which is popularly used for current control in APF (active pass filter). The various types of hysteresis current control (HCC) include single-band, variable-band, fixed-band, frequency-band, and dynamic method; however, PWM and hysteresis modulation are widely used to control the flow of current (Dotelli et al., 2015). Originally, the controller was operated at a constant switching frequency, and consequently, the amplitude of the ripple is dependent on the working conditions. On the other hand, the amplitude of the ripple can be kept constant by using hysteresis control, in which case the switching frequency is dependent on the operational conditions. As mention from (Sonavane & Jadhav, 2015) with the hysteresis current controller, the reference current and actual current from the measuring element is used to generate the switching signal.

In order to control bidirectional DC-DC converter, fixed-band technique is implemented. The implementation of fixed-band hysteresis current control (HCC) derives the switching signal by comparing inductor current signal between the reference current signals, as illustrated in Figure 2.4. In this case, when the inductor current signal exceeds the positive hysteresis band, the switching signal is operated as *"on"* state, whereas when the inductor current signal falls below the negative hysteresis band, the switching signal is changed to *"off"* state.

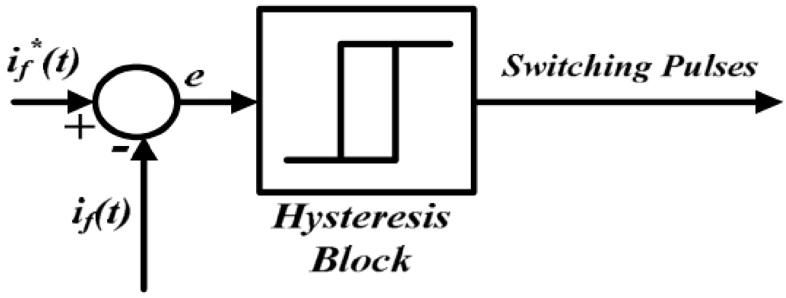

Figure 2.4 Fixed-band hysteresis current control
Source: Vahedi, H., Sheikholeslami, A., & Bina, M. T. (2011).

On the other hand, as shown in Figure 2.5, the variable-band is implemented from error current signal derived from the inductor current signal and the references current signal. The error signal is calculated based on instantaneous reactive power theory. The error current signal then is compared to the reference current signal to produces the switching signal. From this HCC types, the hysteresis band is controlled using fuzzy controller taken from reference current signal and error current signal (Jun & Dazhi, 2009).

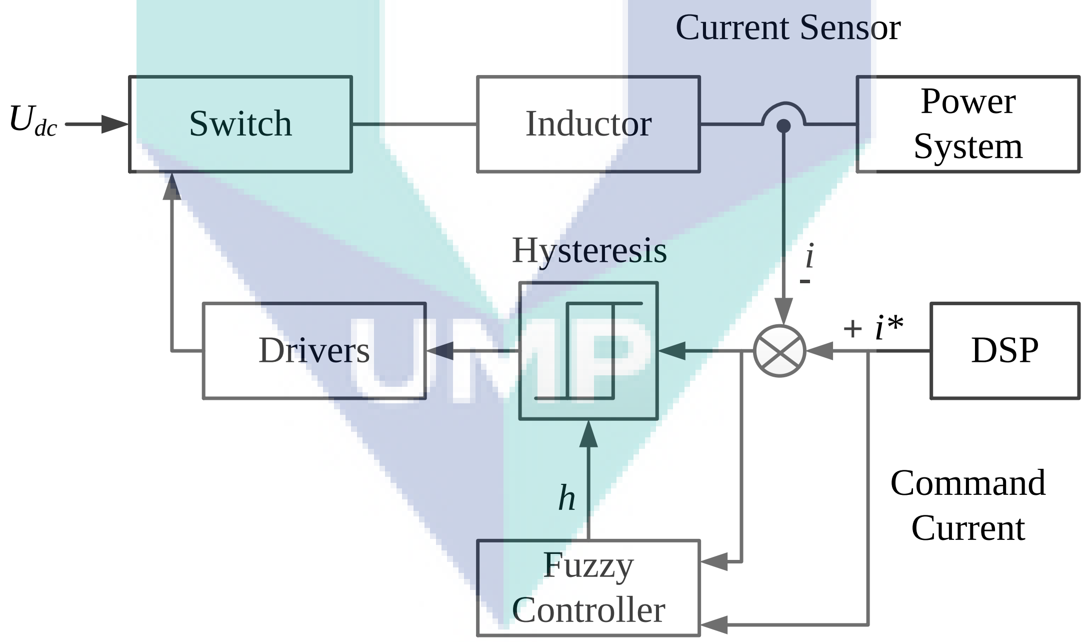

Figure 2.5 Variable hysteresis current control
Source: Jun & Dazhi (2009)

(Dotelli et al., 2015) explained that hysteresis current control has been found to be suitable to be applied in the bidirectional chassis dynamometer. However, ripple is produced from the inductor in the DC-DC converter as a consequent of the variable frequency, however it can be minimized by properly selecting the band size of the torque hysteresis (Ebin & Sreethumol, 2015). Although fixed-band hysteresis current control has some drawback, such as switching frequency is not constant, it is acceptable for pulse generation as its circuit is simple, has fast dynamic response and no sensitivity to the load parameters (Samedaei et al., 2010). Therefore, bidirectional chassis dynamometer is applicable using HCC since it is manipulating load parameters.

The hysteresis current control PWM technique is widely used because it has a fast dynamic response and is easy to implement; it is also capable of inherent peak current limitation and is insensitive to load parameters variation (Marthanda & Marutheswar, 2015) (Peter & Ramchand, 2015). (Komurcugil et al., 2015) founded that, the disadvantages of HCC include variable switching frequency and steady-state error in grid current; also, (Muñoz et al., 2015) explains it produces unpredictable harmonics which may cause unexpected resonance that could harmful to the application. However, the major advantages of hysteresis current control include stability, fast response and good accuracy (Wu et al., 2015). In addition, it is able to reject the disturbance caused by dynamic load, has simple loop design for current compensation and has excellent stability during abnormal condition (Ananth et al., 2013). It has also been found that hysteresis current controller is better applied on current source inverter than voltage source inverter (Kolmakov & Bakhovtsev, 2015).

2.4.2 PID CONTROLLER

Proportional Integral Derivative (PID) controllers are widely used in control systems because of the capability to reduced number of parameters to be tuned. Based on (Kanojiya & Meshram, 2012) studies, PID provide control signals that are proportional to the error between the reference signal and the actual output (proportional action) to integral of the error and to the derivative of the error (derivative action). The transfer function of PID controller is given in Equation 2.1 where T_d defined as parameters to be tuned.

$$K(s) = K_p \left[1 + \frac{1}{T_i\,(s)} + T_d(s)\right] \tag{2.1}$$

$$G(s) = \frac{K_e^{-sL}}{Ts+1} \tag{2.2}$$

Typically in control performance, PID controller function by adjusting the proportional gain (K_P), the integral gain (K_I) and differential gain (K_D) as shown in block diagram in Figure 2.6. One of the widely used tuning method is Ziegler-Nichols method with the step response curve in Figure 2.7. From previous finding (Kanojiya & Meshram, 2012) defines that the response is characterized by two parameters which are delay time, L and time constant, T. As depicted in Figure 2.7 with the tangent line at infection point and noting its intersection with the time axis and the steady state model based on Equation 2.2. However, if the system unable to be derived, experiments is performed to extract the parameters with k, L and T for estimated in the model. Therefore, the controller parameters are tuned according the Zeigler-Nichols method.

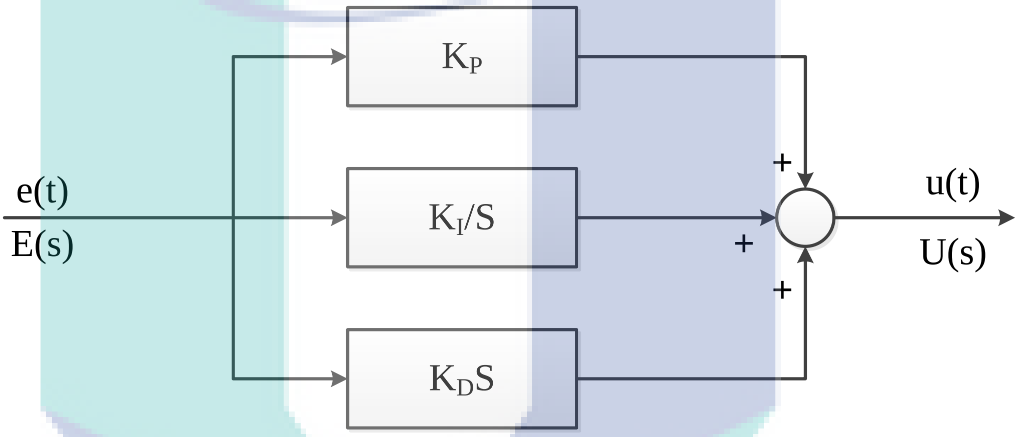

Figure 2.6 Block diagram of PID controller

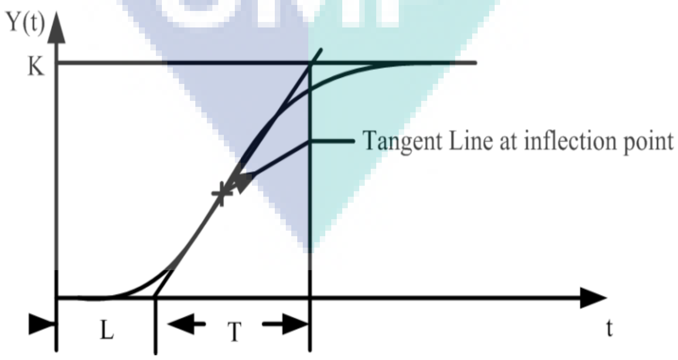

Figure 2.7 Response Curve for Ziegler-Nichols Method

2.5 Bidirectional DC-DC Converter

The bidirectional DC-DC converter is recently used for battery and (or) ultra-capacitor charging and discharging of EV application. The proposed use of bidirectional DC-DC converter in this study, whose structure is as illustrated in Figure 2.8, is to enable the transfer of energy back and forth from battery to the inverter, and vice versa. The supplied current and voltage is characterized by I_1 and V_1 at the prime mover side, and labelled as I_2 and V_2 at the energy storage side. The converter is said to be in buck mode when power flows from the prime mover to the energy storage side, and the converter is in boost mode when power flows in the opposite direction.

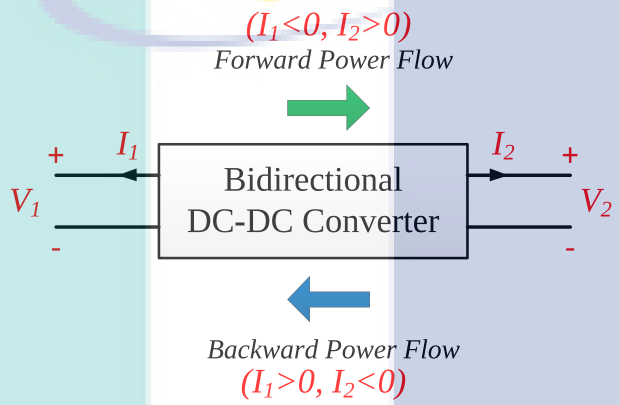

Figure 2.8 Illustration of bidirectional power flow (forward and backward)

DC-DC Converter can be categorized into isolated and non-isolated types. In general, a converter is constructed using either half-bridge, full-bridge, unidirectional or bidirectional topologies. The power flow that happens during buck and boost modes is triggered using signals from switching circuits, using either switches or diodes. Usually a unidirectional semiconductor power switch, such as Metal Oxide Semiconductor Field Effect Transistor (MOSFET) or Insulated Gate Bipolar Transistor (IGBT), is connected in parallel with a diode as unavailability double-sided power switch is not available (Zhang, 2008).

2.5.1 Non-isolated Bidirectional DC-DC converter

Based on (Molavi et al., 2015) and (Du et al., 2010) studies, the basic topologies of non-isolated bidirectional DC-DC converter can be categorized into half-bridge, Cuk, and SEPIC/Luo converter. In addition, derived converter topologies include cascaded half-bridge converter and interleaved half-bridge converter.

A typical non-isolated bidirectional DC-DC converter with half-bridge topology is a combination of buck and boost converter, each of which originally performs in unidirectional manner. Thus, modification from buck and boost topology may result in bidirectional behavior. The bidirectional power flow capability is the effect from the presence of diodes in their structure, which allows current to flow in one direction but not in the opposite direction; this limitation can be overcome by replacing the diodes with controllable switch in its structures.

Based on studies conducted by (Ribeiro et al., 2014), (Manoharan et al., 2013), (Moon et al., 2012) and (Du et al., 2010), it was stated that the non-isolated bidirectional DC-DC converter have better efficiency, and have simpler circuitry compared to that of the isolated bidirectional DC-DC converter. (Patil et al., 2015) has introduced the transformer-less LCL resonant soft-switching bidirectional DC-DC converter for main structures in high step up – step down ratio, high efficiency, low device stress, ZVS turn-on for switches and ZCS turn-on and turn-off for diodes during buck and boost condition.

On the other hand, (Elankurisil & Dash, 2012) and (Vijay & Scaria, 2013) have proven that the non-isolated bidirectional DC-DC converter is limited to low and medium voltage operation. However, (Vijay & Scaria, 2013) found that, with modification using SEPIC converter on the converter operation, the converter is suitable for high voltage in non-isolated application.

Based on Figure 2.9 (Rahman et al., 2015), during the buck mode operation when the power is transferred from high voltage (HV) to low voltage (LV) side, switch *Q1* is an active switch while switch *Q2* is kept off; in this case the converter acts as a step-down converter. On the other hand, in the boost mode operation when the power is transferred from LV to HV side, *Q2* is acts as a controlled switch and *Q1* is kept off; in this case the converter acts as step-up converter. The inductor current is the main element for transferring current flows, thus the auxiliary circuit gives continuous inductor current with constant switching frequency and switching stress. However, no auxiliary circuit is needed for non-isolated to enhance the operation of inductor current (Vijay & Scaria, 2013). The conventional non-isolated converter can be operated in continuous conduction mode (CCM) (Baburaja & Jayakumar, 2013), which was also confirmed in another study (Mohammadi & Farzanehfard, 2015).

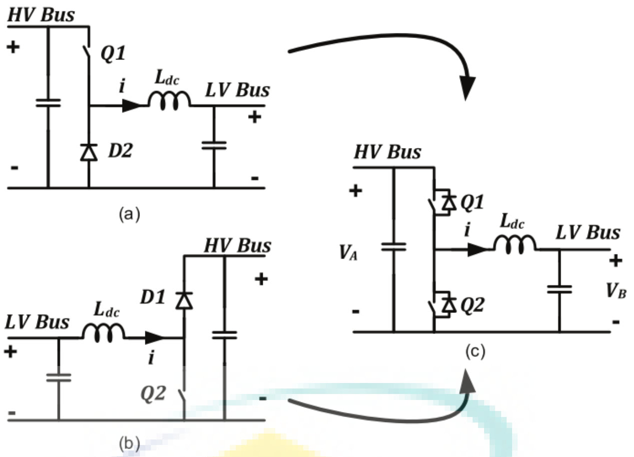

Figure 2.9 (a) Elementary unidirectional buck converter, (b) elementary unidirectional boost converter, and (c) transformation to bidirectional converter by substituting diodes with controllable switch.

Source: Karshenas, Daneshpajooh, & Safaee (2011)

Characterized by a reduced number of components, easy control and low cost, non-isolated bidirectional half-bridge DC-DC converters are very attractive for DC applications, such as renewable energy power systems and vehicles (Ribeiro et al., 2014). The transformer-less bidirectional DC-DC converter is preferred for non-isolated application because of the reduction in size, weight and development costs. This is especially essential when the converter is to be applied in space craft that demands high power but low in weight and small in size (Manoharan & Swarnalatha, 2013). Meanwhile, in EV application, the step-up stage is applied to increase battery voltage during motoring mode, while step-down stage happens to increase the current to makes EV slowing down in regenerative braking mode. Nonetheless, there are some drawbacks using non-isolated topology. To fulfill the low ripple requirement, non-isolated topology requires high inductance value at the battery side in order to smoothen the current that leads to a slower dynamic response (Fardoun et al., 2014). In addition, the use of switch capacitor yield a large switching loss and current stress as a large number of switches is needed to produce high voltage gains as applied in multi-level DC-DC converter (Molavi et al., 2015).

2.5.2 Isolated Bidirectional DC-DC Converter

In a bidirectional DC-DC converter, isolation is normally provided by a transformer, and the added transformer implies additional cost, volume and losses (Rishma et al., 2012); however, since transformer can isolate the two voltage sources and provide impedance matching between them, it is an alternative in those kinds of applications. Full-bridge, half-bridge, a push-pull topology can be categorized as isolated bidirectional DC-DC converter. Typically, isolated bidirectional DC-DC converter is based on the half-bridge in the primary side, whereas the secondary of a high frequency isolation transformer is based on the current fed push-pull (Zhang, 2008). The converter operation is described for both modes; in the presence of a DC bus the battery is being charged, while the battery discharged in the absence of the DC bus. This operation is basically operated in DC uninterruptible power supply (UPS) (Zhang, 2008).

By adding the transformer, the isolated DC-DC bidirectional converter can achieve high step-down or step-up conversion ratio. However, the drawbacks arise from the additional transformer include the increase in the volume and circuit complexity, while reducing its efficiency (Molavi et al., 2015). On top of that, galvanic isolation is required in many application, thus it is mandated by different standards (Karshenas et al., 2011); hence, in terms of safety, galvanic isolation is essential during application (Jiang et al., 2014).

A recent study on non-isolated bidirectional DC-DC converter has shown that the converter has the benefit of lower magnetics bulk, higher efficiency and compact (Patil et al., 2015). Since high frequency is needed to increase power density, which would lead to high switching losses, the losses can be overcome by using a soft switching DC-DC converter. In addition, non-isolated DC-DC converter with soft switching is applicable for a wide range of load in buck and boost operation (Patil et al., 2015).

2.5.3 Half-Bridge Bidirectional DC-DC Converter

The Half-Bridge Bidirectional DC-DC Converter (HBDC) is designed with minimum number of devices. Simultaneously, HBDC implement zero voltage switching (ZVS) on all active switching devices causing minimization in switching losses (Park & Song, 2011). Moreover, HBDC is resulted from the combination of a boost mode in one direction and buck mode in the opposite direction and it has higher efficiency compared to other topologies (Ribeiro et al., 2014).

From previous (Ribeiro et al., 2014) depicted that, the power transferred from the low voltage side (LV bus) to the high voltage side (HV bus) which is in positive direction the converter operates as a boost converter. According Figure 2.10, for high average inductor current values, only IGBT Q2 and diode 1 is conducted. While Q2 is *"on"* state, the inductor voltage can be expressed in Equation 2.3 and the slope of inductor current, I is represent in Equation 2.4. Thus, the combination of Equation 2.3 and 2.4 result the inductor current to positive. Diode, D1 is forward biased (during Q1 command signal is *"off"* and Q2 command signal *"on"* or *"off"* according to control approach) when the inductor current voltage is represent in Equation 2.5. If voltage side (LV bus) is less than voltage side (HV) the converter is operating in boost mode. Therefore, D1 is conducting the inductor current slope in negative. For buck mode condition, the converter transferred power from HV to LV bus with negative direction. It is operated when Q1 is *"on"* and the inductor voltage is given by Equation 2.5. To come out the negative in inductor current slope, voltage side (LV) is less that voltage side (HV) is applying with Equation 2.3 and Equation 2.4. Diode, D2 is forward biased when Q1 command signal is *"off"* and the inductor voltage is given by Equation 2.3. The slope of the inductor current is positive while diode, D1 is conducting.

$$V_L = V_{LV} \tag{2.3}$$

$$\frac{dl}{dt} = \frac{V_L}{L} \tag{2.4}$$

$$V_L = V_{LV} = V_{HV} \tag{2.5}$$

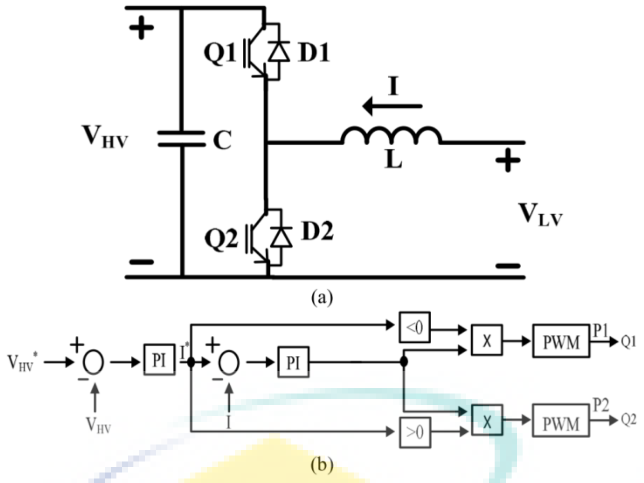

Figure 2.10 Half-Bridge Bidirectional DC-DC Converter (a) Control Circuit (b) Controller

As studied by (Babu & Henry, 2011), it is stated that, half-bridge topology suitable in power reduction because voltage and current stress are less than in full-bridge topology. This half-bridge is preferred in PADU and appropriate to be used for DC machine generating and regenerating consequently from limitation of power rating effects from heat generated at the DC machine. Therefore, to examine the capability of bidirectional power flows from DC machine to power storage (sink/source) and vice versa, Hysteresis Current Controller (HCC) and PID controller are used as PADU controller.

Half-bridge topology is used in PADU because voltage and current stress is less than in that encountered in full-bridge topology. Moreover, half-bridge topology gives higher power (Babu & Henry, 2011), and as such is appropriate to be used in DC machine generation and regeneration. Therefore, to examine the capability of bidirectional power flows from DC machine to battery, and vice versa, hysteresis current control is used as the controller.

2.6 Power Transfer in EV

In EV application, the circuit of the bidirectional DC-DC converter is operated in two modes: motoring mode or regenerative mode. A typical motoring mode occurs when the EV is being accelerated, while regenerative mode happens when it is going downhill. In battery application, the motoring mode and regenerative mode is denoted as charging mode and discharging mode, respectively.

2.6.1 Motoring Mode

The motoring mode is the operation of motor in bidirectional DC-DC converter acts as a load. The motoring mode operation involves the load torque, in which case the motor current is positive, whereas the back EMF is less than motor armature voltage by an amount equal to V_a. Therefore, in buck mode operation, the motor is rotated at the desired speed that can be achieved by adjusting the duty ratio to keep the armature voltage greater than the back EMF (Joshi & Samanta, 2013). However, during buck mode, the battery side acts as a rectifier to produce energy to be fed to the battery (Rahman et al., 2015).

2.6.2 Regenerative Braking Mode

In regenerative mode, EV is going downhill, during which regenerative braking is applied. In this situation, a negative load torque occurs at the motor, which consequently causes the motor current to become negative and raising the motor's back EMF voltage (Joshi & Samanta, 2013). Significant amount of the mechanical energy from the braking vehicle resulting from the regenerative braking is recovered in the storage from reversal power flow (Caricchi et al, 1994). When the vehicle is going downhill, the motor acts as generator, during which power flows from the generator to the storage device (Rahman et al., 2015); in this situation, the bidirectional DC-DC converter is in boost mode. However for safety, dynamic braking system needs during acceleration (Seki et al., 2008).

Bidirectional DC-DC convertor with half-bridge topology is alternately operated in boost and buck modes; each mode is controlled using two independent controllers in which the gain for the two modes are different (Lee et al, 2013). From (Jeongwoo & Douglas J., 2005), the power recovered from regenerative braking mode is complex than motoring mode because of losses occurs. Thus, regenerative braking control is generally used to overcome this situation, in which the reference parameter is modified from charging current to torque.

The bidirectional DC-DC converter is suitable to be used when the drive characteristics of a motor needs to be optimized. In braking mode, it has been found that the efficiency of the motor increases from the utilization of energy (Buvana & Jayashree, 2012).

Hence, bidirectional DC-DC converter can be used for measuring the performance of a chassis dynamometer because the energy produced by the drum is not dissipated as heat.

2.7 Summary

This chapter describes the different types of dynamometer and it characteristics. The introduction of chassis dynamometer with their capability has been discussed in this section for better selection of power circuit and control circuit in bidirectional chassis dynamometer design. In addition, the appropriate motor type is selected according to the capability with the design of bidirectional chassis dynamometer.

Furthermore, literature reviews are carried out on the hysteresis current control employed as the controller of current flows of bidirectional DC-DC converter. Finally, the proportional and integrated (PID) control strategy is presented to be employed as part in DC machine control strategy which is manipulating torque performance according to required tests.

The EV power management system and the topology of bidirectional DC-DC converter as energy transfer and energy storage is also presented. Half-Bridge bidirectional DC-DC Converter is suitable in for bidirectional chassis dynamometer due to the advantages discusses in this chapter. Thus, power analysis from Electric Vehicle (EV) is adapted for briefly explanations on how this bidirectional chassis dynamometer operates. The graphical form of literature review is depicted in Appendix A.

CHAPTER 3

METHODOLOGY

3.1 Introduction

This chapter presents the control design of half-bridge bidirectional DC-DC converter (HBDC) to be used on a chassis dynamometer with the capability to perform tests on EV. The road load condition of chassis dynamometer is also described. Overall system of bidirectional Chassis Dynamometer is presented in Section 3.2. The arrangement of simulation design and its parameter are described in Section 3.3. The details of HBDC topology and controller are briefly explained in Section 3.4. In Section 3.5, the simulation control strategy with Hysteresis Current Controller (HCC) and PID controller is presented. In Section 3.6, detailed of analysis of the power flow of HBDC is given.

3.2 Bidirectional Chassis Dynamometer Operating Principles

In this study, to be able to test the performance of an EV, a HBDC is designed to be used in a chassis dynamometer to operate the Vehicle Under Test (VUT). The proposed design consists of a half-bridge bidirectional DC-DC converter as the main component to perform chassis dynamometer road load condition and EV tests. In this application, two voltage source are used: 1) a DC machine (as generator) with which the EV, as VUT, is performed in inclination mode, declination mode and normal mode tests then 2) a storage (sink/source) to enable the DC machine imitate the road load condition at the drum for regenerative braking tests. Figure 3.1 and Figure 3.2 shows the chassis dynamometer in normal condition tests and in regenerative braking tests, respectively.

The bidirectional DC-DC converter structure of the proposed chassis dynamometer is based on half-bridge converter topology. The voltage source of the HBDC is supplied from a DC machine when chassis dynamometer is in normal condition (generating mode); meanwhile, when VUT is in braking mode, the HBDC changed to a power source (sink) to supply or distribute power. In PSIM simulation, the shaft of the DC machine is coupled to the shaft of the drum for the mechanical power to be measured by the chassis dynamometer, whereas the rotation of the drive wheels of EV under test is generated from the electrical energy of the battery.

In VUT motoring mode (normal or EV in driving mode), as shown in Figure 3.1, the battery of the EV supplies energy to the motor via the controller to propel the tires, which consequently rotates the drum of the bidirectional chassis dynamometer in the direction shown. In this condition, the DC machine functions as a generator as the drum is coupled to the DC machine, and the generated power is transferred through the bidirectional DC-DC converter to be stored in the power sink in the chassis dynamometer.

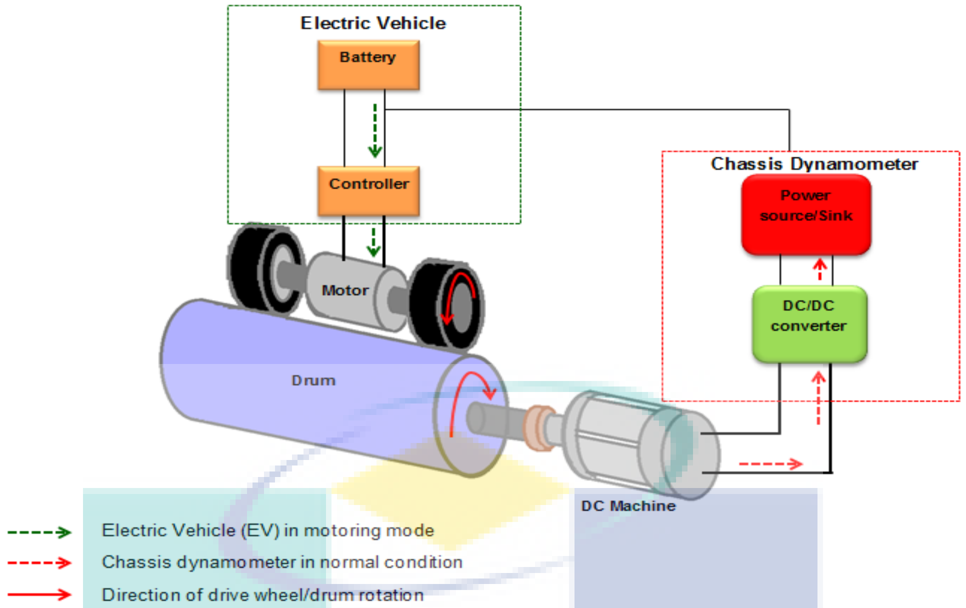

Figure 3.1 Vehicle Under Test (VUT) and Chassis dynamometer indication during normal condition

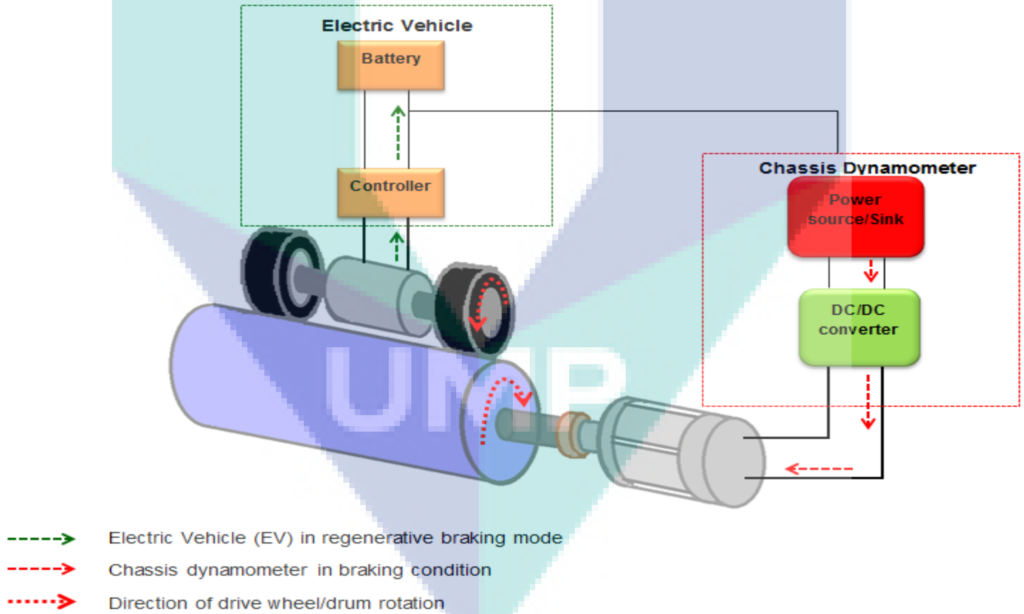

Figure 3.2 Vehicle Under Test (VUT) and Chassis dynamometer during regenerative braking condition

3.3 Simulation, Design and Parameters

The scope of the research is focusing on bidirectional chassis dynamometer with the capability of modified HCC technique in half-bridge bidirectional DC-DC converter for EV testing. Nevertheless, no hardware implementation for bidirectional chassis dynamometer in this research as simulation using PSIM is implemented. It is focuses on development of HBDC and HCC and PID controller which DC machine as output. PSIM is specifically designed for power electronics and motor control simulation. With the capability of minimum sampling time, the analysis of bidirectional DC-DC converter changes is clearly stated in PSIM simultaneously helps to confirm the PWM switching strategy (Kim et al., 2010). Consequently, the usage of dynamometer drum is neglected and unattached in this simulation because prime mover (VUT) is directly coupled to the DC machine (dynamometer) to evaluate testing performance. In this research, theoretical method is used to clarify the calculating for actual performance with dynamometer drum.

3.3.1 Bidirectional Chassis Dynamometer Sizing

Table 3.1 represent the parameters of a 2 kW DC machine and VUT, respectively. The power rating for bidirectional chassis dynamometer is set to 2 kW consequently applicable for an EV in the range of 2 kW. This rating represents the maximum capability of the bidirectional chassis dynamometer to absorbed and generated power of the testing. The parameters design is shown in Table 3.1 with similar internal parameters of DC machine and prime mover to setting of dynamometer and VUT 2 kW conveniently to PADU. Thus, the setting of moment of inertia is different because to setting the prime mover with light weight vehicle of VUT. The inertia at prime mover is less than DC machine to capable testing with bidirectional.

Figure 3.3 shows for simulation purposes; VUT is applied as a prime mover whereas the dynamometer is applied as a DC machine. The performance of the VUT is varied depending on the demands during testing mode. The demand is referred to power needs by DC machine to perform either in buck mode or boost mode to evaluate testing condition. The demanded power is different between testing because normal condition tests includes inclination, declination and steady-state test thus regenerative braking tests are evaluating VUT while driving, braking and stop. The Desired Current, I_d, is commanded to control the DC machine performance tests. When VUT performs normal condition test with inclination test, DC machine demanded a power to emulate dynamometer with inclination test. This condition implemented by the desired current, I_d in PADU to control the power demanded by DC machine to performs tests. Besides, I_d is taken from the Driver's Aid screen (displays road load condition), in which drive cycle for dynamometer testing is available.

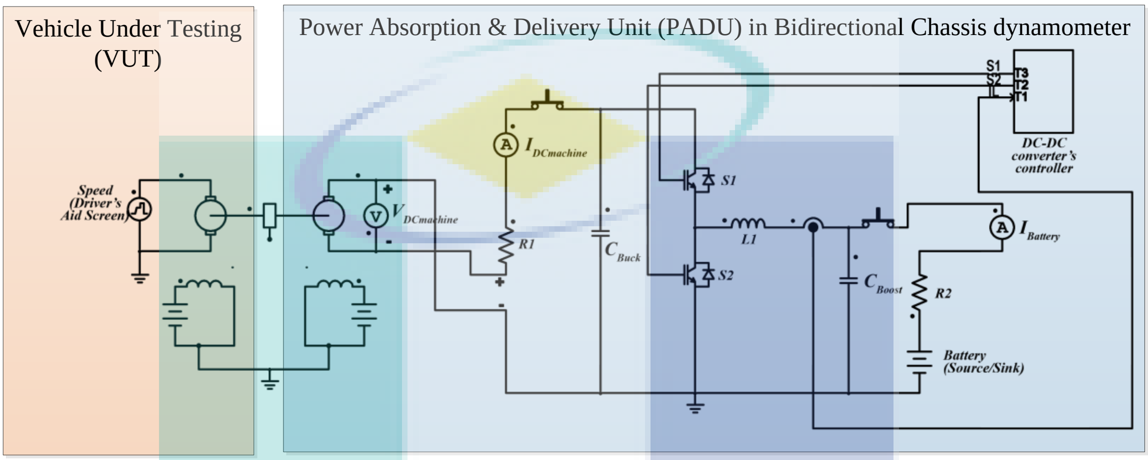

Figure 3.3 Half-bridge bidirectional DC-DC converter topology on chassis dynamometer

The current performance of buck and boost test parameters are shown in Table 3.2 and Table 3.3 respectively. The tests condition is including normal condition test and regenerative braking test. PADU voltage are defines as V_{IN} for input voltage and V_{OUT} for output voltage. At every condition PADU voltage are similar and the desired current, I_d is set according to -3.5 A to 8 A due to the capability of PADU performs with 2 kW at normal condition and -1 kW at regenerative braking. The desired current, I_d is set to 0 A until 8 A for normal condition tests therefore 0 A until -4 A for regenerative braking tests. The I_d value is setting minimum with -4 A and maximum with 8 A according to rating power for bidirectional chassis dynamometer is from -1 kW and 2 kW. From (Zhang, 2008) discussion, it should be notice that a positive current setting is given for normal condition test and negative current setting is given for regenerative braking test. Thus negative is preferable to be neglected in this application and changed as input or output according to direction flow.

Table 3.1 Parameters of Dynamometer as DC Machine and VUT as prime mover using PSIM

	PARAMETERS	DC MACHINE	PRIME MOVER (EV)
	Moment of Inertia	1 kgm^2	0.4 kgm^2
	Voltage (rated), V_t	250 V	250 V
	Speed (rated), n	1500 rpm	1500 rpm
	Resistance, R_a	0.5 Ω	0.5 Ω
Armature	Inductance, L_a	0.01 H	0.01 H
	Current (rated), I_a	10 A	10 A
	Resistance, R_f	75 Ω	75 Ω
Field	Inductance, L_f	0.02 H	0.02 H
	Current (rated), I_f	1.6 A	1.6 A

Table 3.2 Current performs buck mode in PADU for normal condition tests.

	Case	Desired Current, I_d (A)	Voltage from DC machine, $V_{dyno(e)}$ (V)	PADU Voltage, V_{IN}= V_{OUT}	Voltage from Sink/Source, V_{ss} (V)	Power at Sink/Source, P_{SS} (W)
1	Inclination	2 to 8	250	>250	0	<464
2	Declination	8 to 3	250	>250	0	>1960

Table 3.3 Current performs boost mode in PADU for regenerative braking tests.

	Case	Desired Current, I_d (A)	Voltage from DC machine, $V_{dyno(e)}$ (V)	PADU Voltage, V_{IN}= V_{OUT}	Voltage from Sink/Source, V_{ss} (V)	Power at Sink/Source, P_{SS} (W)
1	VUT drive	-3.5	0	>200	200	835
2	VUT brake	-3.5 to 0	0	>200	200	835 to 70
3	VUT stop	0	0	>200	200	0

3.3.2 Driving Resistance Sizing

Chassis dynamometer drum is an important part in the design of chassis dynamometer as the performance of a VUT can be determined through the rotation of the drum. The DC machine parameter is set near to 2 kW to test the vehicle (EV). Throughout the research, DC machine is employed to supply or absorb energy from bidirectional DC-DC converter in investigating the performance of bidirectional power flow in both directions.

A chassis dynamometer operates by absorbing the output power produces by an engine of a vehicle test to be transferred to a DC machine that acts as a load. In many chassis dynamometer applications, such as eddy current, hydraulic and AC generator, the power absorbed by the drum is usually dissipated as heat. The performance of a VUT can be measured through simultaneous operation of load variation and parameter measurement. Load variation refers to the process of manipulating dynamometer drum's inertia to emulate road load condition, while parameter measurement is associated with the power, torque and speed measurements using various sensors, normally installed at the load cell. Chassis dynamometer implicates an absorbing power output from the VUT allow different loads to be applied on drum for various testing procedures (Bennetts, 2002).

However, conventional chassis dynamometer is focused on measuring power delivered by vehicle that is dependent on road condition. Several chassis dynamometer that could emulate the physical system configuration, inertia and friction calibration techniques, and control software have been developed; the driving resistance VUT and chassis dynamometer rules are detailed in this section.

The direction of force applied during chassis dynamometer testing is illustrated in Figure 3.4. The inertia from the vehicle and the force on the chassis dynamometer assist in the emulation of actual road load condition on the drum of the chassis dynamometer. As different vehicles have different mass, inertia simulation must be employed to provide realistic loading during transient proceedings (Matthews et al., 2009).

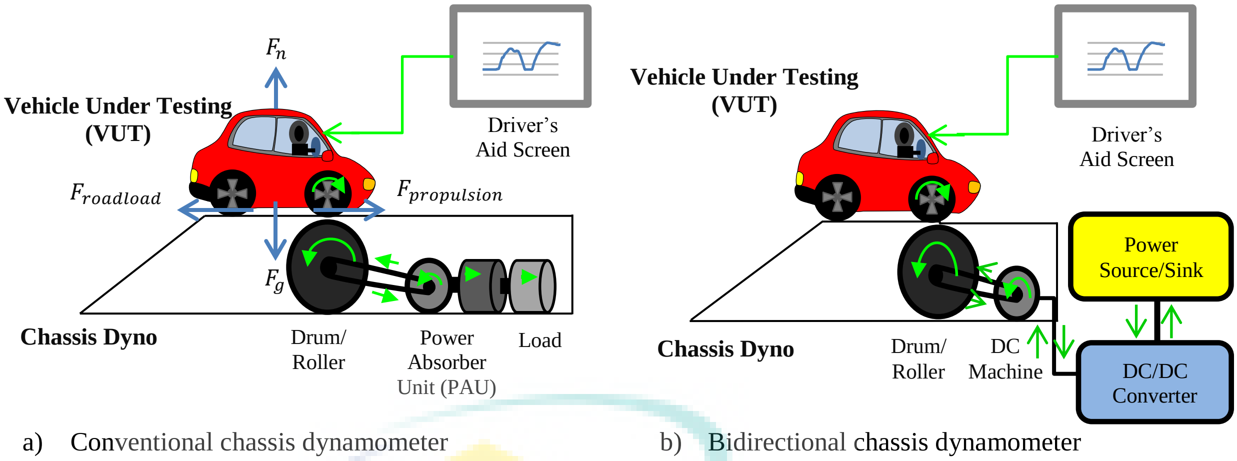

Figure 3.4 Comparison between conventional and bidirectional chassis dynamometer

The force acting on the vehicle can be calculated using Equation 3.1 and Equation 3.2, where m_{car} is the weight of the vehicle to be calculated, with acceleration and gravitational forces taken into account. The gravitational force is equal to the net force is as expressed in Equation 3.3 because the directions of the two forces are in parallel.

$$F_{car} = m_{car}a \tag{3.1}$$

$$F_g = m_{car}g \tag{3.2}$$

$$F_n = F_g \tag{3.3}$$

Equation 3.4 expresses the frictional force, $F_{roadload}$, in which its direction is opposite to the applied force as shown in Figure 3.4. Frictional force is due to the traction of the vehicle, while applied force is due to the propulsion of the vehicle.

$$F_{roadload} = \mu F_n \tag{3.4}$$

Since $F_{roadload}$ is derived based on frictional force, the values for vehicle force, F_{car}, or applied force, $F_{propulsion}$, can be defined using Equation 3.5.

$$F_{car} = F_{propulsion} - F_{roadload} \tag{3.5}$$

Based on equations above, the total road-load of the vehicle is calculated using Equation 3.6, and the road condition emulated by the wheels is then delivered to the chassis dynamometer. Torque is generated to provide realistic load and consists of forces that are constants, F_c, or dependent on acceleration, F_a, or vehicle velocity, F_v. The total force applied on the wheels is calculated as in Equation 3.7.

$$F_w = F_a + F_v + F_c \tag{3.6}$$

$$F_v = A_v + Bv + Cv^2 \tag{3.7}$$

The acceleration force can be expressed as $F_a = m_{car}\frac{dv}{dt}$, and the constant force $F_c = A_c$. Setting, $A = A_c + A_v$ (Matthews et al., 2009), the total load can be expressed as:

$$F_{total(load)} = A + Bv + Cv^2 + m_{car}\frac{dv}{dt} \tag{3.8}$$

The chassis dynamometer emulates the total road load to make vehicle experiences road condition, and consequently power performance of the vehicle can be measured. The instantaneous dynamometer power is defined as in Equation 3.9.

$$P = \tau\omega = F.v \tag{3.9}$$

where P is the power produced by the vehicle and τ is the associated torque. The power required must be considered to determine how much torque should be added when conducting the test (Jirawattanasomkul & Koetniyom, 2000). From Equation 3.10 and Equation 3.11, the parameters of chassis dynamometer, including drum radius, distance of load cell and moment of inertia, can be determined from the structure, while angular frequency, ω and force, F is obtained from measurement method.

$$P_{propulsion} = \left(m \times \frac{\partial(V)}{\partial t} + F_{roadload}\right) \times v \tag{3.10}$$

$$P_{dyno} = F_{total(load)} \times V_{dyno} \tag{3.11}$$

3.4 Power Electronics Design

The topology of half-bridge bidirectional chassis dynamometer is illustrated in Figure 3.5 that consists of half-bridge topology to perform as bidirectional DC-DC converter, with which the DC machine absorbs and delivers power and the prime mover acts as the vehicle under test (VUT). The system is classified as VUT that is performs road load condition and DC machine as dynamometer which absorbed and delivered power through PADU to be stored. The testing performances are evaluated at PADU power analysis. The analysis of power flow direction shows either normal condition tests or regenerative braking tests.

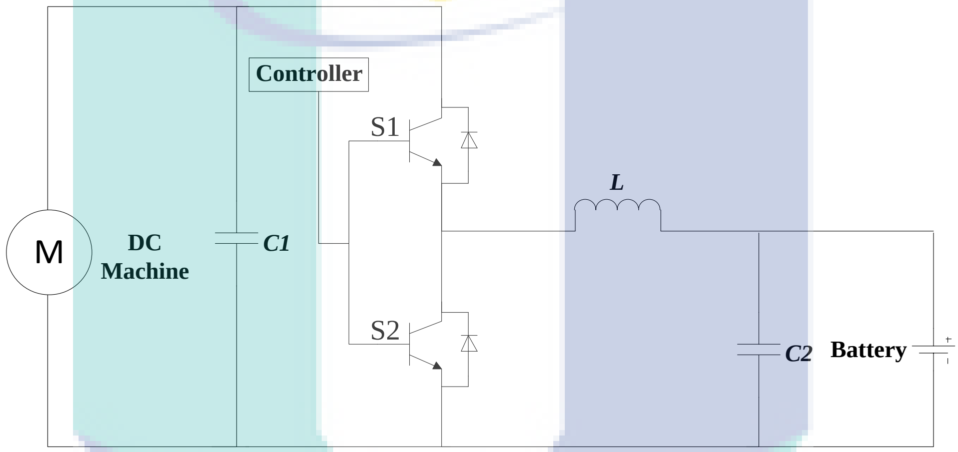

Figure 3.5 Half-bridge bidirectional DC-DC converter topology.

3.4.1 Topology and Parameter of Bidirectional DC-DC Converter

The circuit of bidirectional DC-DC converter uses the half-bridge topology as shown in Figure 3.5, which commonly includes a buck switch, *S1* and a boost switch, *S2*. The HBDC with non-isolated structure is implemented in buck and boost modes to operate bidirectional power flow. In this study, bidirectional capability of the system has been proven as energy is transferred from the DC machine to the storage in motoring mode, while the reverse is true in braking mode. The current that flows in the circuit is shaped by the switching actions of switch *S1* and *S2*, controlled by current controller. Table 3.4 shows parameter in HBDC to indicate the system operated bidirectional. The values of V_{in} and V_{out} in Table 3.4 is originated from the converter topology in Figure 3.5. The parameter used show both V_{in} and V_{out} as input during buck mode or boost mode.

Certainly, during buck mode, V_{in} is defined as input voltage with 96 V. However, during boost mode, V_{out} is operated as input voltage and set with 30V.

Table 3.4 Parameter of HBDC using PSIM for buck and boost mode.

Parameter	Value
Input Voltage, V_{in} (buck mode)	96 V
Input Voltage, V_{out} (boost mode)	30 V
Capacitor, *C1* & *C2*	470 µF
Inductor, *L*	1367 mH

To accomplish bidirectional energy flow, the arrangement of buck mode condition and boost mode condition during operation is shown in Figure 3.6, in which the operation of bidirectional power flow involved four sub-intervals. Initially, the operation starts with the input voltage, V_{IN} as supply and the operation is in buck mode in Interval I and Interval II. As shown in Figure 3.6 (a), in Interval I, switch *S1* is activated while *S2* is in inactive mode. The circuit currently transfers energy from V_{IN} to the output voltage that causes the output voltage V_{OUT} to be reduced. However, in Interval II, as depicted in Figure 3.6 (b), *S1* and *S2* are both turned *"off"*, thus current flows through diode *D2*, which is in parallel with *S2*.

Then, the half-bridge bidirectional DC-DC converter is operated in boost mode during interval III and IV; during this intervals power flow_from V_{OUT} to V_{IN}, which is the reverse of that in buck mode. As shown in Figure 3.6(c), in Interval III, power flows in the circuit as *S2* is activated while *S1* is inactive. Thus, V_{OUT} starts to supply energy through *S2* which is then absorbed by V_{IN}. Then, in Interval IV, both *S1* and *S2* are deactivated, the operation is similar to that in Interval II but energy flows in the opposite direction.

Half-bridge topology is preferred in PADU because the fact that the power devices (IGBT switches) function in complementary mode and have bidirectional load and source half-bridge converter certainly not operates in discontinuous conduction mode (Al-sheikh et al., 2014). Certainly, half-bridge topology function by pairing means when *S1* is "*on*", *S2* is "*off*" and vice versa simultaneously reducing current peaks as well as stress on components. Since current and switches stress are lower, the efficiency of half-bridge topology is better than full-bridge topology (Du et al., 2010). Therefore previous finding (Elankurisil & Dash, 2012) and (Park & Song, 2011) shows that losses occurs more due to the operation of four switches of full-bridge meanwhile half-bridge topology reduces switching losses due to minimize of switches usage.

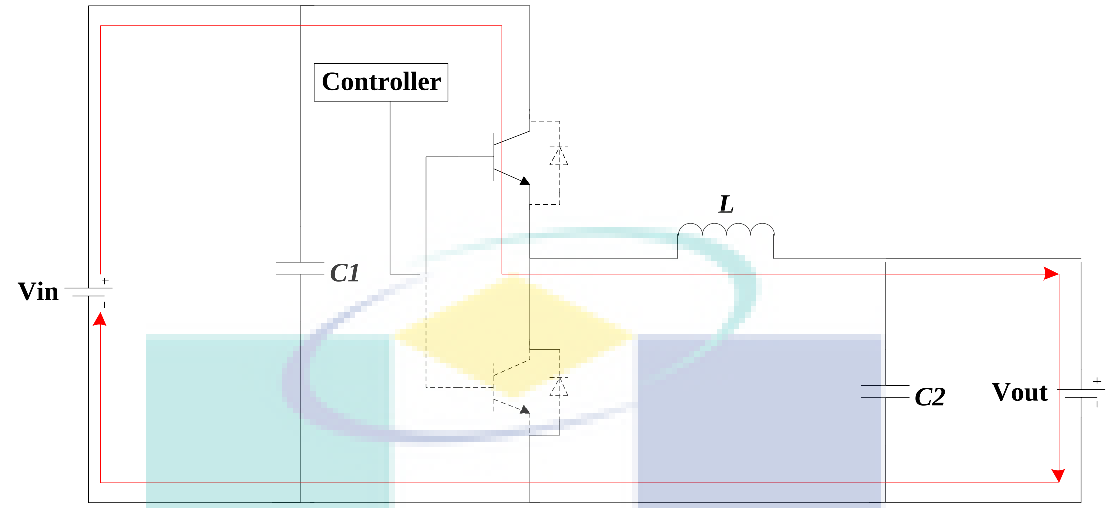

(a) Interval I (buck mode)

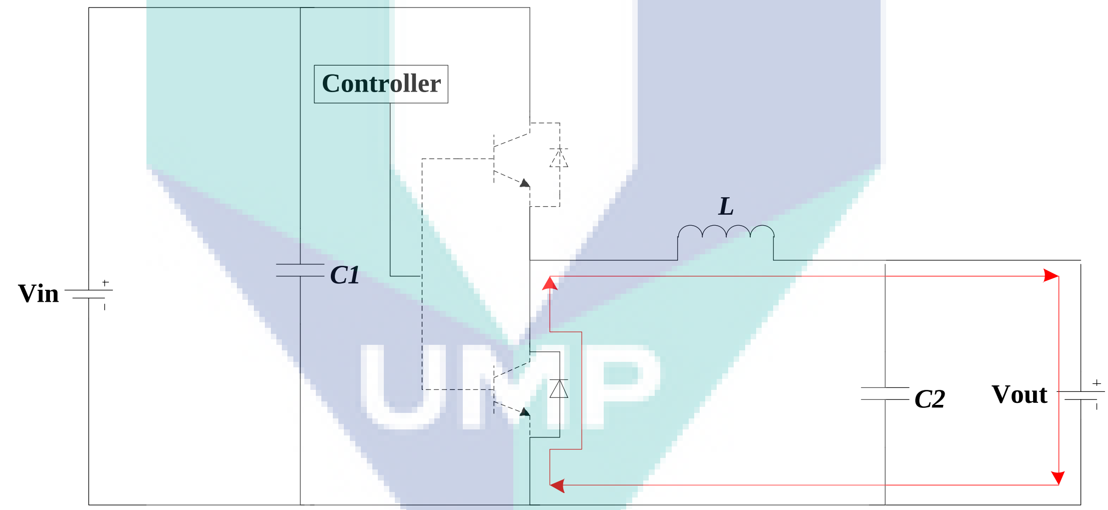

(b) Interval II (buck mode)

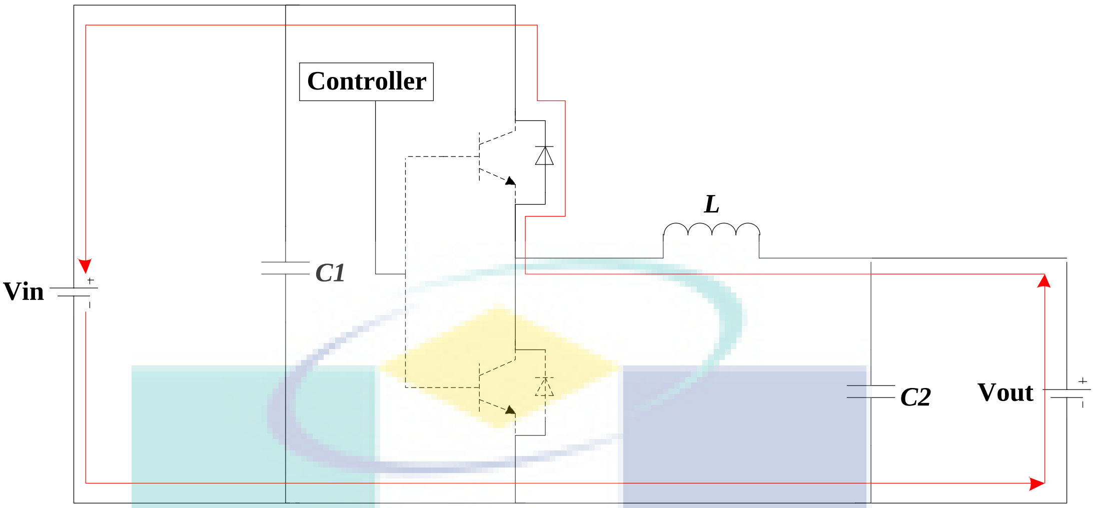

(c) Interval III (boost mode)

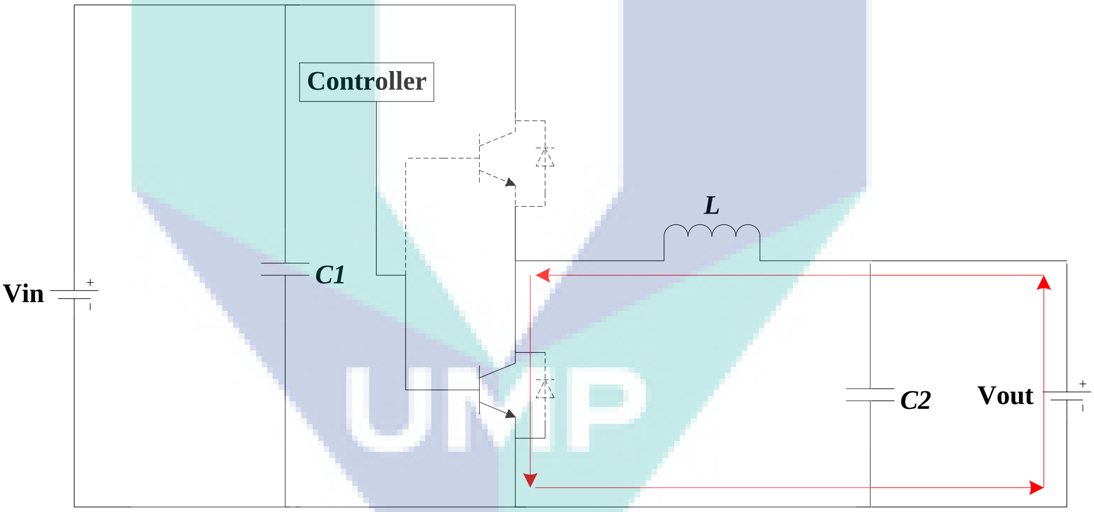

(d) Interval IV (boost mode)

Figure 3.6 Operation principle of Half-bridge bidirectional DC-DC converter with current flow.

3.5 Control Strategy

Control strategy for bidirectional chassis dynamometer consists of inner loop control and outer loop control. The outer loop is the control of speed and torque of the DC machine, while the inner loop is the control of current during power flow in bidirectional DC-DC converter operation.

3.5.1 Outer Loop: Proportional, Integrated & Derivatives (PID) Control

Figure 3.7 shows the block diagram of the Half-Bridge Bidirectional DC-DC Converter's (HBDC) as outer loop that is used to manipulate the internal torque of the DC machine during road load condition. It can result the reference current, I_{ref} of HBDC to switching in normal condition tests or regenerative braking tests. Thus, desired current, I_d is applied to perform the testing capability within -4 A to 8 A current. The PID controller is employed to control the actual value from internal torque as required by the testing condition. The result from PID signal is then transferred to the inner loop of this system. The speed at DC machine is operated according torque performance as speed and torque relation curve in Figure 3.8.

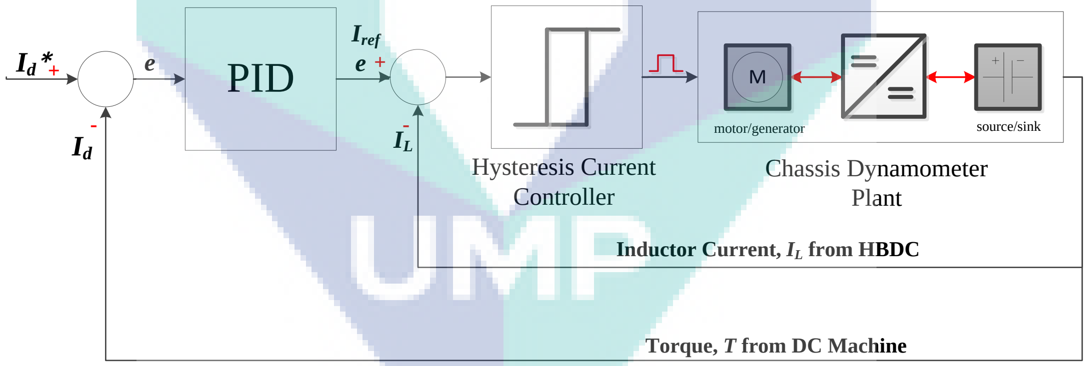

Figure 3.7 Block diagram of outer loop of half-bridge bidirectional DC-DC converter

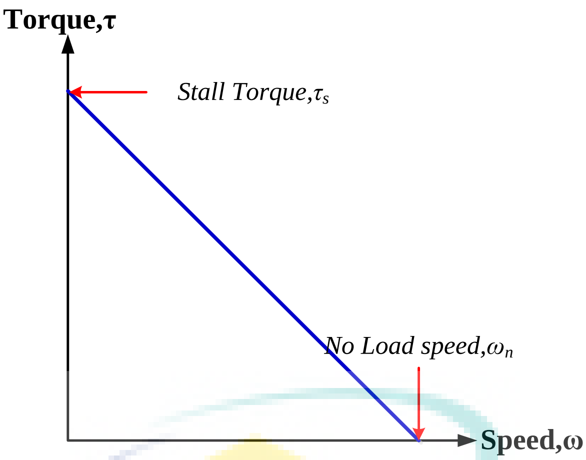

Figure 3.8 DC Motor Torque and Speed Curve

To tune the coefficients of the PID controller for the DC machine, the Zeigler-Nichols is applied with the plants exhibits the response curve in Figure 3.9. The response curve is the first order system with transportation delay. There are two parameters in response curve with delay time, L and time constant, T. These parameters are determined by a tangent line at inflection point in response curve and noting its intersections with the time axis and the steady state value. Therefore the plant model is expressed in Equation 3.12 (Joshi, 2013).

$$G(s) = \frac{Ke^{-sL}}{Ts+L} \tag{3.12}$$

$$K_I = \frac{K_P}{T_I} \tag{3.13}$$

$$K_D = K_P \times T_I \tag{3.14}$$

The parameters of PID controller of the approximate model can be carried out from experiments. Table 3.5 explains Ziegler-Nichols tuning method to define the response curve of the system. As K_P is presents from Table 3.5, accordingly parameter K_I and K_D can be found out using Equation 3.13 and Equation 3.14. Based on the response curve, the PID parameters for PADU are tabulated in Table 3.6.

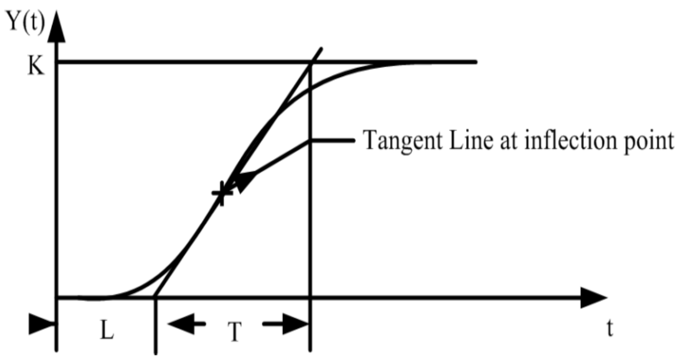

Figure 3.9 Response curve for Zeigler-Nichols parameters

Table 3.5 Ziegler-Nichols tuning method

Controller type	K_P	T_i	T_d
P	T/L		
PI	0.9T/L	L/0.3	
PID	1.2T/L	2L	0.5L

Table 3.6 Tuned PID coefficients for HBDC

$\mathbf{K_P}$	1.2
$\mathbf{K_I}$	0.0045
$\mathbf{K_D}$	0.005

3.5.2 Inner Loop: Hysteresis Current Control

Figure 3.10 depicts the block diagram of the inner loop of the hysteresis current controller that controls the direction of current flow in the bidirectional chassis dynamometer, either from the DC machine to the storage (source/sink) or from the storage to the DC machine. The switching in the HCC uses the half-bridge topology, in conjunction with switch *S1* and switch *S2*.

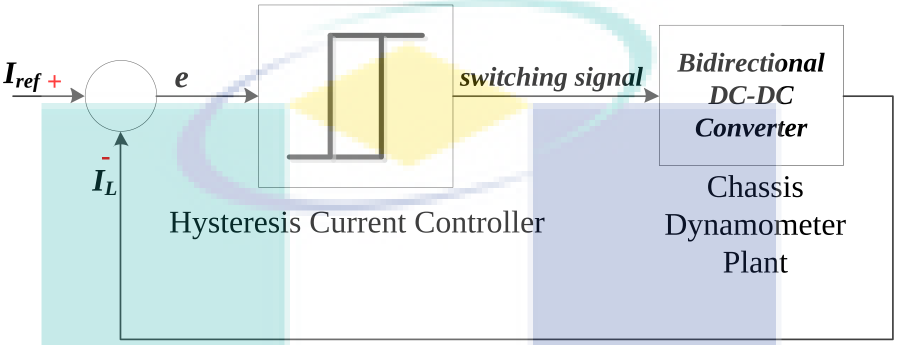

Figure 3.10 Block diagram of inner loop of hysteresis current controller

The main function of the HCC in bidirectional DC-DC converter is to enable the energy storage to sink the power from DC machine operating in generator mode, and for the storage to supply power to the DC machine when the machine is operating in motoring mode. This shows that the HBDC is capable of bidirectional power transfer. However, to reduce losses during conduction and switching, modification has been made to the original HCC.

As shown in Figure 3.11, in the positive region of the hysteresis band, the DC machine operates in generative mode, which imitate inclination/uphill, normal or declination/downhill road load conditions. Meanwhile, in the negative region of the band, the machine operates in motoring mode to move the drum in the dynamometer, during which the driver use the brake to decreases the rpm of the drum; this mode let the machine imitates actual road condition when going downhill.

In the operation of the bidirectional chassis dynamometer, the HCC compares the inductor current I_L from the HBDC with the reference current I_{ref} obtained from the PID. As shown in Figure 3.11, I_{ref} is centred within a hysteresis band that lies between $I_{ref(+)}$ (upper limit) and $I_{ref(-)}$ (lower limit). When I_L is bigger than I_{ref}, the converter operates in buck mode, but it operates in boost mode when I_L is smaller than I_{ref}. Also, when I_L is bigger than $I_{ref(+)}$ or lower than $I_{ref(-)}$, the hysteresis controller limits and switches the direction of the inductor current so that the inductor current stays withi n the specified band. A PWM switching signal obtained from the limiting and switching actions is sent to switches *S1* and *S2* in the bidirectional DC-DC converter to produce the inductor current, I_L. Consequently, for buck mode switch *S1* is *"on"* and switch *S2* is *"off"* when the inductor current triggered from negative band to positive band inside the envelope of hysteresis band. While boost mode, switch *S1* is *"off"* and switch *S2* is *"on"* and the inductor current flow from the positive band to the negative band of the hysteresis envelope. Also, the dynamometer is in generative mode when the inductor current is in the positive region of the hysteresis band, while regenerating mode happens when the inductor current is in the negative region of the hysteresis band.

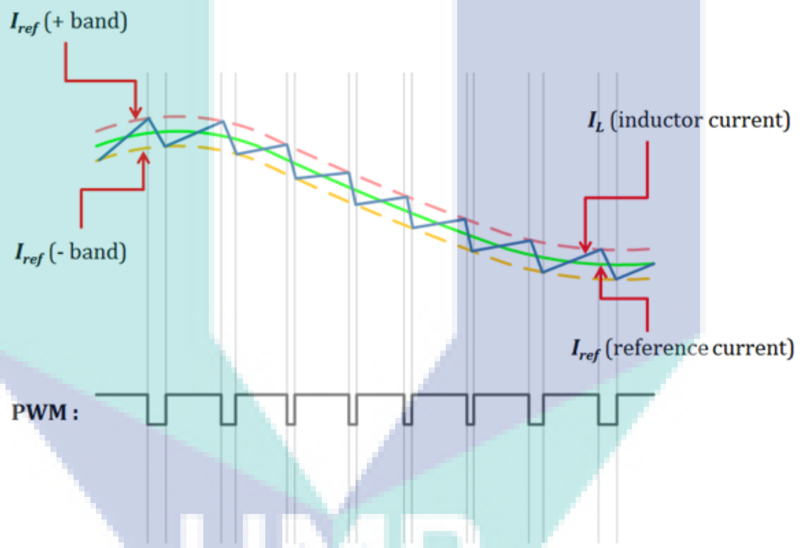

Figure 3.11 Hysteresis Current Control sequence

With the conventional logic control of HCC, some issues are encountered during zero crossing, the transition of the inductor current from the positive region to the negative region of the hysteresis band, and vice versa. Essentially, the issue is including increases of power losses effects from inductor current ripple during zero crossing. Concurrently, the increasing of switching frequency can cause increase of the heat and damage to the switching device (Hong et al., 2014). To enhance the performance of the logic control during conduction and switching, this study proposed to implement a new logic control for the HCC, which is a modification of the original circuit. The proposed circuit would reduce losses in the bidirectional chassis dynamometer.

3.5.3 Modified Hysteresis Current Control

Figure 3.12 shows a conventional logic control of a hysteresis current control in HBDC using two comparators. In both figures, the negative terminals of the comparator are connected to the reference current I_{ref} in order to construct the hysteresis band, while the positive terminals are connected to the inductor current I_L. The outputs from the comparators are fed to a S-R flip-flop. The inductor current originates from inductor *L1* of HBDC, while *S1* and *S2* are the switching signal used to activate the associated switching devices (Yao et al., 2009); the switches are operated in generating mode during positive I_{ref} and regenerative mode during negative I_{ref}.

In this study, a modification of the former circuit was done, as shown in Figure 3.13. The basic operation of this modified logic control is similar to that of the conventional circuit. However, in conjunction with the output from comparator 3, the output from the S-R flip-flop are used to activate the AND gate and the OR gate to generate signals *S1* and *S2*. With the circuit, the transition between buck mode and boost mode and vice versa becomes zero, which consequently reduce losses during switching.

In spite of the advantages offered by HBDC, further research is needed to improve the performance and overall control and management of the hysteresis current control. In addition, to improve the performance of hysteresis current control, further study on the various techniques to produce the hysteresis band is needed. The switching signal rules of the hysteresis current control are shown in Table 3.7.

Table 3.7 Switching Signal Rules

Mode	**Switch (S1)**	**Switch (S2)**	**Inductor Current (I_L)**
Buck Mode	ON	OFF	Increasing
Buck Mode	OFF	OFF	Decreasing
Boost Mode	OFF	ON	Decreasing
Boost Mode	OFF	OFF	Increasing

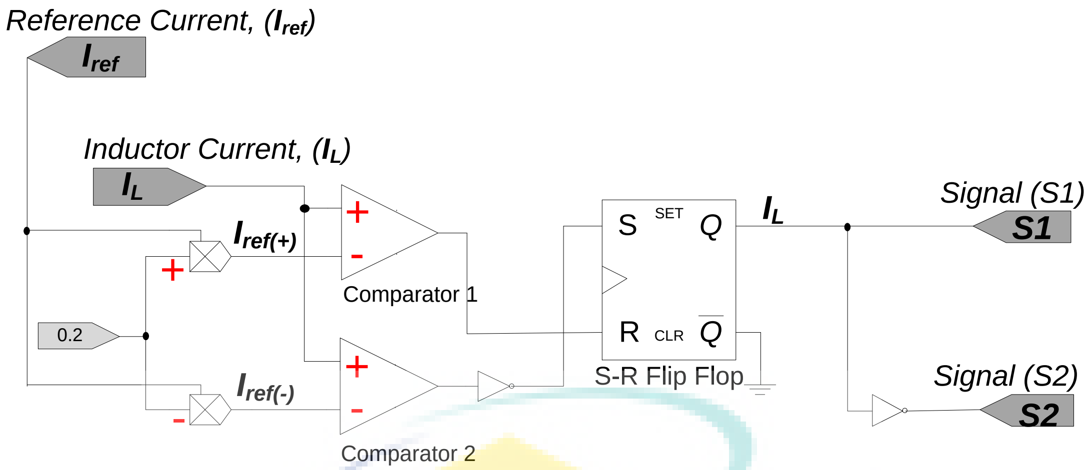

Figure 3.12 Conventional logic control of Hysteresis Current Controller in HBDC

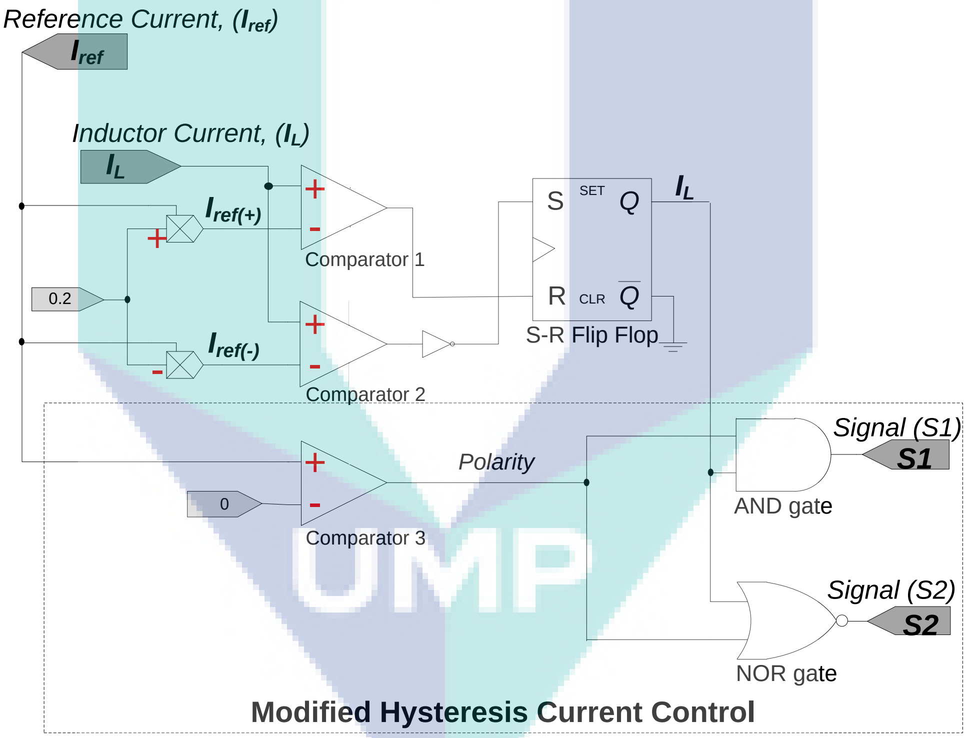

Figure 3.13 Proposed logic control of Hysteresis Current Controller in HBDC

3.6 Power Flow Design

Figure 3.14 shows the power management (power flow) and the timing diagrams applied to the bidirectional chassis dynamometer during VUT. Road load condition is the reference for the driver to perform on the vehicle while VUT. Road load condition is a situation during which the driver experiences driving resistance, like when the vehicle is going uphill (inclined condition), going downhill (declined condition) or when the road surface is flat (normal condition). The road load condition in chassis dynamometer is similar to real on road condition.

The different speeds and torques of the DC machine is controlled to make the machine emulate the road load condition, which is used to control the operation of the bidirectional chassis dynamometer. This is to facilitate the measurements be conducted on the VUT, whether it is in incline condition, decline condition, steady condition or during braking. The next section explains the speed and torque control of the bidirectional chassis dynamometer.

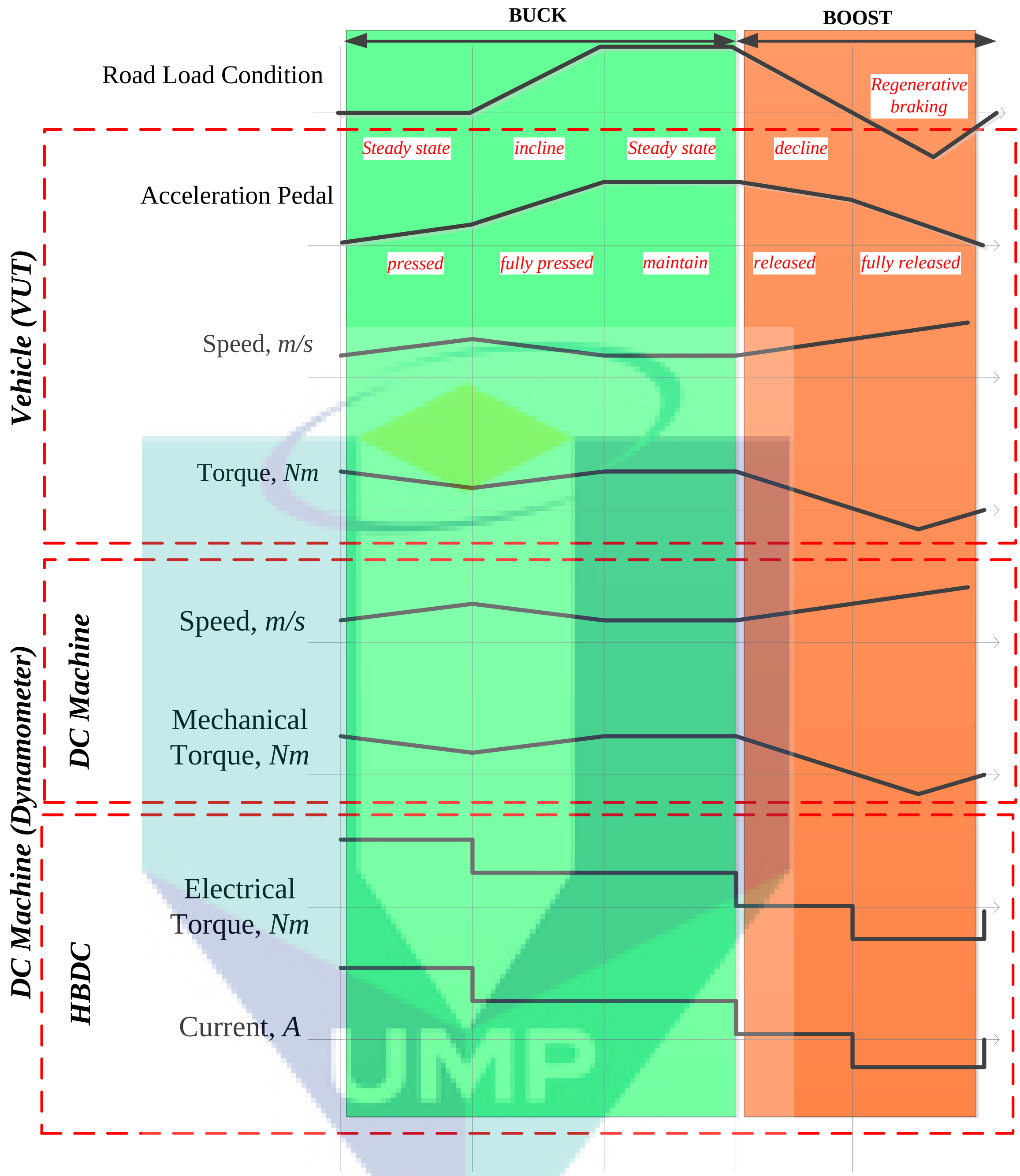

Figure 3.14 Timing diagram of bidirectional chassis dynamometer during VUT

3.6.1 Mode 1: Normal Condition Mode (Normal & Inclination)

Figure 3.14 shows the power management of bidirectional chassis dynamometer, such as speed, mechanical torque, internal torque and current from DC machine. In Mode 1, when the DC machine is in generative mode and the DC-DC converter is in buck mode, power is transferred from the DC machine to the energy storage medium. In buck mode operation, the acceleration pedal of the VUT is pressed, which causes speed to increase and mechanical torque to decrease. The acceleration pedal affects the road load condition, whether it is in normal mode or inclination mode. Inclination mode occurs when the acceleration pedal is fully pressed and VUT experiences uphill condition, while normal mode happens when the acceleration pedal is maintained in a constant condition, during which the propulsion of the VUT imitated normal road load condition.

From the Figure 3.14, it is observed that the rotating dynamometer drum affects the speed and mechanical torque of the VUT, which shows that the performance of the dynamometer can represent that of the DC machine and the speed and mechanical torque are measured from the dynamometer drum. The drum emulates the VUT, while the DC machine acts as a generator. The DC machine supplies power to the DC-DC converter to be stored in the sink (source). The DC-DC converter controlled the modes of the road load conditions. From the results obtained, it should be noted that in buck mode, current is positive in polarity and high in magnitude when the pedal is fully pressed. Also, high current is required when VUT is experiencing uphill road condition, which causes the dynamometer more difficult to rotate.

3.6.2 Mode 2: Regenerative Braking Mode

Regenerative braking mode is a condition that represents VUT is braking, when the acceleration pedal is released that causes the DC-DC converter to trigger a signal to the dynamometer to operate in boost mode. In this mode, the DC machine acts as a motor and obtain its power from the sink (source). The effect on the dynamometer is that the speed of the VUT is reduced and its mechanical torque is increased as it get easier to turn the drum. In this situation, the driver will reduce the speed by releasing the acceleration pedal, while simultaneously pressing the brake pedal; for EV application, this is called as regenerative braking.

From the results, it was also found that the speed and internal torque of the dynamometer resemble that of the VUT, as how the VUT would have performed in real road load situations. Moreover, on releasing the acceleration pedal, the DC-DC converter is in boost mode that causes the current to flow from the sink (source) to the DC machine, which consequently turns the drum faster as if the VUT is going downhill. In this mode, regenerative braking tests can be performed on the EV.

3.6.3 Power Loss

The power transfer of bidirectional chassis dynamometer performance is translated in Figure 3.14 and Figure 3.16. The performance of DC machine during normal condition and VUT during regenerative braking is stated.

However, no hardware implementation is carried out for bidirectional chassis dynamometer in the research as simulation using PSIM is implemented, and consequently, the usage of dynamometer drum is neglected. Moreover, the dynamometer drum is not attached in this simulation method because prime mover (VUT) is directly coupled to the DC machine when the performance of the bidirectional chassis dynamometer is evaluated. For dynamometer drum force, theoretical method is used in calculating the actual performance of conventional chassis dynamometer. Thus, conduction losses and switching losses is highlighted in power electronics part.

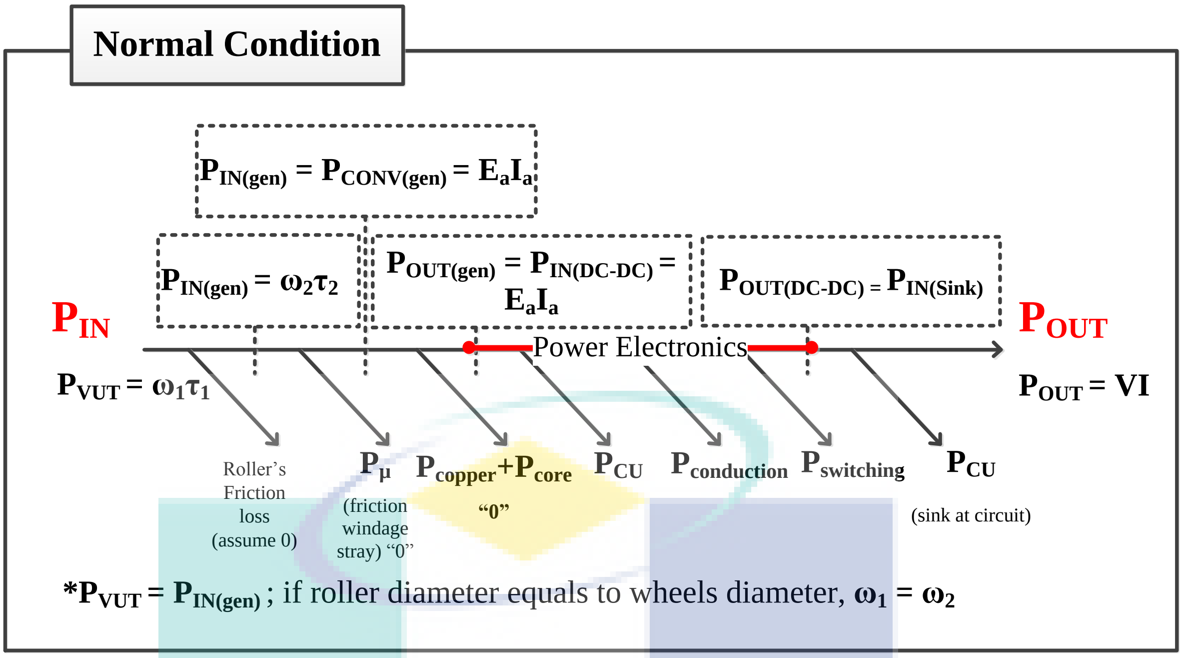

Figure 3.15 Power flow of bidirectional chassis dynamometer during normal mode

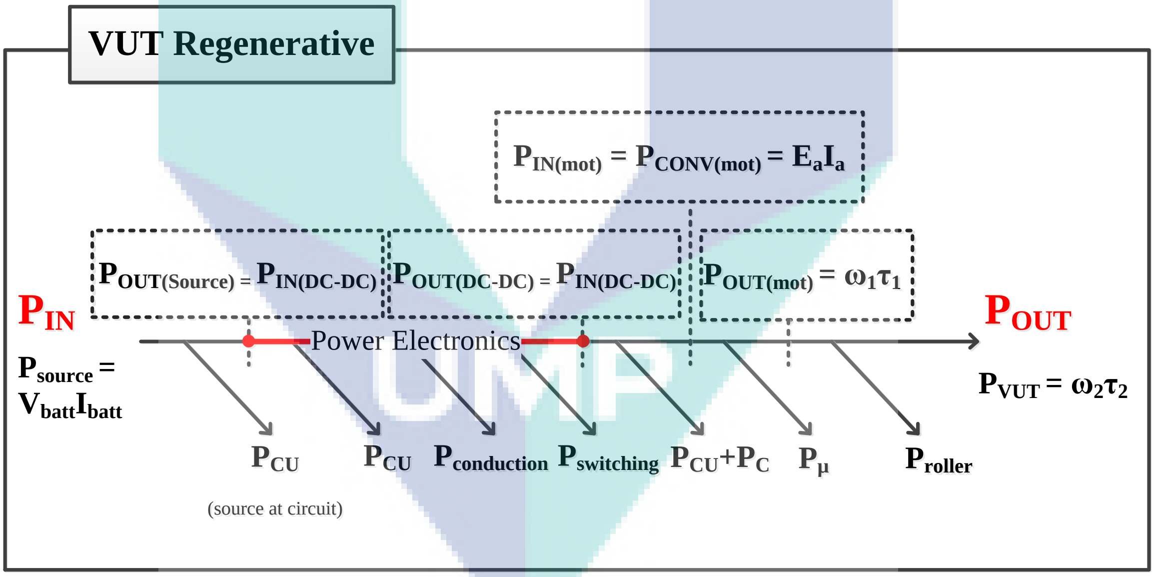

Figure 3.16 Power flow of bidirectional chassis dynamometer of VUT during regenerative braking mode

From previous discussion, (Piris-Botalla et al., 2014) mention that, the power losses analysis includes those produced by the auxiliary circuit and evaluated considering to the DC voltages of the power supplies constant. The occurrence of losses in a switching device can be classified in three types: off-state, conduction and switching losses. (Ghasem Hosseini et al., 2005) mention that the leakage current during the off-state is negligibly small; therefore the power losses during this state can be neglected. As a result in converter model only conduction losses and switching losses are calculated.

The expression of power losses are obtained considering both conduction and switching losses produced from DC machine. The IGBT power losses are evaluated as function of the gate threshold voltage during switching transitions. The conduction losses are evaluated for each IGBT according to its current waveform and conduction interval (Piris-Botalla et al., 2014). The conduction power losses of the IGBT can be determined as functions of the rms current and its on-state equivalent resistance, Rds_{on}, and the diode calculation losses can be calculated using Equation 3.16 where $V_{F(ix)}$ defines the diode forward voltage as a function of current flowing through it. Finally, Equation 3.17 expressed the total conduction losses in IGBT devices.

$$P_{cTx} = \left(\sqrt{\frac{1}{2\pi}\int_{\gamma_1}^{\gamma_2} i_x^2 \, d\theta}\right)^2 Rds_{on} \tag{3.15}$$

$$P_{cDx} = \frac{1}{2\pi}\int_{\gamma_1}^{\gamma_2}\left(-V_{F(i_x)} i_x\right) d\theta \tag{3.16}$$

$$P_{cx} = 2(P_{cTx} + P_{cDx}) \tag{3.17}$$

Both expressions in Equation 3.18 and Equation 3.19 are evaluating the energies dissipated at the turn-off and turn-on switching transitions whereas functions of the instantaneous current at the switching angle. Therefore, t_{ri-on} is the rising current time, t_{fv-on} is the falling voltage time, t_{rv-off} is the rising voltage and t_{fi-off} is the falling current time which can obtain using the information provided by datasheet.

$$E_{off(i_x)} = \frac{1}{2} V_x |i_x| \left(t_{ri-on} + t_{fv-on}\right) \tag{3.18}$$

$$E_{on(i_x)} = \frac{1}{2} V_x |i_x| \left(t_{rv-off} + t_{fi-off}\right) \quad (3.19)$$

Thus, Equation 3.20 and Equation 3.21 determine the turn-off power losses and the turn-on power losses. The total losses on switches is express in Equation 3.23 where P_{swx} defines as P_{onTx} or P_{offTx} depends on switch operation under dissipative or natural switching mode with turn-on or turn-off, respectively.

$$P_{offTx} = E_{off(ix)} f_{sw} \quad (3.20)$$

$$P_{onTx} = E_{on(ix)} f_{sw} \quad (3.21)$$

$$P_{Dxoff} = V_x Q_f f_{sw} k_v \quad (3.22)$$

$$P_{tswx} = P_{cx} + 2(P_{swx} + P_{Dxoff}) \quad (3.23)$$

In this research, the losses encounter in HBDC is directly measured using PSIM simulation. Figure 3.17 shows the IGBT Module with HBDC topology, with DC machine as input supply, gating signal from controller and four extra nodes on the top. These four nodes are for the power losses, and they are (from left to right): (1) transistor conduction losses P_{Q_cond}, (2) transistor switching losses P_{Q_sw}, (3) diode conduction losses P_{D_cond}, and (4) diode switching losses P_{D_sw}. These losses are for the whole IGBT module where these are in the form of electric currents, and will flow out of these nodes. Measurement for losses values, ammeter is attached to each node (Tech, 2014).

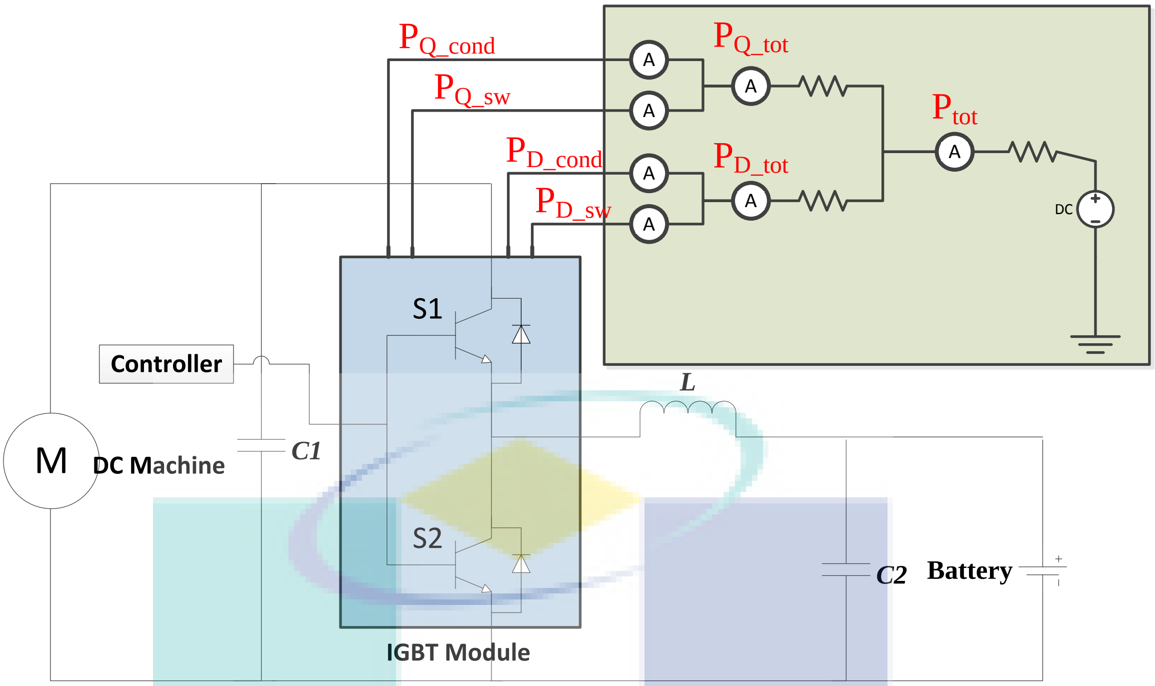

Figure 3.17 The HBDC circuit for the loss calculation of bidirectional chassis dynamometer using PSIM

3.7 Summary

This chapter explains the proposed method implemented in the bidirectional chassis dynamometer, and the vehicle parameter for the overall operation of the dynamometer. Also, a DC machine is used as chassis dynamometer and a motor as a prime mover to imitate the behaviour of the vehicle. The power flow of the DC machine as generator (motor) is presented.

A hysteresis current controller, used as the main controller in the study, is proposed. The modified HCC produces a switching signal to the half-bridge bidirectional DC-DC converter. To control the circuit operation, the modified HCC is designed to operate in buck mode during normal condition and regenerative braking condition. Moreover, for measuring torque and speed emulated from the prime mover, the PID controller is implemented in the bidirectional chassis dynamometer. Lastly, the derived current, torque and speed have been presented in order to explain operation principle of the bidirectional power flow.

With the half-bridge topology, the bidirectional power flow is capable to perform with minimum switching device. Thus, with the different power flow, the testing occurs in bidirectional chassis dynamometer can be analyses. During Buck mode, normal condition tests are conducted with inclination, declination and steady state test. However, for the opposite direction, regenerative braking tests with VUT in driving, VUT in braking and VUT while stopping test can be evaluated.

The power of bidirectional DC-DC Converter is analyses from the occurrences of testing condition. The power transfer is analyses to prove that the capability of bidirectional chassis dynamometer from the testing. It also includes the power losses encounter during testing occurs. The switching losses and conduction losses are conducted to evaluate the different performance of conventional HCC and modified HCC.

CHAPTER 4

RESULTS AND DISCUSSION

4.1 Introduction

This chapter analyses the performance of a 2 kW bidirectional chassis dynamometer operating in conjunction with the proposed Half-Bridge Bidirectional DC-DC Converter (HBDC) controlled by a hysteresis current controller (HCC) and PID controller. The proposed bidirectional DC-DC converter is used to control energy transfer from VUT and to control energy produced from storage (sink/source). The 2 kW of power is transferred from the DC machine to the storage (sink/source) by Power Absorption and Delivery Unit (PADU) during buck mode. Meanwhile, boost mode is applied to transfer 1 kW of power from storage (sink/source) to execute the DC machine. This chapter also describes the control strategy of HCC and PID in HBDC; the HCC is controlling current performance and PID is capable to manipulating the torque of the DC machine. In addition, results of power transfer are obtained from normal condition tests and regenerative braking tests are documented in this chapter.

4.2 Hysteresis Current Controller (HCC)

As mentioned in Chapter 3, the modified hysteresis current control (HCC) was applied and has been compared to the conventional HCC. The results obtained from the modified and the conventional HCC is compared in this section. To control current in PADU, I_L and I_d are used as sensing points to indicate bidirectional current flow. The comparison of the HCCs shows the differences in the switching signals at *S1* and *S2*, zero transition, switching losses and conduction losses.

4.2.1 HCC Switching

Comparison of the conventional HCC with the proposed modified HCC is conducted to show the mode transition at zero crossing. The results of the simulation, such as HCC current flow, conduction losses and switching losses, are discussed in this section. In the bidirectional DC-DC converter, the mode transition from charging mode to discharging mode is needed in EV application, and according to (Hasan et al., 2008), improper control of storage charging and discharging will affect the battery's lifetime. Different block diagram arrangements are used to simulate the conventional HCC and the modified HCC.

The switching signals *S1* of IGBT 1 and *S2* of IGBT 2 in PADU for the conventional HCC and the proposed modified HCC are respectively shown in Figure 4.1 and Figure 4.2. It is noted that the switching waveforms are different between the two HCCs. In the conventional HCC, the switching signals S1 and S2 are triggered during the same mode causing the switches to be turned "*on*" and turned "*off*" all of the time, and this situation will result in an increased switching loss and conduction losses in the system. However, in the modified HCC, the switching signals *S1* and *S2* are activated by the signal received from HCC during different modes. *S1* is activated during buck mode (in positive region), while *S2* is activated during boost mode (in negative region), and this will consequently reduce switching loss and conduction loss at zero transition. Thus, the proposed modified HCC is better suited than the conventional HCC to be applied in the bidirectional chassis dynamometer.

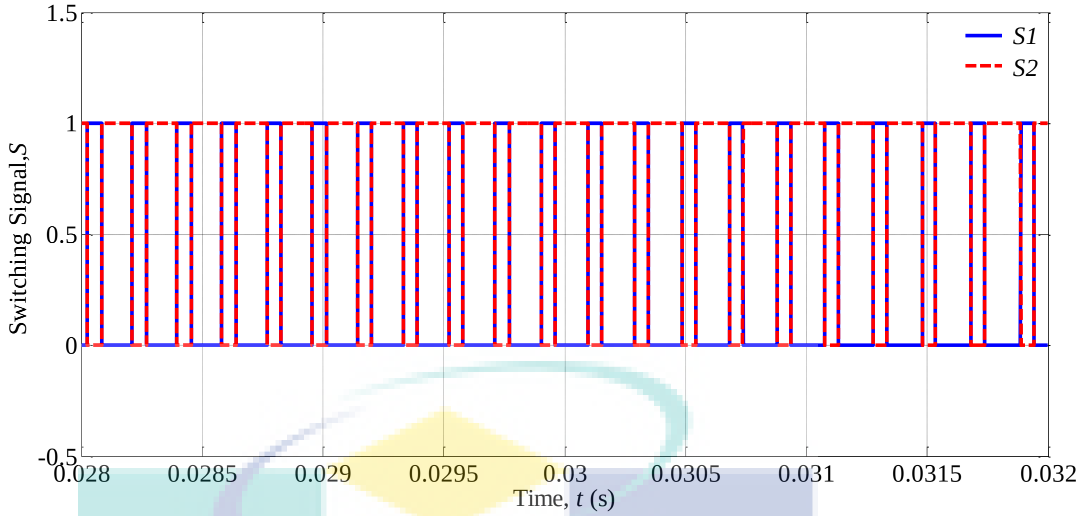

Figure 4.1 Switching Signals *S1* and *S2* in HBDC using conventional HCC

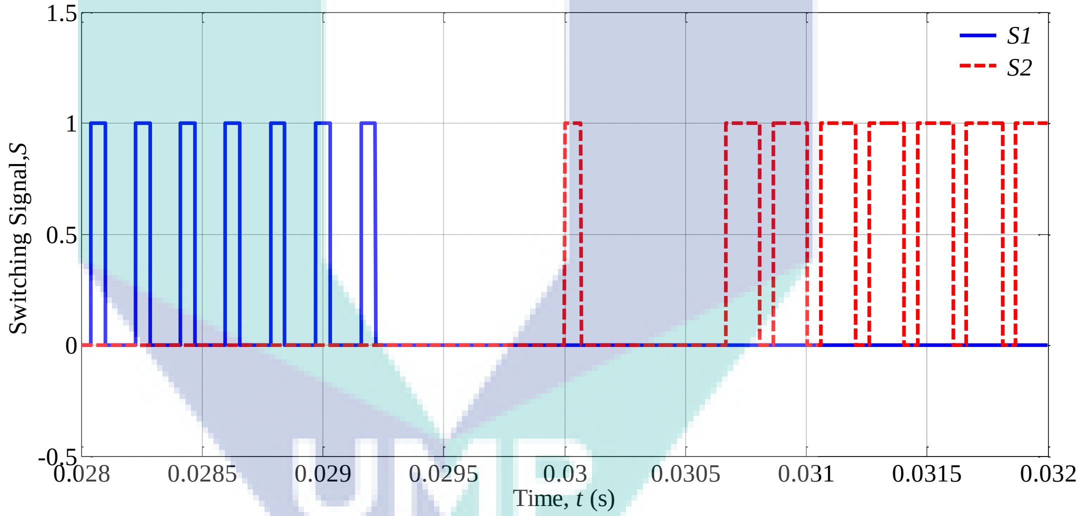

Figure 4.2 Switching Signals S1 and S2 in HBDC using modified HCC

4.2.1.1 Modified HCC during Buck Mode Operation

The entire system with HBDC topology has been tested under buck mode and boost mode, executed using the reference current, I_{ref} step response with the desired values. Figure 4.3 shows the switching response of the HCC in buck mode operation, showing reference current I_{ref}, inductor current I_L, and hysteresis band (HCC envelope) between Iref $_{(-)}$ (lower band) and $I_{ref\,(+)}$ (upper band). It is noted that I_L is conducted within the hysteresis band and when I_L reaches $I_{ref\,(-)}$ or $I_{ref\,(+)}$, the switching signal *S1* changes state; when I_{ref} = 25 A, the duty cycle of *S1* is almost 100 %. Also, the relationship between *S1* and I_L is such that when *S1* is "*on*", I_L increases from $I_{ref\,(-)}$ to $I_{ref\,(+)}$ within HCC envelopes; however, on reaching $I_{ref\,(+)}$, I_L decreases to $I_{ref\,(-)}$ as *S1* in "*off*" state. This action continues to the end of response.

Meanwhile, Figure 4.4 shows the response of the HCC-controlled switching signals *S1* and *S2* as I_{ref} is stepped up from 10 A to 25 A in buck mode. It is noted that the duty cycle of the switching signal *S1* changes from having a short duty cycle to a longer duty cycle when I_{ref} is stepped up, while *S2* always remained switched "*off*". I_L produces a higher frequency ripple inside the HCC envelope when I_{ref} = 10 A, but decreases to a lower frequency when I_{ref} is stepped up to 25 A, which leads to the different duty cycle as mentioned above. This change in the duty cycle is due to the increase in the demand of current from HCC, which consequently affects the switching signal *S1*.

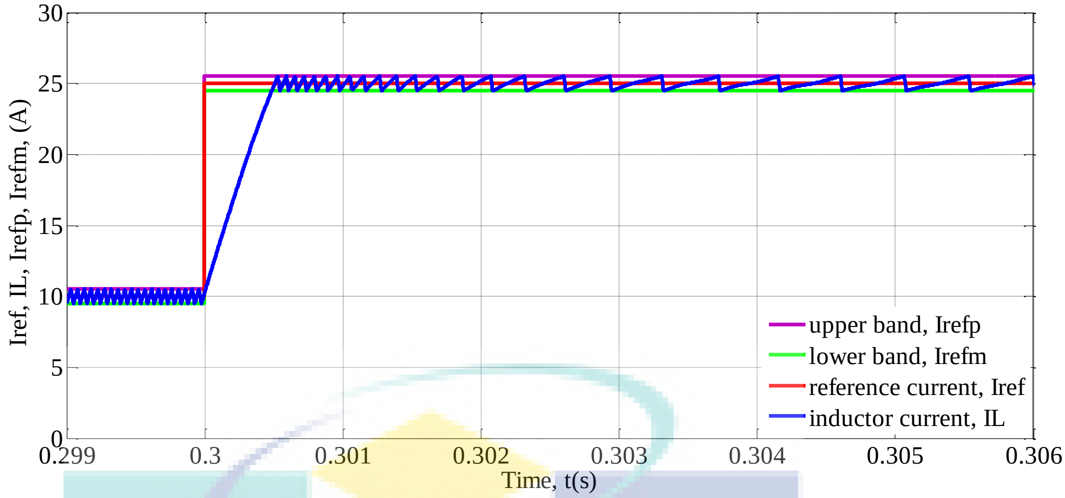

Figure 4.3 Performance of modified HCC parameters during buck mode showing I_L, I_{ref}, $I_{ref\,(+)}$ and $I_{ref\,(-)}$ with step response from 10 A to 25 A

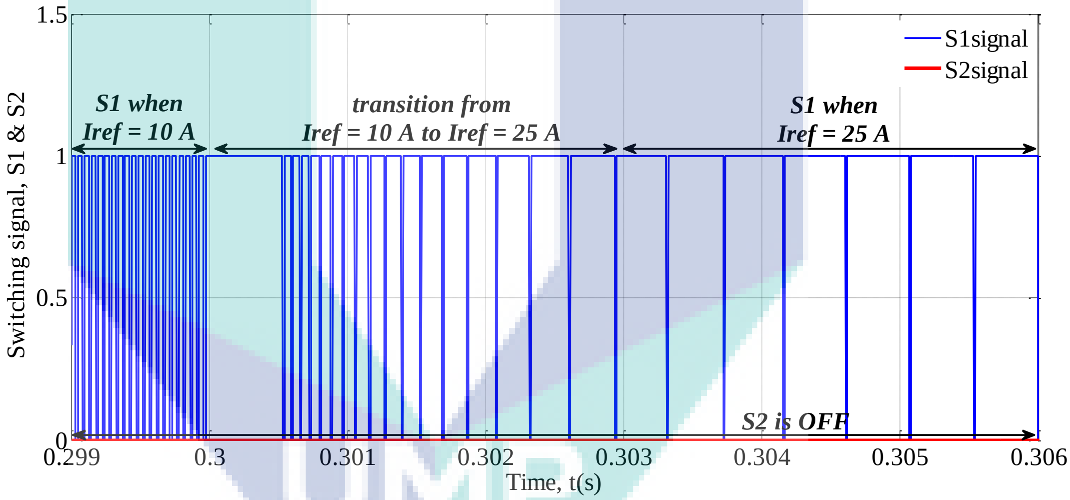

Figure 4.4 Duty Cycle of Switching Signals *S1* and *S2* during buck mode in HBDC using modified HCC

4.2.1.2 Modified HCC during Boost Mode Operation

In boost mode operation, I_{ref} is stepped down from -5 A to -15 A, and however the operation in this mode is similar to that in buck mode operation, the performance is evaluated in negative region of the graph. Figure 4.5 shows the parameters of the modified HCC operated in boost mode, during which *S2* is turned "*off*" when I_L reaches $I_{ref\,(+)}$, while *S1* is always turned "*off*". When *S2* is turned "*on*", the inductor current, I_L decreases from $I_{ref\,(+)}$ to $I_{ref\,(-)}$ in the hysteresis band. Simulation of HBDC with HCC is designed to turn "*off*" the signal *S1* throughout the boost mode operation. In addition, during the step change in I_{ref}, the oscillation of I_L within the hysteresis band decreases from a higher frequency when I_{ref} = -5 A to a lower frequency when I_{ref} = -15 A.

Figure 4.6 shows the duty cycles of the switching signals *S1* and *S2* during boost mode operation. While *S1* is "*off*" throughout the operation, the duty cycle of *S2* is higher when I_{ref} = -5 A compared to that when I_{ref} = -15 A, taking values in between during the transition.

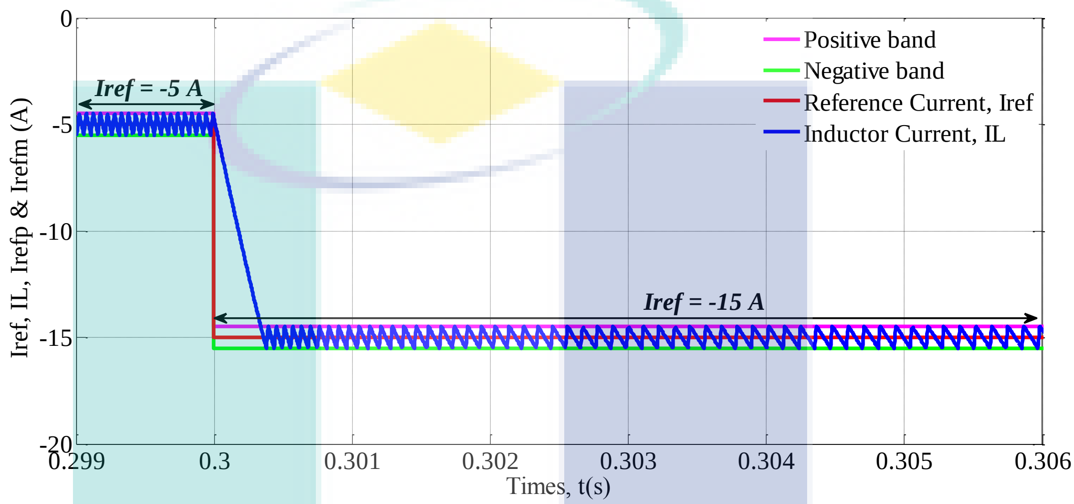

Figure 4.5 Performance of modified HCC parameters during boost mode showing I_L, I_{ref}, $I_{ref\,(+)}$ and $I_{ref\,(-)}$ with step response from -5 A to -15 A

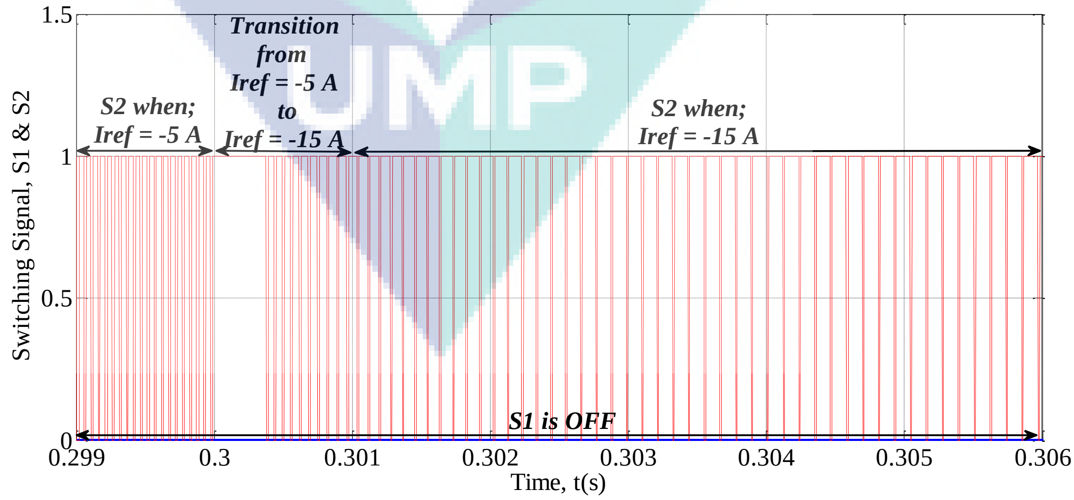

Figure 4.6 Duty Cycle of Switching Signals *S1* and *S2* during boost mode in HBDC using modified HCC

4.2.2 HCC at Zero Transition

4.2.2.1 Conventional HCC

Figure 4.7 shows the performance of the conventional HCC when the operation changes from buck mode operation (positive region) to boost mode operation (negative region). It is noted that the inductor current, I_L is wave-shaped to follow the reference current, I_{ref}, during which I_L oscillates within the hysteresis band between $I_{ref\,(+)}$ and $I_{ref\,(-)}$. It is observed that when condition changes from buck mode to boost mode, I_L continues to oscillate as usual, even during the zero transition zone. Thus, in conventional HCC, the oscillation of I_L is identical in both regions, including in the zero transition zone.

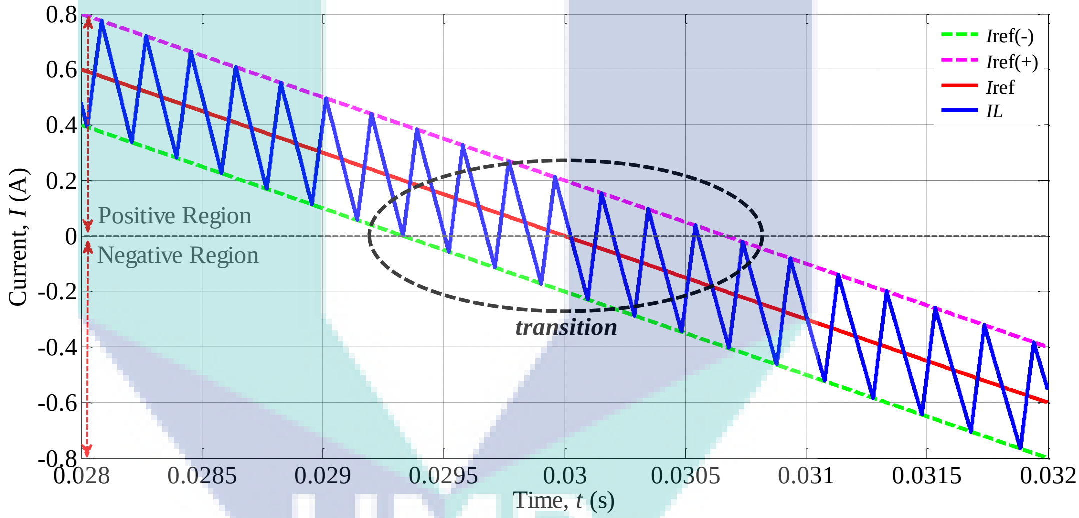

Figure 4.7 Performance of modified HCC in the zero transition region

4.2.2.2 Modified HCC

Figure 4.8 shows the performance of the modified HCC at zero transition. In the positive region (buck mode), the inductor current I_L oscillates within the HCC envelope, but stops oscillating and becomes zero when $I_{ref\,(-)} = 0$ A. The inductor current stays at that value until $I_{ref} = 0$ A, during which a single oscillation occurs as the negative region receives an incomplete envelope for I_L to continue its oscillation. However, when $I_{ref\,(+)}$ is approaching 0 A, I_L resumes its oscillation within the HCC envelope in the negative region (boost mode). Hence, in the modified HCC, the inductor current I_L stops oscillating during the transition from buck mode to boost mode, that is in the region when $I_{ref\,(-)} = I_{ref} = I_{ref\,(+)} = 0$ A.

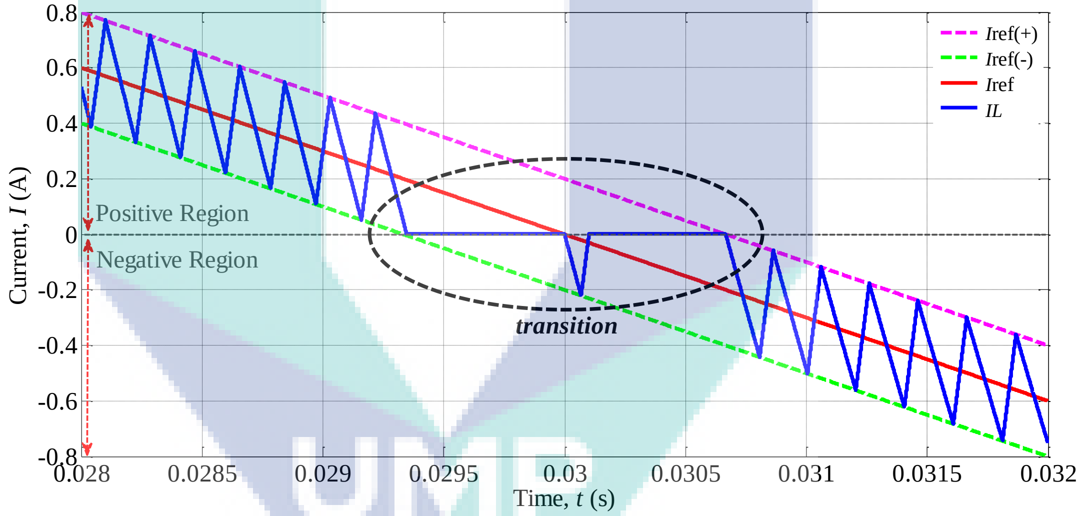

Figure 4.8 Performance of modified HCC in the zero transition region

4.2.3 HCC Switching Losses and Conduction Losses

Switching losses of the conventional HCC and modified HCC are shown in Figure 4.9 and Figure 4.10, respectively, from which it is noted that the performance of the two HCCs differs in the region of zero transition. For both the conventional HCC and the modified HCC, the switching losses are approximately 9 W when it is in "*off*" state. The losses in the conventional HCC is between 2 W and 4 W during transition that occurs in the interval between 0.0295 s to 0.0305 s, while no losses occur in the modified HCC during the transition except during the single oscillation that occurs in the inductor current.

Conduction loss of conventional HCC and modified HCC are shown in Figure 4.11 and Figure 4.12, respectively. Similar to switching losses, the conduction losses of the modified HCC is smaller than that of the conventional HCC as I_L ceases to flow in the modified HCC in the zero transition region, while the current continue to flow in the conventional HCC. It is noted that a conduction losses of up to 0.1 W occur in the conventional HCC during zero transition between the interval 0.0295 s until 0.0305 s. However, no conduction losses occur in the modified HCC during same interval, which consequently reduces the overall losses of the HBDC.

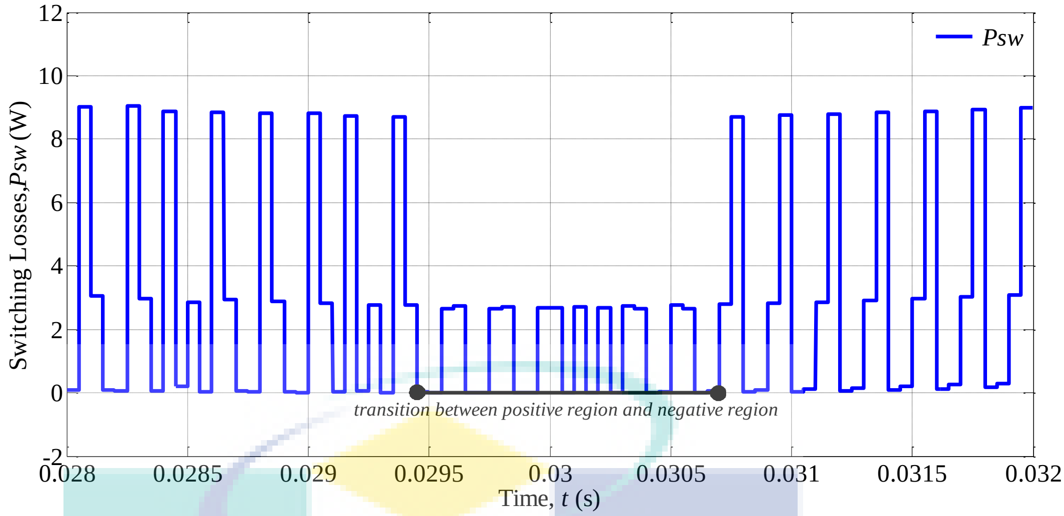

Figure 4.9 Switching Losses in Conventional HCC

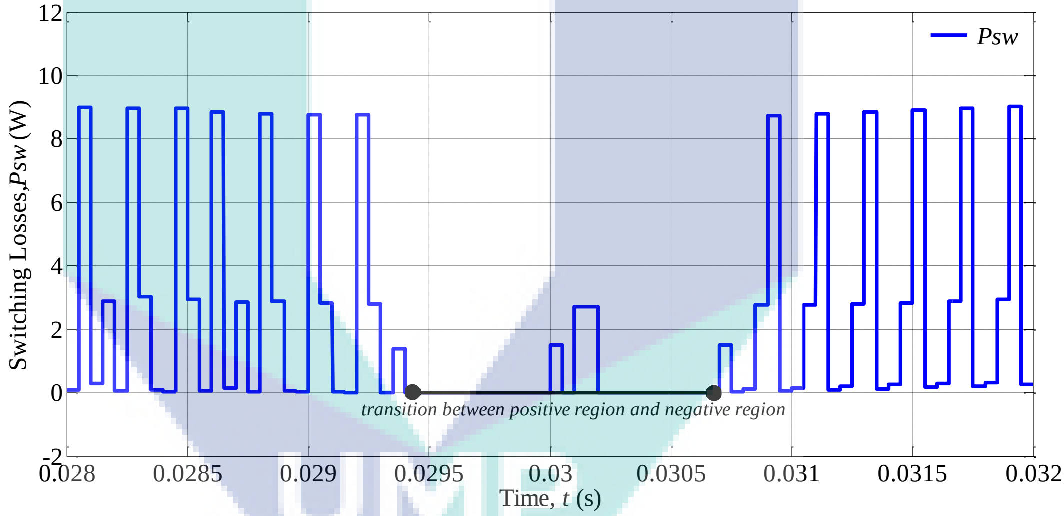

Figure 4.10 Switching Losses in Modified HCC

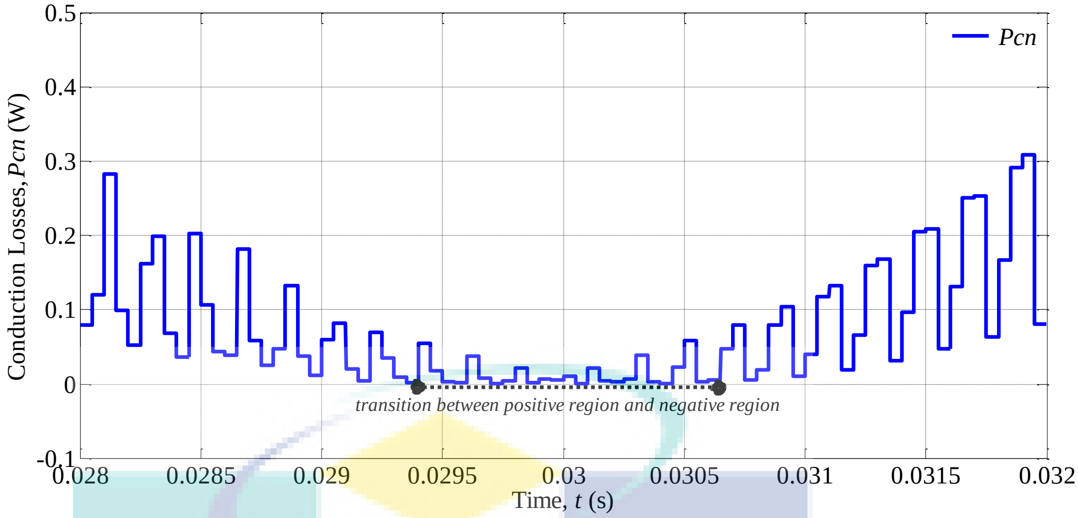

Figure 4.11 Conduction Losses in Conventional HCC

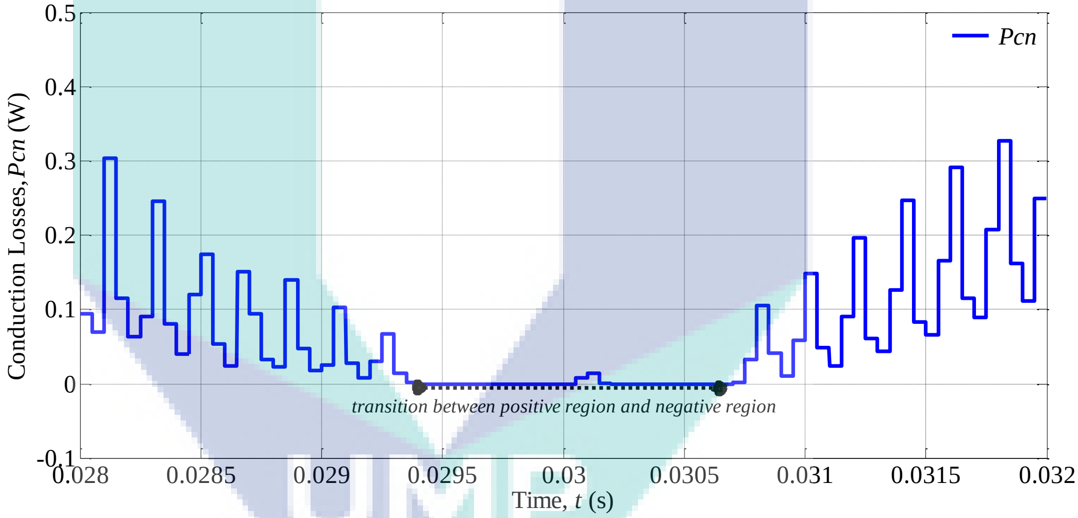

Figure 4.12 Conduction Losses in Modified HCC

4.2.4 Discussion

At zero crossing during transition buck mode and boost mode, the modified HCC can be simplified as new technique which is different with previous technique. The advantages of the modified HCC are switching at HBDC reduced and single switch, S1 or S2 will be triggered in a mode. As a result, reduces switching losses and conduction losses in the system mainly at zero crossing. Comparison of conventional HCC and modified HCC at zero crossing, switching signal, switching losses and conduction losses is tabulated in Table 4.1. The analysis indicates that the switching losses and conduction losses performance. Figure 4.13 shows the calculated losses of the conventional HCC and the proposed modified HCC, and it is found that the switching losses contribute to the bulk of the power losses. According the bar chart, the total switching losses in the interval between 0.028 s to 0.032 s of the modified HCC is 4.5 J, while that of the conventional HCC is 6.3 J. Consequently, total switching losses is reduced to 28.21% and conduction losses are reduced to 7.69%. Without oscillation at zero crossing, reduction in power losses of the modified HCC occurs. The reduction power loss is contributed by the modified logic circuit, resulting in a higher efficiency due to lower inductor conduction, and lower switching and conduction losses (Ribeiro et al., 2014) and (Lin et al., 2013).

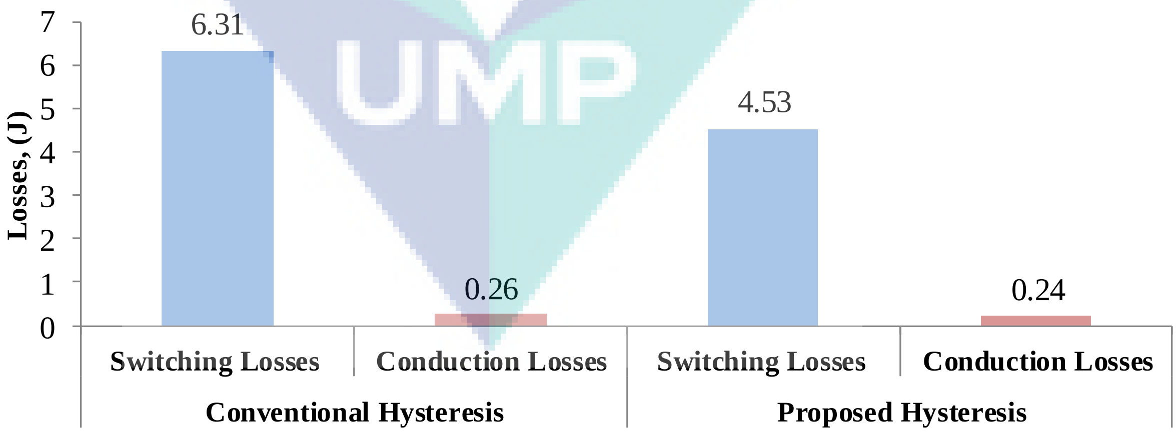

Figure 4.13 Comparison of total losses in the interval between 0.028 s to 0.032 s of conventional HCC and modified HCC

Table 4.1 Summary of conventional and modified technique of HCC

Conventional Hysteresis Current Controller Technique	**Modified Hysteresis Current Controlller Technique**
(a) Performance of HCC in the zero transition region	
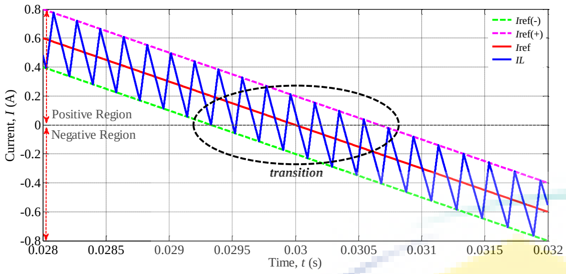	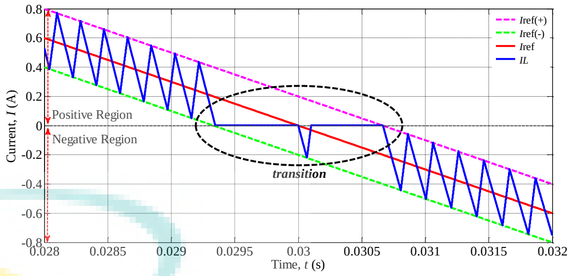
(b) Switching Signals *S1* and *S2* in HBDC using HCC	
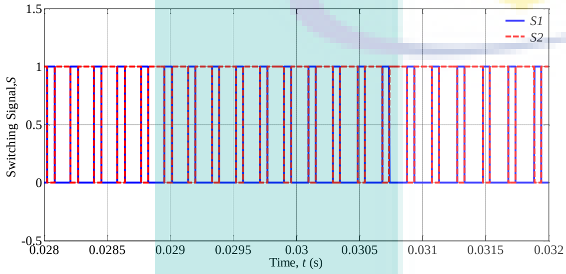	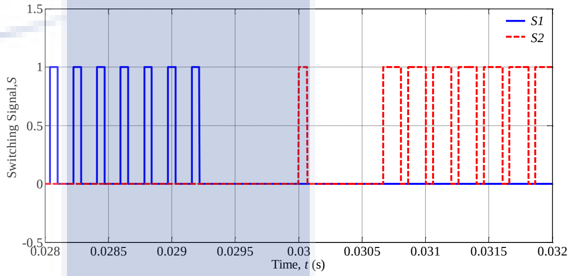
(c) Switching Losses in HCC	
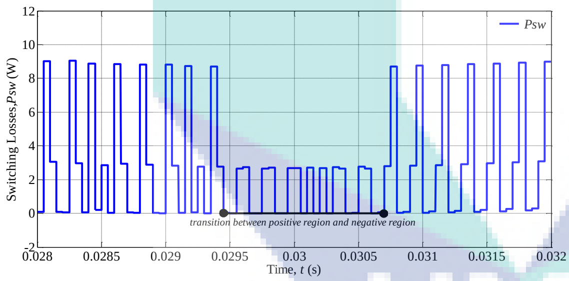	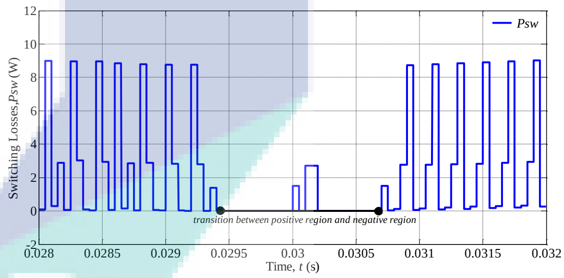
(d) Conduction Losses in HCC	
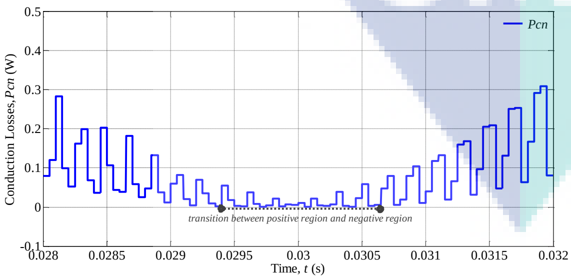	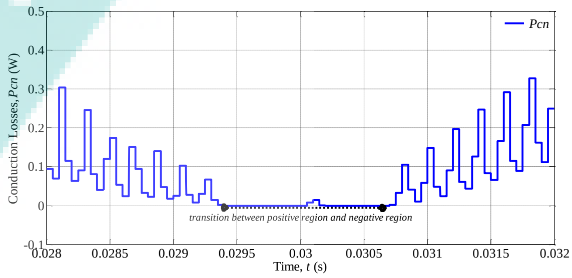

4.3 Bidirectional Chassis Dynamometer Testing

4.3.1 Introduction

From the methodology mentioned in Chapter 3, testing on the bidirectional chassis dynamometer is performed using HCC as inner loop, while PID controller is employed as the outer loop. The inner loop is used to regulate current of PADU during buck mode and boost mode. With the presence of torque from the DC machine, PID controller is used as an outer loop for controlling the torque produced from the DC machine. Combination of the two controllers in bidirectional chassis dynamometer will be described in this section.

4.3.2 Normal Condition Tests

In this system, I_L acts as a feedback to indicate the direction of current flow during buck mode and boost mode. According to the results obtained, the flow of current in PADU is related to performance of current in the DC machine or storage (source/sink). During boost mode, power is demanded in the DC machine to tests regenerative braking. In this condition, the storage (source/sink) acts as the source that supplies power to the DC machine. On the other hand, in buck mode, power is supplied by the DC machine to the storage and will be discuss in this subsection.

4.3.2.1 Step Response (steady state)

Table 4.2 shows the results obtained when the bidirectional chassis dynamometer was tested in normal condition, with step response of desired current I_d set to 8.0 A in buck mode and -3.5 A in boost mode. Desired current is set to 8 A due limits to achieving to 2 kW for normal condition tests. Thus, -3.5 A is limits for regenerative braking tests with 1 kW.

Table 4.2 Steady-state test results of bidirectional chassis dynamometer operated captured at desired current with I_d (8 A) in buck mode and I_d (-3.5 A) in boost mode.

MODE	SET	MEASURED					
	Desired Current, I_d (A)	Actual Current, I_a (A)	VUT Current, I_{VUT} (A)	Speed, n (rpm)	Torque, τ (Nm)	Power from VUT, P_{VUT} (W)	Power at Sink/Source, P_{SS} (W)
Buck (steady state)	8.0	7.99	4.16	1558.70	12.75	2081.75	1983.23
Boost (steady state)	-3.5	-3.51	-1.82	1568.07	-5.56	-910.75	-935.57

Figure 4.14 shows the step response obtained from tests performed on the capability of PADU in the bidirectional chassis dynamometer, in which the actual current I_a, taken from the DC machine, is compared to the desired current I_d. Using the PID controller, I_a is being controlled by I_d in order to dictate the internal torque of DC machine. During the testing of the dynamometer, I_a should be in the range of I_d as the value of I_d will correspond to the performance of the DC machine in emulating the road load condition.

Figure 4.15 shows the step response of VUT current, in which I_{VUT} from VUT is changes from 4.16 A (buck mode) to -1.82 A (boost mode) when the desired current I_d is step-changed from 8 A (buck mode) to -3.5 A (boost mode). In buck mode, the VUT acceleration pedal is pressed to resemble normal road load condition tests as the direction of current flow is opposite of that in the boost mode.

Figure 4.16 and Figure 4.17 respectively show the speed, n, and torque, τ, of the DC machine when the desired current I_d is step-down from 8 A to -3.5 A. It is noted that, as a result of the step-down in I_d, the speed of the machine during steady state mode increases very slightly from 1558.70 rpm to 1568.07 rpm. However, the torque of the DC machine decreases from 12.75 Nm to -5.56 Nm due to the change in the flow direction of I_d, and thus I_a, which causes the machine's inertia to increase. At the same time, the torque of the VUT is also negative as it is in regenerative braking mode; in this mode, the VUT's acceleration pedal is slightly released due to increasing speed so as to maintain normal speed condition.

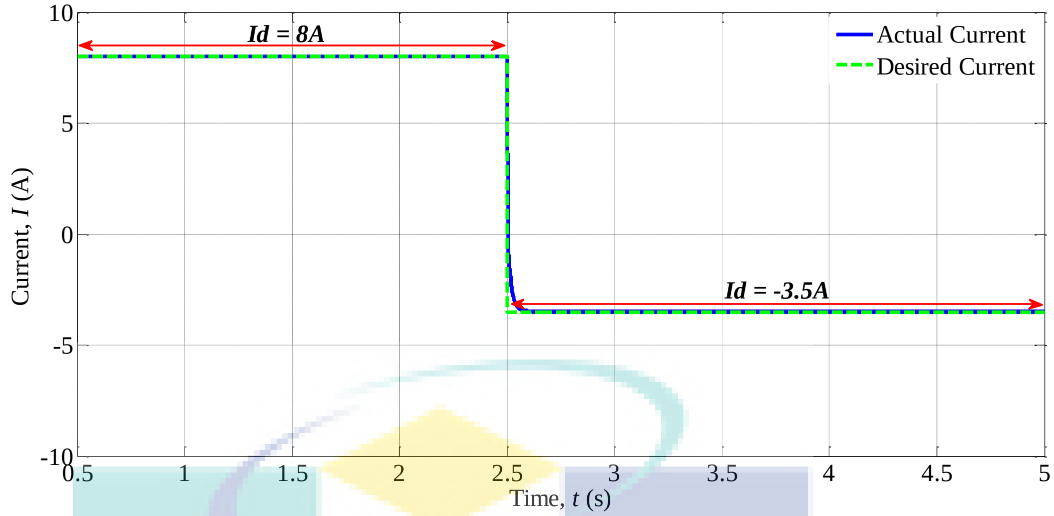

Figure 4.14 Step response of the bidirectional chassis dynamometer using desired current, I_d with 8.0 A (buck mode) and -3.5 A (boost mode).

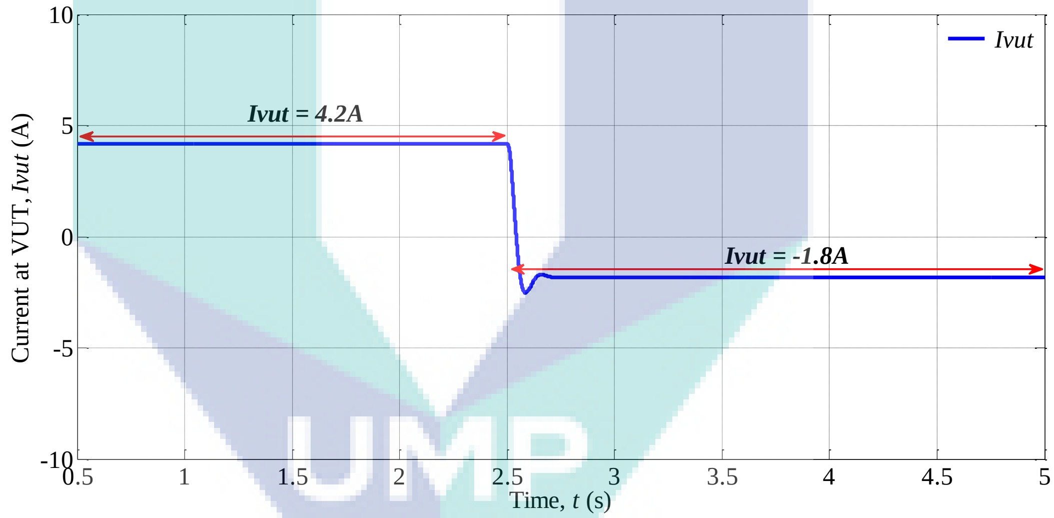

Figure 4.15 Step response of VUT current, I_{VUT} with desired current at 8.0 A (buck mode) and -3.5 A (boost mode) to test the bidirectional chassis dynamometer

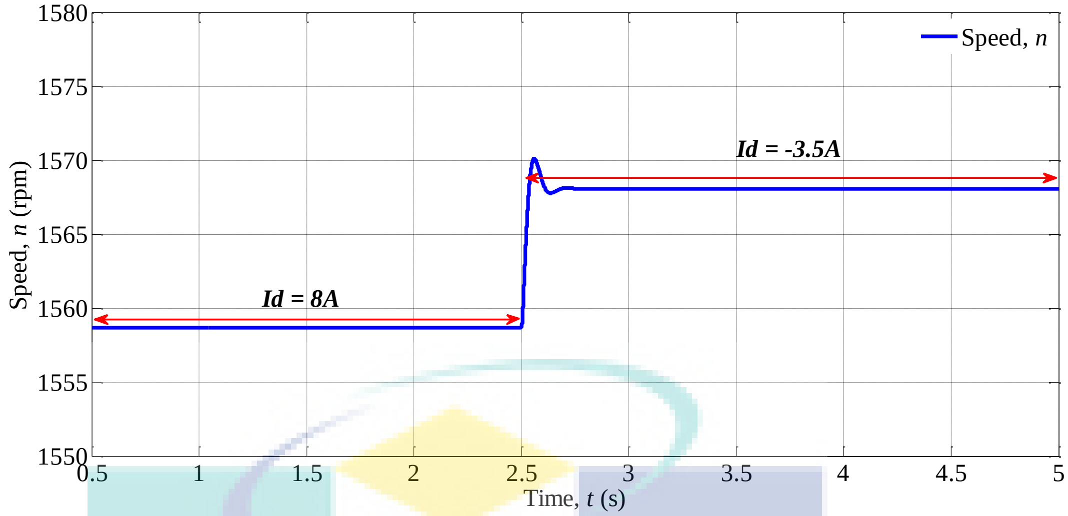

Figure 4.16 Speed of DC machine during steady state tests.

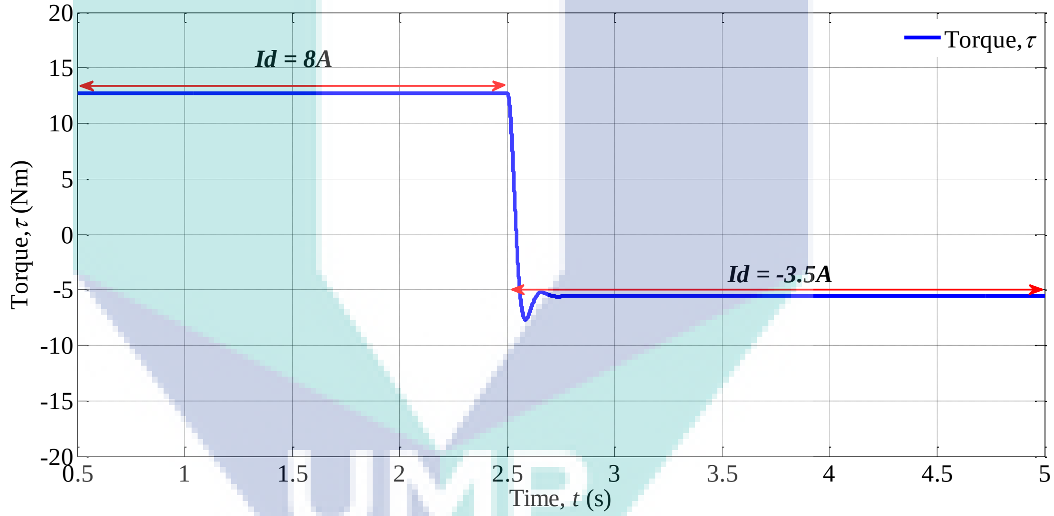

Figure 4.17 Torque of DC machine during steady state tests.

4.3.2.2 Inclination Current

Figure 4.18 show the graph obtained from inclination test conducted on bidirectional chassis dynamometer to emulate uphill condition with the desired current I_d changed from 2.0 A in normal state to 8.0 A in inclined state. During this test, PADU is operated in buck mode, which makes the DC machine performing in generating mode. The value of I_d was set up to correspond to the torque of the DC machine in order to control the power produced by the machine during generating mode to be stored in (sink/source) storage. Moreover, the generated current at the DC machine can be controlled using PID controller. From the figure, it is noted that the actual current I_a steadily follows the desired current I_d. Note that I_a is used as a feedback for the PID to manipulate the performance of the DC machine.

Table 4.3 shows the values of various parameters obtained from conducting the inclination test on the bidirectional chassis dynamometer when I_d is step-change from 2.0 A to 8.0 A. It is noted that during the test the power from VUT increases from 520.44 W to 2065.22 W, while the power at the storage increases from 464.95 W to 1967.03 W.

Table 4.3 Set and measured values obtained from inclination tests.

MODE	**SET**	**MEASURED**					
	Desired Current, I_d (A)	Actual Current, I_a (A)	VUT Current, I_{VUT} (A)	Speed, n (rpm)	Torque, τ (Nm)	Power from VUT, P_{VUT} (W)	Power at Sink/Source, P_{SS} (W)
Buck (steady state)	2.0	1.99	1.04	1563.59	3.18	520.44	464.95
Buck (incline)	2.0 increasing to 8.0	1.99 increasing to 7.95	1.04 increasing to 4.11	1563.59 decreasing 1558.75	3.18 increasing to 12.75	520.44 increasing to 2065.22	464.95 increasing to1967.03

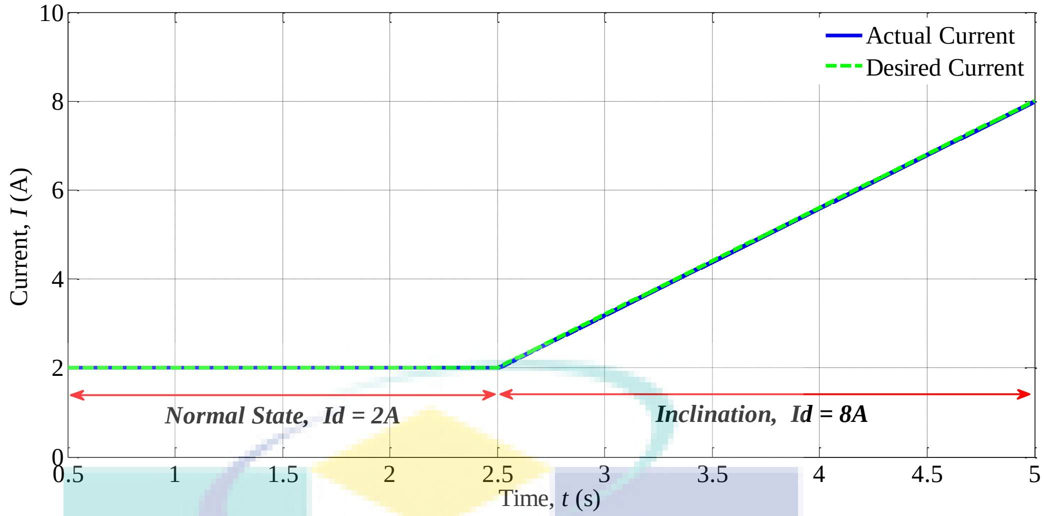

Figure 4.18 Comparison of I_d and I_a obtained from inclination test on bidirectional chassis dynamometer emulating uphill condition with *Id* step-change from 2.0 A to 8.0 A.

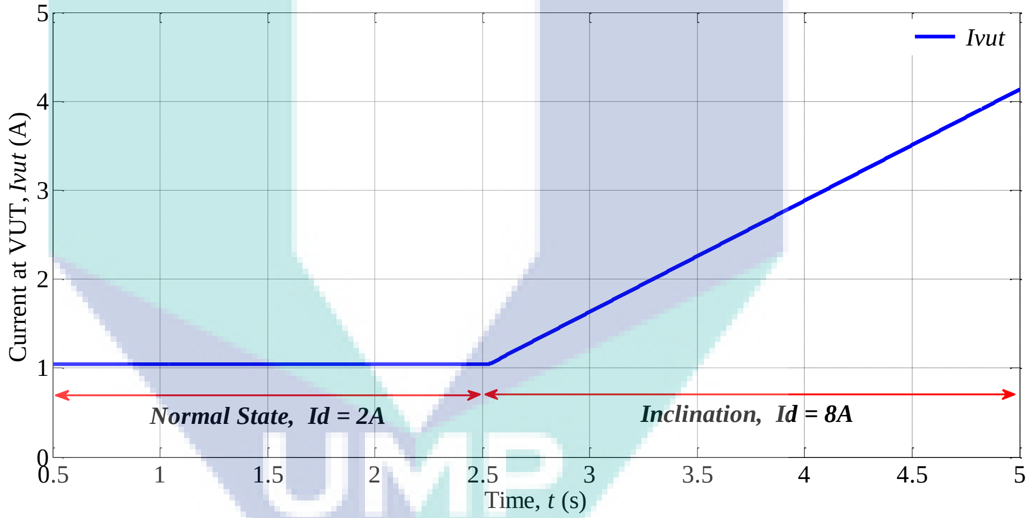

Figure 4.19 Graph of I_{VUT} obtained from inclination test on bidirectional chassis dynamometer emulating uphill condition with I_d step-change from 2.0 A to 8.0 A.

Figure 4.19 shows the VUT current I_{VUT} obtained from the inclination test on bidirectional chassis dynamometer emulating uphill condition, during which the VUT current increases from 1.04 A to 4.11 A. During acceleration, VUT follows the command drive cycle as the driver needs to press the acceleration pedal according to the drive cycle displayed on driver's aid screen. In the simulation, a compensating VUT is used as the prime mover.

During inclination mode, the speed of the DC machine gradually decreases from 1563.59 rpm to 1558.75 rpm as shown in Figure 4.20, while the torque produced gradually increases from 3.18 Nm to 12.75 Nm as shown Figure 4.21. Thus, the acceleration pedal of the VUT is depressed when undergoing uphill road condition, the speed of the DC machine decreases, while its torque increases.

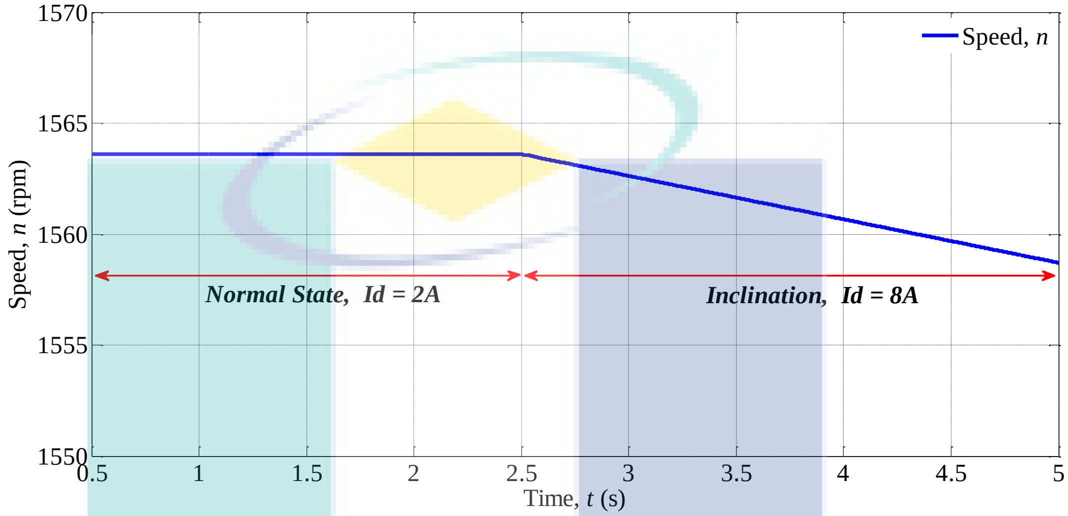

Figure 4.20 Speed of DC machine during inclination tests.

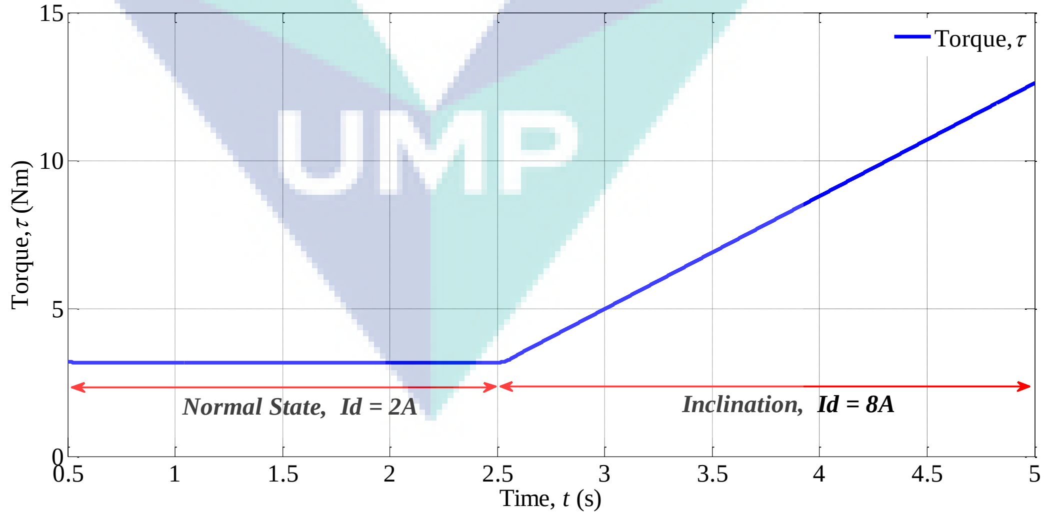

Figure 4.21 Torque of DC machine during inclination tests.

4.3.2.3 Declination Current

Other than the inclination test, the bidirectional chassis dynamometer was also tested in declination mode under normal condition. As shown in Figure 4.22, the actual current I_a very closely tracks the desired current I_d when the latter was changed from 8 A to 3 A. In this mode, the DC machine is managing the VUT as the machine is experiencing downhill road load. Meanwhile, Figure 4.23 shows the change in VUT current from 4.16 A to 1.62 A during the declination test that causes the speed of the DC machine to increase from 1558.70 rpm to 1562.71 rpm, while Figure 4.25 shows the decrease in torque from 12.27 Nm to 4.94 Nm. However, the results obtained may be affected by the small values of I_d used to control the DC machine. In the actual situation, the driver will be able to release the acceleration pedal as the drum helps to roll the wheels of the vehicle. The results obtained indicate a downhill road load because the driver is experiencing similar road conditions. Table 4.4 shows the measured values obtained from declination test when desired current I_d is changed from 8.0 A to 3.0 A.

Table 4.4 Results obtained from declination test.

MODE	**SET**	**MEASURED**					
	Desired Current, I_d (A)	Actual Current, I_a (A)	VUT Current, I_{VUT} (A)	Speed, n (rpm)	Torque, τ (Nm)	Power from VUT, P_{VUT} (W)	Power at Sink/Source, P_{SS} (W)
Buck (steady state)	8.0	7.99	4.16	1558.70	12.27	2081.74	1983.45
Buck (decline)	8.0 decreasing to 3.0	7.99 decreasing to 3.07	4.16 decreasing to 1.62	1558.70 increasing to 1562.71	12.27 decreasing to 4.94	2081.74 decreasing to 810.15	1983.45 decreasing to 738.51

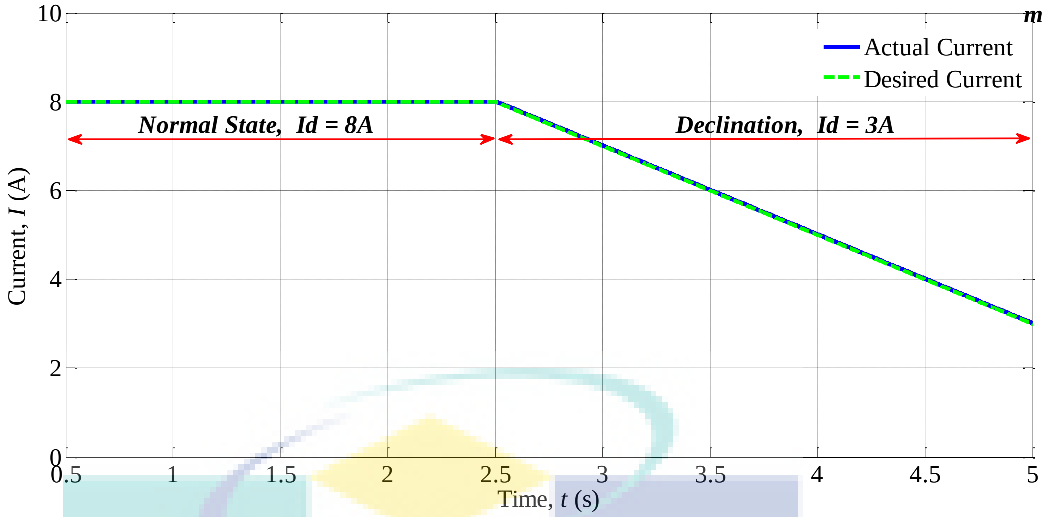

Figure 4.22 Declination test on bidirectional chassis dynamometer emulating downhill condition with desired current, I_d changed from 8.0 A to 3.0 A.

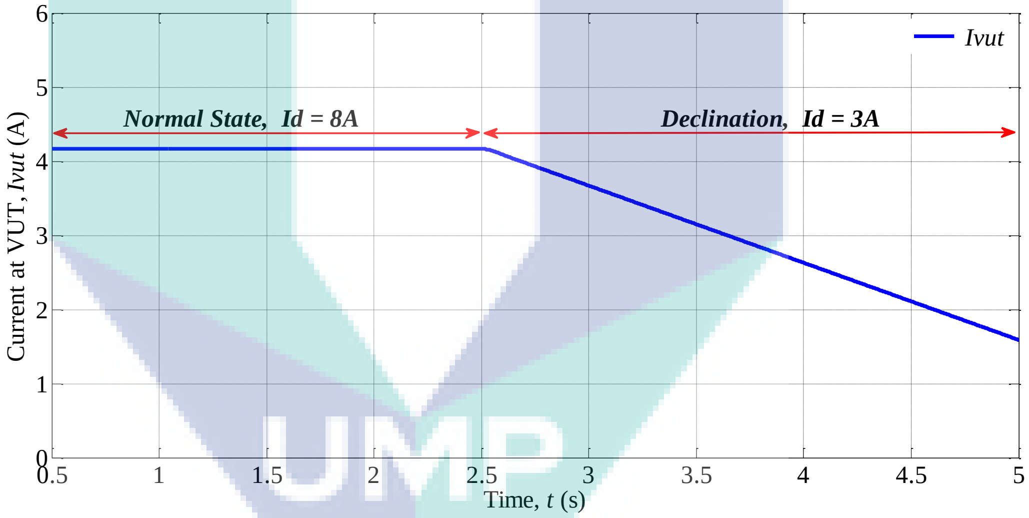

Figure 4.23 Declination test on bidirectional chassis dynamometer emulating downhill condition showing changes in VUT current.

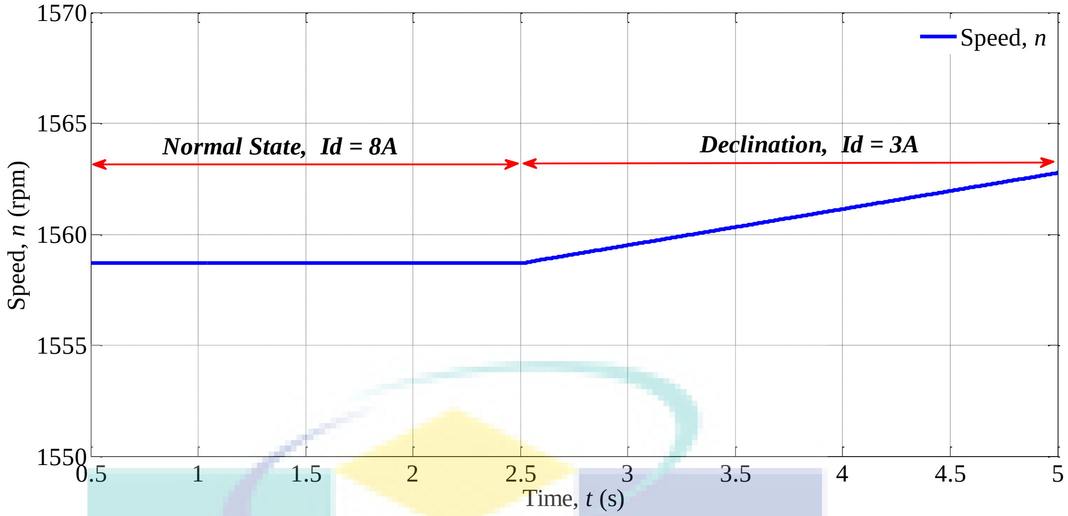

Figure 4.24 Speed of DC machine during declination test.

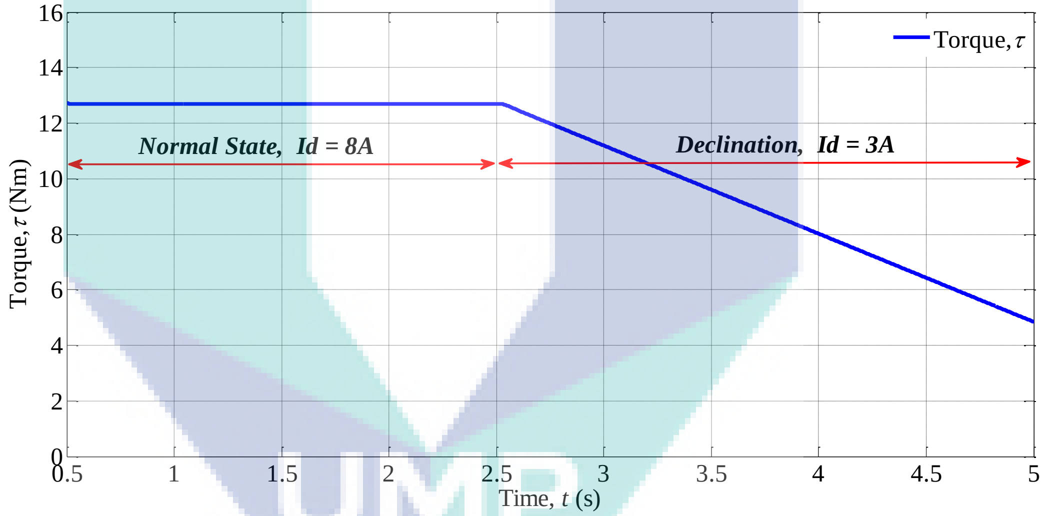

Figure 4.25 Torque of DC machine during declination test.

4.3.2.4 Discussion

The results obtained from steady-state test, inclination test and declination test show the performance of the bidirectional chassis dynamometer in normal condition. Under normal condition, the speed and torque of the DC machine changes to emulate road load conditions, similar to a conventional chassis dynamometer.

4.3.3 Regenerative Braking Tests

This section describes the simulation of regenerative braking tests conducted on the bidirectional chassis dynamometer operated in boost mode, but to better explain the regenerative braking test, the results of buck mode and boost mode are included to show the bidirectional power flow in the dynamometer. In boost mode, an input voltage of 90 V is set at the storage (sink/source), during which current flows in shown at the negative region, while the output voltage is V_{dyno}. During regenerative braking, power from the storage P_{SS} is delivered to the dynamometer as P_{dyno}. Also, the tests were conducted in three testing condition: VUT in drive condition, VUT in stop condition and VUT in braking condition.

4.3.3.1 VUT in Drive Condition

During VUT in drive condition test, VUT is operated in driving position, while the DC machine is controlled to function in regenerative braking condition. Consequently, the speed of the DC machine is increased when the operation of the machine is changed from normal condition mode to regenerative mode, which reverses the direction of desired current flow. However, during this change, VUT is maintained in driving condition, while the DC machine demand power to propel the VUT, which results in the increase in the torque of DC machine. During this test, the current flow performs in the negative region to emulate VUT performance in order to maintain the torque of DC machine similar to VUT.

In the simulation, testing started with normal condition to resemble normal road_load, in which two modes are tested, which are buck mode (positive region) and boost mode (negative region), as shown in Figure 4.26. Initially, before regenerative braking is executed, the bidirectional chassis dynamometer experiences a normal road load. However, at t = 2.5 s, the desired current I_d is set to -3.0 A to change the dynamometer to operate in boost mode, which consequently causes the system to be in regenerative braking condition. To achieve regenerative braking testing, the actual current I_a is controlled to follow I_d, while simultaneously, VUT is in drive position as the acceleration pedal keep is pressed. Figure 4.27 shows VUT current, I_{VUT} of -1.56 A obtained during the test, and since VUT is in drive position, I_{VUT} stays at -1.56 A during the interval 2.5 s until 5.0 s, while, Table 4.5 shows the results obtained during regenerative braking test in drive condition.

Table 4.5 Regenerative braking test results when VUT in drive condition

MODE	**SET**	**MEASURED**					
	Desired Current, I_d (A)	Actual Current, I_a (A)	VUT Current, I_{VUT} (A)	Speed, n (rpm)	Torque, τ (Nm)	Power from VUT, P_{VUT} (W)	Power at Sink/Source, P_{SS} (W)
Buck (VUT drive)	2.0	1.99	1.04	1563.58	3.18	520.44	464.93
Boost (VUT drive)	-3.0	-2.99	-1.56	1567.66	-4.76	-780.65	-809.75

Figure 4.28 and Figure 4.29 respectively show the speed and torque of the bidirectional chassis dynamometer as a result of the step-change in I_d (and I_a) from 2.0 A to -3.0 A. The speed during regenerative braking tests increases from 1563.58 rpm in buck mode to 1567.66 rpm due to the change in current flow direction. Simultaneously, a torque of 3.18 Nm in buck mode decreases to -4.76 Nm in boost mode, causing the VUT to operate in regenerative braking mode due to the decrease in I_d.

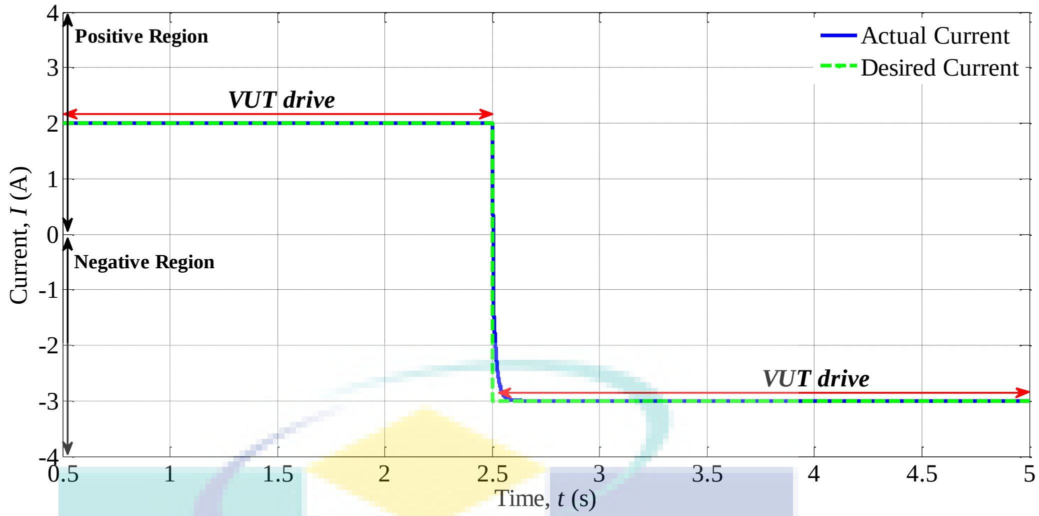

Figure 4.26 Step response of bidirectional chassis dynamometer when desired current I_d is step-changed from 2.0 A (buck mode) to -3.0 A (boost mode) with VUT in drive condition.

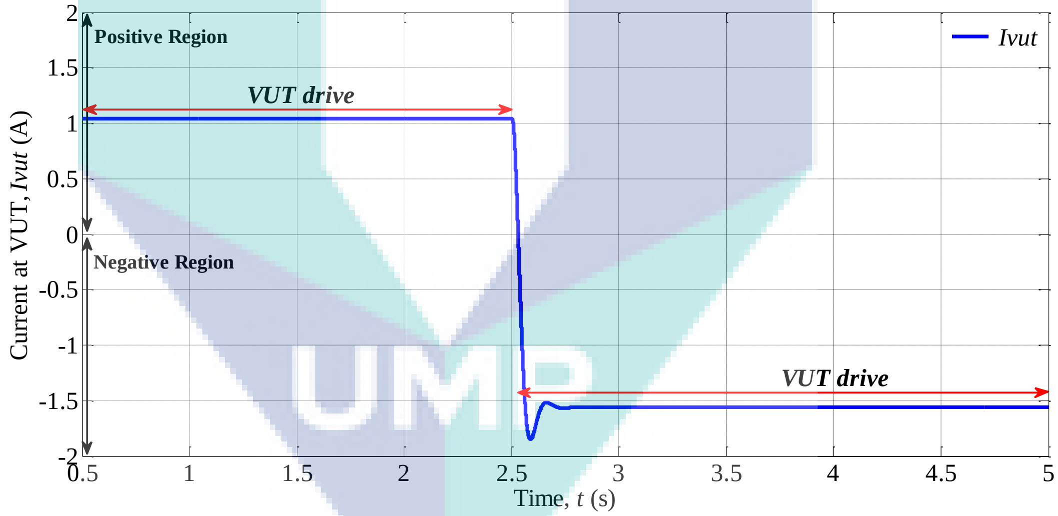

Figure 4.27 Step response of VUT current I_{VUT} obtained from bidirectional chassis dynamometer tested with VUT in drive condition.

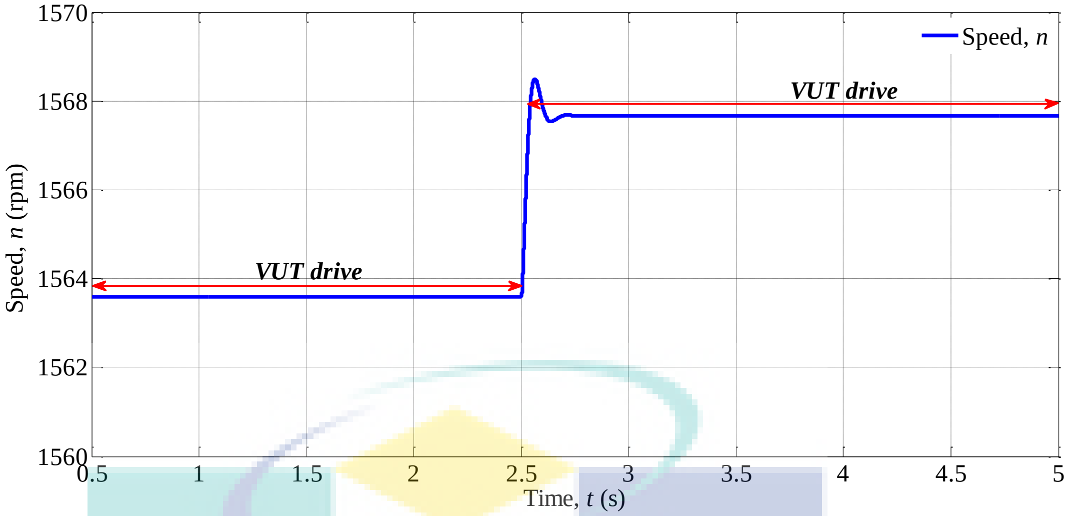

Figure 4.28 Speed of DC machine during normal condition and regenerative braking.

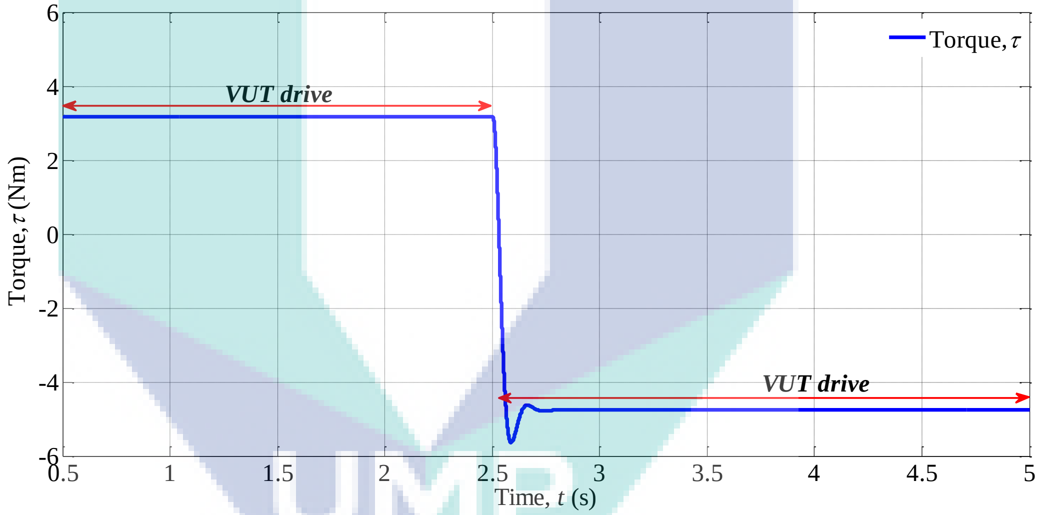

Figure 4.29 Torque of DC machine during normal condition and regenerative braking.

4.3.3.2 VUT in Stop Condition

Figure 4.30 shows the desired current I_d and actual current I_a during the regenerative braking tests with VUT in stop condition. Regenerative braking testing started with normal road load condition then at t = 2.5 s, I_d is step-change from 2.0 A to -3.0 A to test regenerative braking. When VUT is stopped, the bidirectional chassis dynamometer is still being driven, as shown in Figure 4.31, during which I_{VUT} = 0 A shows that no braking occurs. Table 4.6 shows the results of the regenerative braking test in stop condition.

Speed and torque characteristics of the DC machine with VUT in stop condition are respectively shown in Figure 4.32 and Figure 4.33. Note that the speed and torque of the machine are affected by the reversal in the flow direction of I_d. The speed of the DC machine at normal road load with I_d = 2.0 A is constant at 1563.58 rpm; when VUT is changed to boost mode, VUT rapidly stops and I_{VUT} = 0 A, which increases the speed of the DC machine to 1697.04 rpm. There is no load when VUT is in stop condition, but the increase in the speed is because energy is still being supplied in boost mode. However, when there is no load, load torque becomes zero; thus. DC machine torque is 0 Nm when VUT stops.

Table 4.6 Regenerative braking test results when VUT in stop condition

MODE	**SET**	**MEASURED**					
	Desired Current, I_d (A)	Actual Current, I_a (A)	VUT Current, I_{VUT} (A)	Speed, n (rpm)	Torque, τ (Nm)	Power from VUT, P_{VUT} (W)	Power at Sink/Source, P_{SS} (W)
Buck (VUT drive)	2.0	1.99	1.04	1563.58	3.18	520.44	438.49
Boost (VUT stop)	-3.0	-2.99	0	1697.04	0	0	-901.87

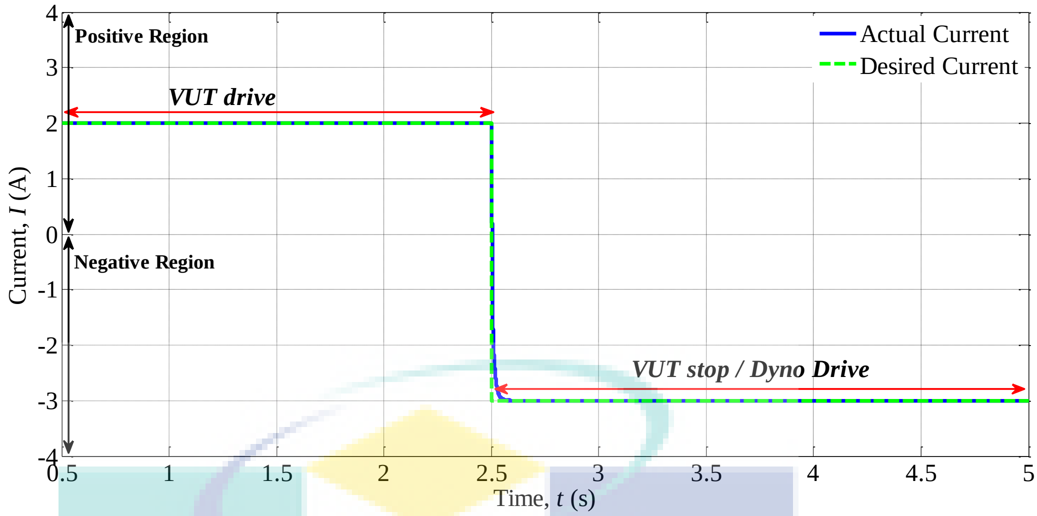

Figure 4.30 Step response of bidirectional chassis dynamometer when desired current I_d is step-changed from 2.0 A (buck mode) and -3 A (boost mode) with VUT in stop condition.

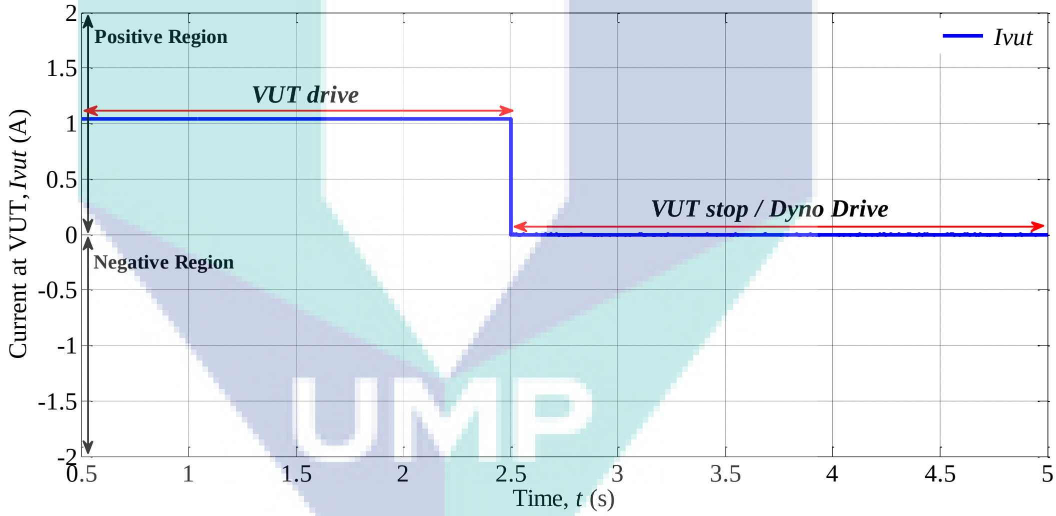

Figure 4.31 Step response of VUT current I_{VUT} when bidirectional chassis dynamometer is tested with VUT in stop condition.

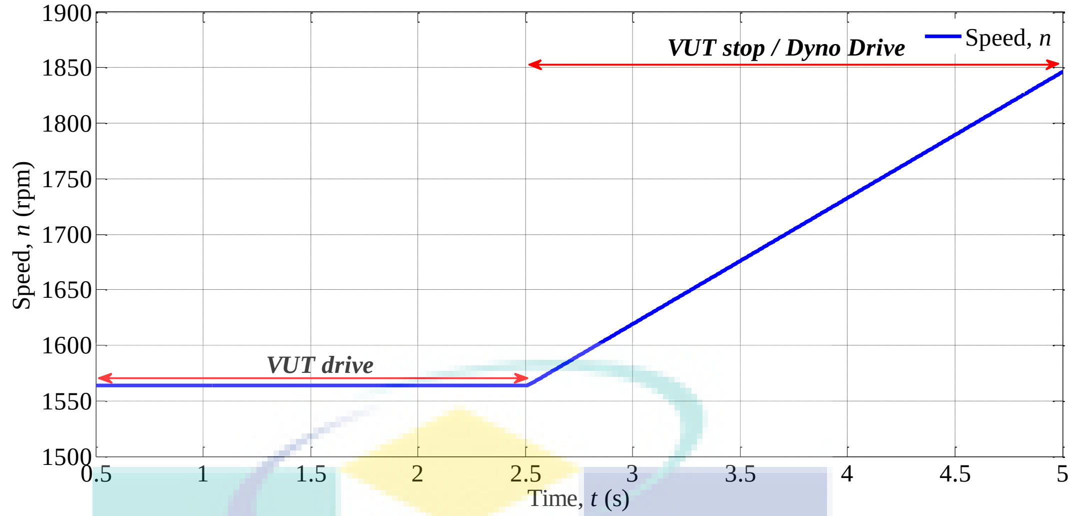

Figure 4.32 Speed of DC machine in regenerative braking with VUT in stop condition.

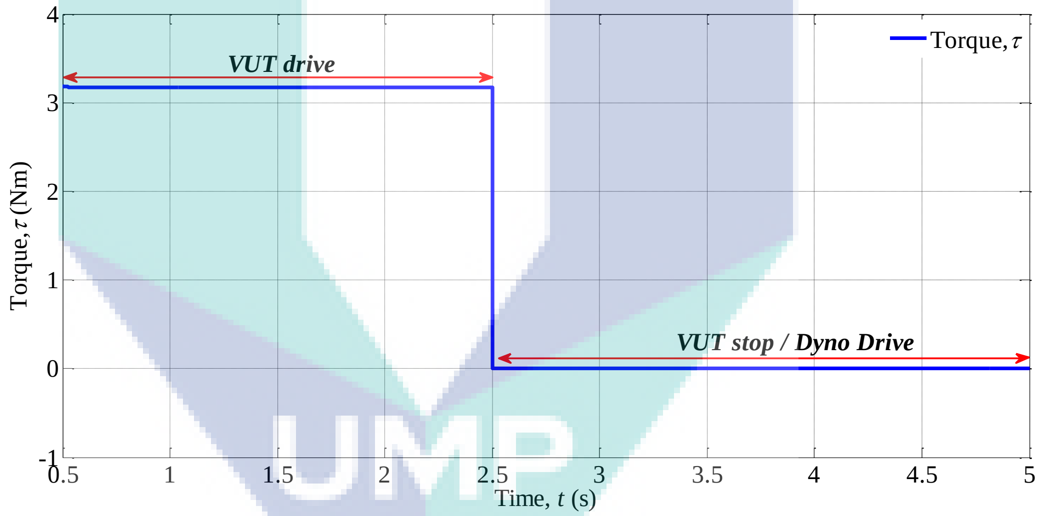

Figure 4.33 Torque of DC machine in regenerative braking with VUT in stop condition.

4.3.3.3 VUT in Brake Condition

Figure 4.34 shows the desired current and the actual current from DC machine to obtain regenerative braking tests with VUT in drive state, brake state and stop state. Simultaneously, Figure 4.35 shows the VUT current analysis during the testing. In the beginning, VUT is started with normal condition and DC machine emulates normal load which yields results that are similar to that obtained in previous section on VUT in drive condition as I_d = 2.0 A. Then, at t = 2.5 s, the acceleration pedal of VUT is still in driving mode and Id is changed to -3.0 A. It is causes VUT experiencing regenerative braking mode and resulting I_{VUT} = -1.56 A and power at VUT is now delivered to the battery. Concurrently, at 2.5 s, overshoot occurs at I_{VUT} due to changes of current flow direction at DC machine. The Prime mover of VUT is unattached with PID controller thus causes an overshoot at I_{VUT}. Next, VUT is put in braking condition at t = 3.5 s, I_d is set to 0 that causes I_{VUT} to increase to 0 A, during which the dynamometer emulates regenerative braking of VUT. To complete the test, the VUT in stop condition is also recorded with I_{VUT} is 0. Table 4.7 is the tabulation of the various parameters obtained from the test.

Table 4.7 Regenerative braking test results when VUT in drive state, VUT in brake state and VUT in stop state.

MODE	**SET**	**MEASURED**					
	Desired Current, I_d (A)	Actual Current, I_a (A)	VUT Current, I_{VUT} (A)	Speed, n (rpm)	Torque, τ (Nm)	Power from VUT, P_{VUT} (W)	Power at Sink Source, P_{SS} (W)
Buck (VUT drive)	2.0	1.99	1.04	1563.58	3.18	520.44	438.49
Boost (VUT drive)	- 3.0	- 2.99	-1.56	1567.66	-4.76	-780.65	-809.75
Boost (VUT brake)	-3.0 increasing to 0	-2.99 increasing to 0	1.56 decreasing to 0	1567.66 decreasing to 1565.22	-4.76 increasing to 0	780.65 decreasing to 0	809.75 decreasing to 70.91
Boost (VUT stop)	0	0	0	1565.22	0	0	-70.91

Figure 4.36 and Figure 4.37 respectively show the speed and torque of the DC machine during regenerative braking test with VUT in drive state, brake state and stop state. When VUT is in driving condition, the speed of the DC machine is 1567.66 rpm and decreases to 1565.22 rpm when VUT is in braking condition. Overshoot occurs because speed is fixed by VUT performance and unattached with PID. Meanwhile, the torque of the DC machine changes from - 4.76 Nm when VUT is in brake state to 0 Nm at VUT is in stop state. After braking, VUT is stopped at time t = 4 s, but even though the torque on the DC machine is 0 Nm, the DC machine continues to rotate at 1565.22 rpm.

Due to suddenly changes of DC machine direction, I_{VUT} experience a regenerative braking condition with static acceleration pedal. During changes of normal condition test to regenerative braking test, overshoot occurs at I_{VUT}. As mention in chapter 3, VUT is prime mover at power circuit. Thus overshoot at I_{VUT} occurs because power circuit for VUT is unattached with other control circuit to control VUT performance. PID controller is attached with DC machine to control the dynamometer testing performance.

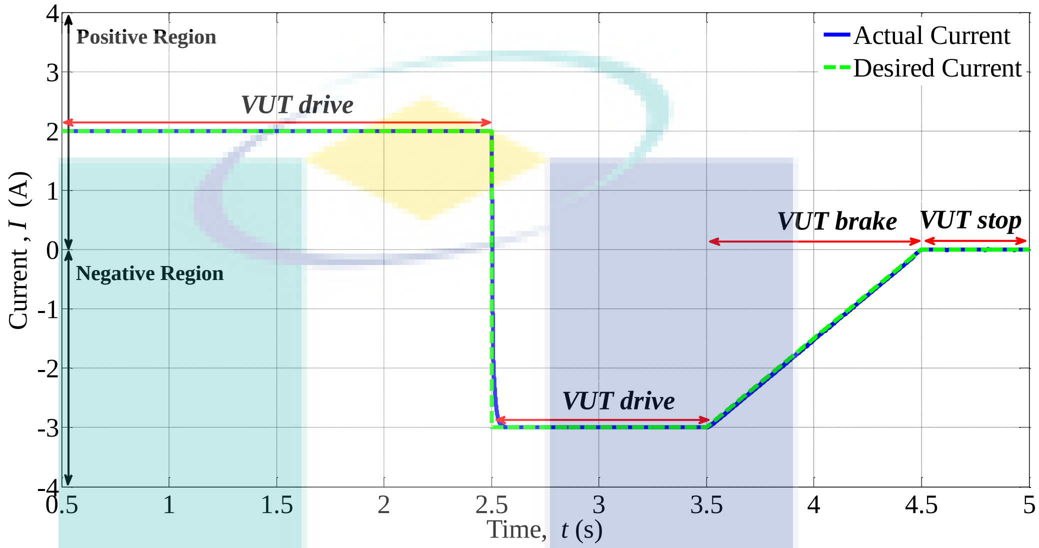

Figure 4.34 VUT overall performance during regenerative braking tests with desired current, *Id* with 2.0 A (buck mode) and -3 A (boost mode).

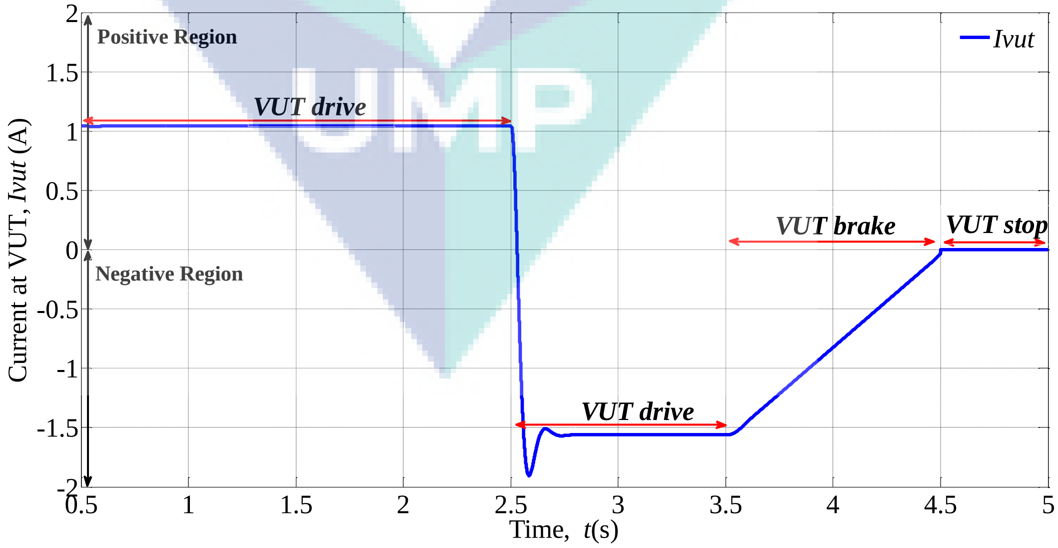

Figure 4.35 VUT current during regenerative braking tests with I_d= 2.0 A (buck mode) and I_d= -3.0A (boost mode).

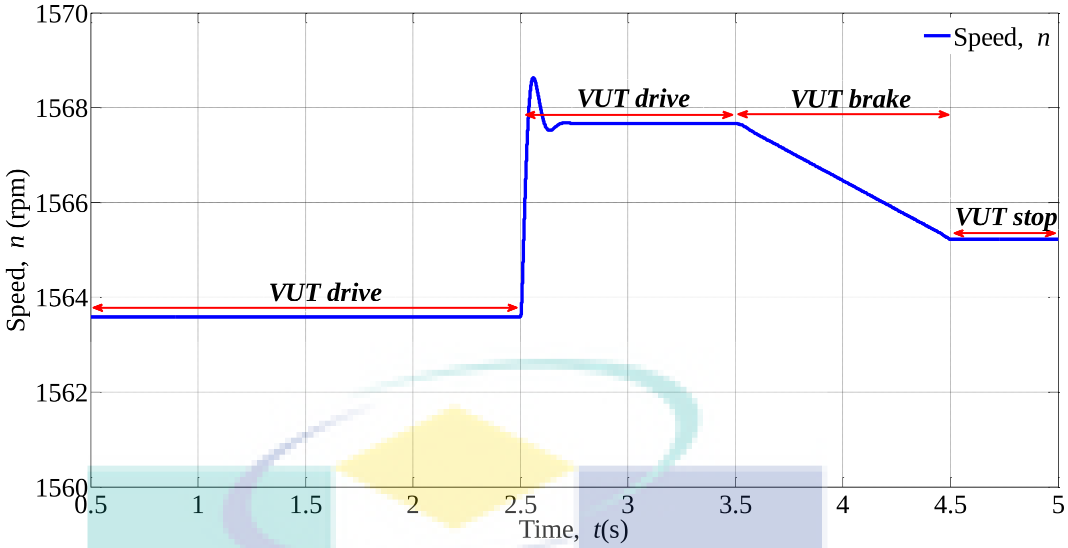

Figure 4.36 Speed of DC machine during normal condition and regenerative braking.

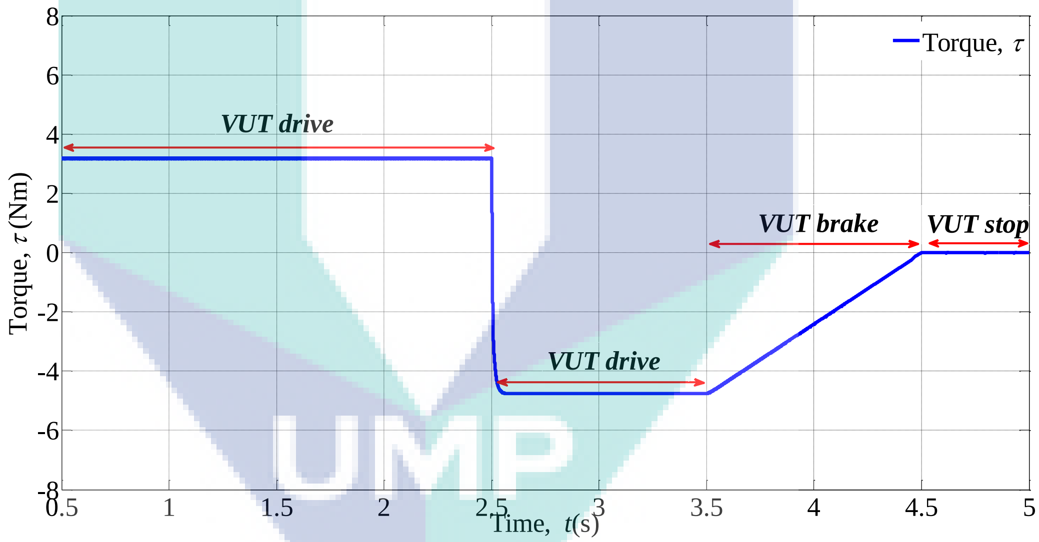

Figure 4.37 Torque of DC machine during normal condition and regenerative braking.

4.3.4 Discussion

From the results obtained from the regenerative braking test conducted on the bidirectional chassis dynamometer with VUT operated in drive state, brake state and stop state, it can be seen that the performance of the dynamometer is affected by the different states of VUT. When the chassis dynamometer is in regenerative braking mode and VUT in braking condition, the dynamometer emulates the braking condition of VUT. Similarly, when VUT is either in driving condition or braking condition or stopping condition, the DC machine is affected by the condition of VUT. This implies that the DC machine emulates VUT during regenerative braking condition. Thus the bidirectional chassis dynamometer can be applied in testing regenerative braking condition.

4.4 Bidirectional Chassis Dynamometer Power Transfer Analysis

4.4.1 Introduction

The previous section has discussed tests of VUT in normal condition and regenerative braking. The power transfer analysis of bidirectional chassis dynamometer is verified during normal condition with steady state test, inclination test and declination test. Thus, regenerative braking tests were conducted with different VUT conditions: VUT in drive condition, VUT in stop condition and VUT in brake condition. In this section, the bidirectional results of the system are evaluated and analysed, and the power transfer in bidirectional chassis dynamometer in relation to the power management for the entire system is discussed.

4.4.2 Normal Condition Test

Figure 4.38 illustrates the power flow diagram of bidirectional chassis dynamometer in normal condition test. The input power P_{IN} to the system is supplied electrically to the VUT as $P_{VUT(e)}$, which is then mechanically transmitted to the storage (sink/source), while the power at the sink/source, P_{SS}, as the output power, P_{OUT}. Since the mechanical parameter is not included in bidirectional chassis dynamometer, mechanical power losses is neglected. It is noted that P_{VUT}, P_{dyno} and P_{PADU} have different values.

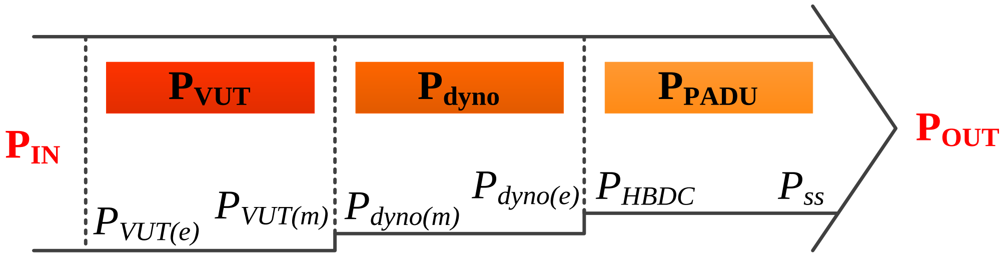

Figure 4.38 Power flow diagram of bidirectional chassis dynamometer in normal condition test.

4.4.2.1 Step Response (Steady State) Test

The power transfer of bidirectional chassis dynamometer in normal condition during buck and boost mode in response to step-change test is shown in Figure 4.39. Power transfer of 2000 W is achieved with I_d set to 8.0 A in buck mode, while power transfer achieved is -900 W with I_d set to -3.5 A in boost mode ("-" sign in power is neglected since direction of current flow reverses during regenerative braking). The magnification of the power transfer in normal condition is shown in Figure 4.39 (a) and (b) however, the details of the regenerative braking mode will be explained in subsection 4.4.3.

The testing was conducted in steady state, and the generated power by VUT, $P_{VUT(e)}$, is constant at 2081.75 W in buck mode, as shown in Table 4.8. The generated power is transmitted to the dynamometer as $P_{VUT(m)}$, which is directly related to $P_{dyno(m)}$ in producing power at the DC machine. Since $P_{VUT(m)}$ and $P_{dyno(m)}$ are connected to each other in mechanical propulsion, $P_{VUT(m)}$ and $P_{dyno(m)}$ have values of 2075.55 W. Since the power generated at the DC machine is absorbed by PADU, $P_{dyno(e)}$ is stored in the storage (sink/source). $P_{dyno(e)}$ supplies PADU with 2070.47 W of power to execute the switching, which produces an output power of 1983.23 W. When the DC machine is in generative mode, the output power occurs at the storage (sink/source), P_{SS}.

Table 4.8 Power management during steady state tests in normal condition.

Power	$P_{VUT(e)}$,(W)	$P_{VUT(m)}$,(W)	$P_{dyno(m)}$,(W)	$P_{dyno(e)}$,(W)	P_{ss},(W)
Buck Mode	2081.75	2075.55	2075.55	2070.47	1983.23
Boost Mode	910.75	913.35	913.35	917.86	935.57

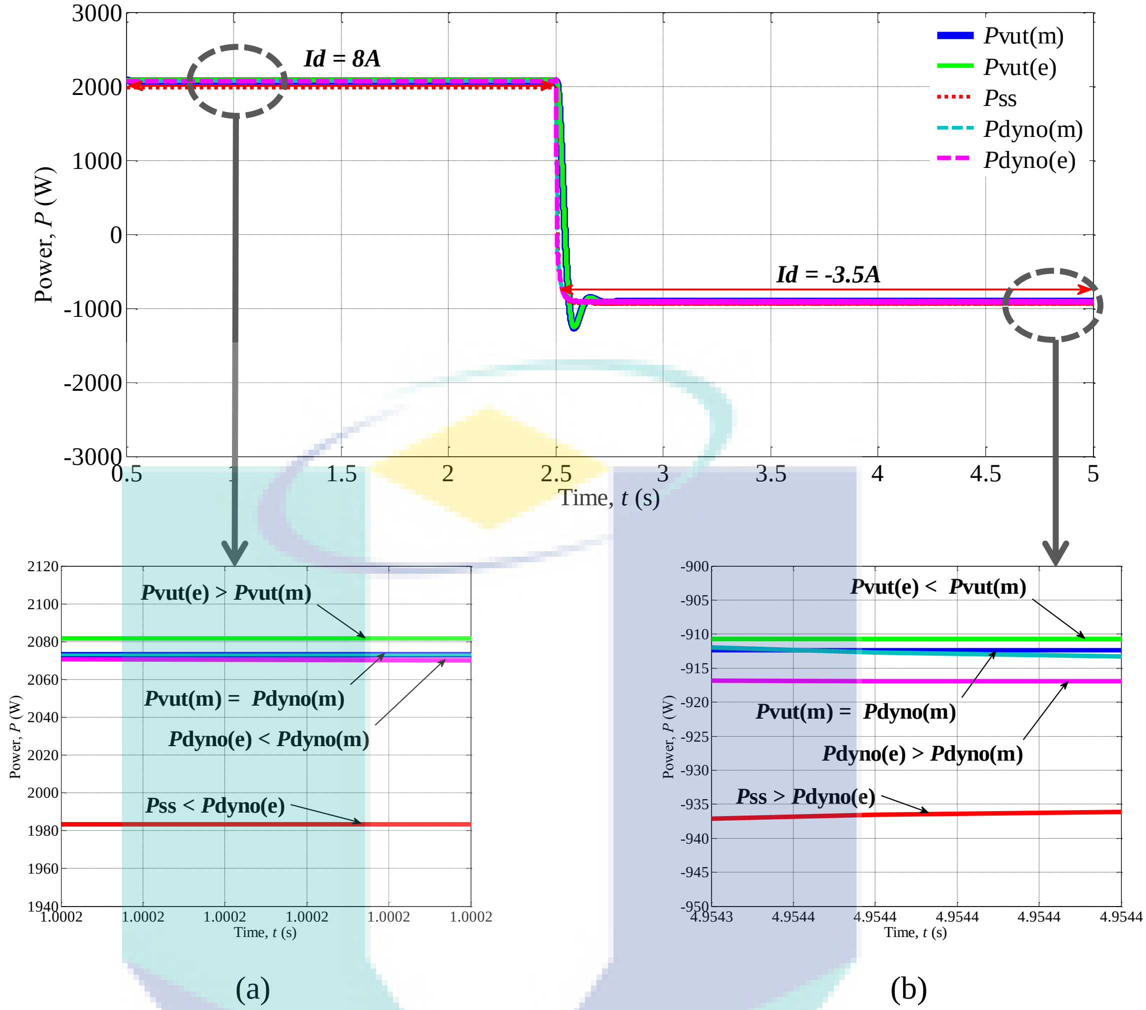

Figure 4.39 Power transfer of bidirectional chassis dynamometer during buck and boost modes in normal condition, including $P_{VUT(m)}$, $P_{VUT(e)}$, $P_{dyno(m)}$, $P_{dyno(e)}$ and P_{SS} with magnification of (a) Buck mode and (b) Boost mode power transfer.

The overall power transfer that happen during this test is as summarized in Table 4.9. During normal condition test, the electrical power, $P_{VUT(e)}$ = 2081.75 W, is greater than its mechanical power, $P_{VUT(m)}$ = 2075.55 W; thus, $P_{VUT(e)}$ is the input power to the system. However, the DC machine's mechanical power $P_{VUT(m)} = P_{dyno(m)}$ = 2075.55 W because the mechanical force from VUT causes the mechanical shaft of the machine to rotate. Meanwhile, the power generated from the DC machine acts as electrical power to produce the input power for PADU, $P_{dyno(e)}$ = 2070.47 W. The output power from PADU is then transmitted to the storage (source/sink), P_{SS} = 1983.23 W, which will become the input power to the system during regenerative braking tests.

Table 4.9 Complete power management during normal condition test with step response

Mode	VUT (Prime Mover)	Dyno (DC machine)	PADU (HBDC)
Buck	$P_{VUT(e)} > P_{VUT(m)}$	$P_{dyno(m)} > P_{dyno(e)}$	$P_{dyno(e)} > P_{ss}$
	$P_{VUT(m)} = P_{dyno(m)}$		
Boost	$P_{VUT(e)} < P_{VUT(m)}$	$P_{dyno(m)} < P_{dyno(e)}$	$P_{dyno(e)} < P_{ss}$
	$P_{VUT(m)} = P_{dyno(m)}$		

4.4.2.2 Inclination Test

Figure 4.40 step response shows the step response of steady state and inclination state conducted in normal condition. In steady state, with I_d is set to 2.0 A, power transfer of 500 W is obtained. However, in inclination state, power transfer increases from 500 W to 2000 W when I_d is increased from 2.0 A to 8.0 A. The magnification of a part of the figure is shown in Figure 4.40.

The results obtained for the steady state in the inclination test is similar to that obtained from the steady state test performed earlier, hence the previous discussion is also applicable here. As shown in Table 4.10, the electrical power generated by VUT, $P_{VUT(e)}$ with 520.44 W in steady state buck mode increases to 2065.22 W in inclined boost mode. However, the mechanical power of the VUT, $P_{VUT(m)}$ (2061.73 W), is less than the mechanical power of the dynamometer, $P_{dyno(m)}$ (2070.11 W) as the VUT is experiencing an uphill condition during the test. This situation causes the torque of DC machine to increase, which causes the inertia of the VUT to increase and, consequently, decreasing its speed. Thus, the power generated at the DC machine is absorbed by PADU, $P_{dyno(e)}$ to be stored in the storage (sink/source). $P_{dyno(e)}$ supplies PADU with 2067.54 W of power to execute the switching from steady state mode to inclined mode, which produces an output power of 1967.03W. When the DC machine is in generative mode, the output power P_{SS} occurs at the storage (sink/source).

Table 4.10 Power management results during incline tests in normal condition

Power	$P_{VUT(e)}$,(W)	$P_{VUT(m)}$,(W)	$P_{dyno(m)}$,(W)	$P_{dyno(e)}$,(W)	P_{ss},(W)
Buck Mode (steady state)	520.44	519.95	519.85	519.62	464.95
Buck Mode (incline)	520.44 increasing to 2065.22	519.95 increasing to 2061.73	519.85 increasing to 2070.11	519.62 increasing to 2067.54	464.95 increasing to 1967.03

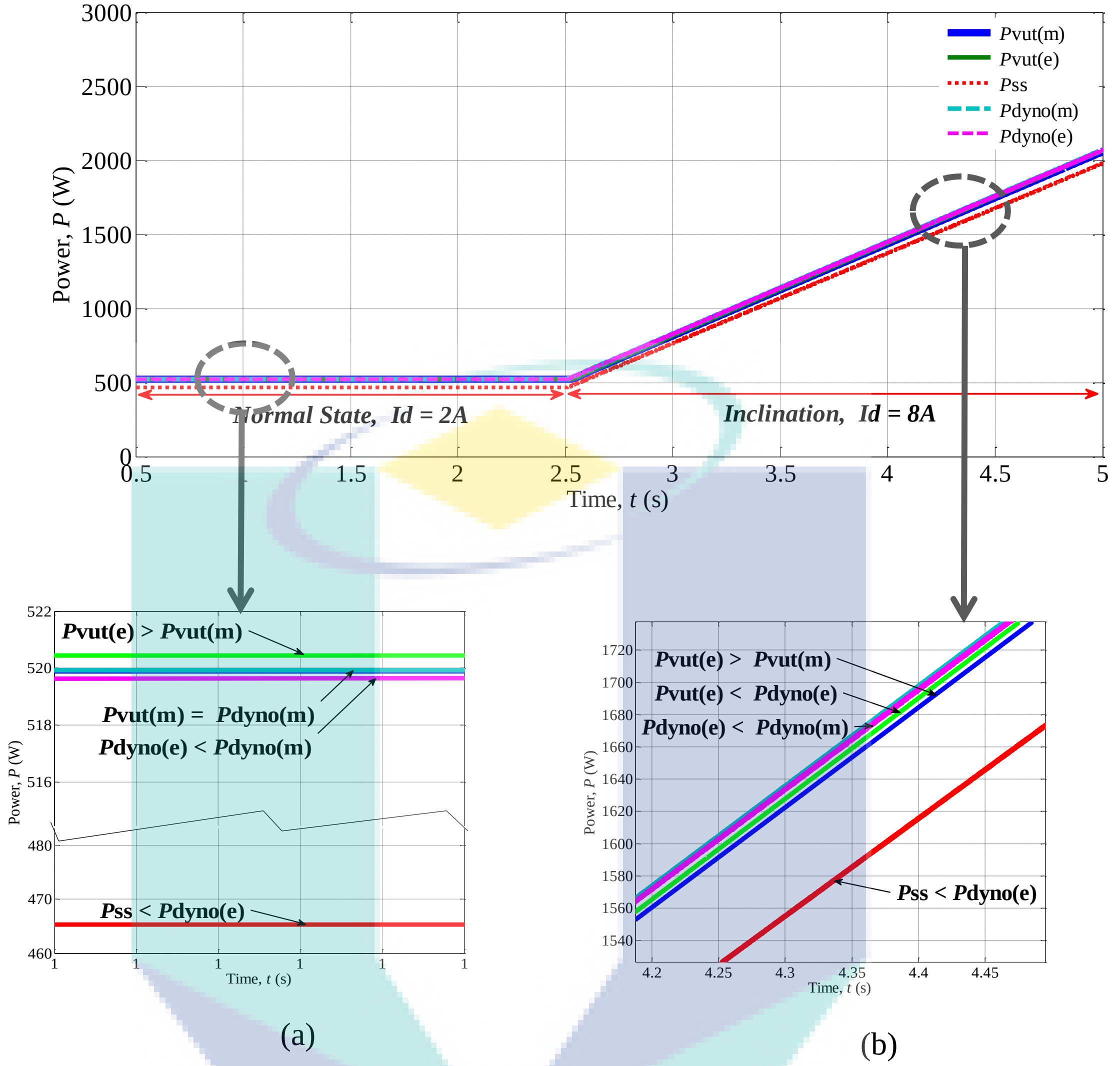

Figure 4.40 Power transfer of bidirectional chassis dynamometer during buck mode in normal condition with inclination test including $P_{VUT(m)}$, $P_{VUT(e)}$, $P_{dyno(m)}$, $P_{dyno(e)}$ and P_{ss} with magnification of results obtained from inclination tests during normal condition: (a) Buck mode (steady state), and (b) Buck mode (incline).

The overall power transfer that occur during the inclination test is summarized in Table 4.11. In steady state test, $P_{VUT(e)}$ is found to be greater than $P_{VUT(m)}$ ($P_{VUT(e)} > P_{VUT(m)}$) because VUT produces energy to be transmitted to the DC machine. However, inclination test shows that $P_{VUT(m)}$ is less than $P_{dyno(m)}$ ($P_{VUT(m)} < P_{dyno(m)}$) because the internal torque of VUT is different from that of the DC machine as the mechanical force from the DC machine is imposed on the mechanical shaft of VUT. Since DC machine internal torque is higher than that of the VUT, the DC machine emulates uphill road load to VUT. The power generated from the DC machine becomes the input power $P_{dyno(e)}$ (2067.54 W) to PADU, which is then stored as P_{SS} (1967.03 W) in the storage (source/sink). P_{SS} is the power that is used during regenerative braking tests. However, during regenerative braking tests, instead of being the stored power, P_{SS} changes its role by supplying power to the system.

Table 4.11 Power management in normal condition with inclination test

Mode	VUT (Prime Mover)	Dyno (DC machine)	PADU (HBDC)
Buck	$P_{VUT(e)} > P_{VUT(m)}$	$P_{dyno(m)} > P_{dyno(e)}$	$P_{dyno(e)} > P_{ss}$
	$P_{VUT(m)} = P_{dyno(m)}$		
Buck (incline)	$P_{VUT(e)} > P_{VUT(m)}$	$P_{dyno(m)} > P_{dyno(e)}$	$P_{dyno(e)} > P_{ss}$
	$P_{VUT(m)} \neq P_{dyno(m)}$; $P_{VUT(m)} < P_{dyno(m)}$		

4.4.2.3 Declination Test

Figure 4.41 shows the power management resulting from a step response of the bidirectional chassis dynamometer in a steady state and declination state while in normal condition. During steady state test, desired current, I_d, is set to 8.0 A and power transfer is 2000 W; however, in declination test, power decreases from 2000 W to 750 W when is decreased from 8.0 A to 3.0 A. The magnification of a part of the above figure is shown in Figure 4.41.

In general, the power from VUT is transferred to the DC machine, and then to the dynamometer, before being absorbed by PADU to be stored at storage (sink/source). The explanation for the results obtained in the steady state is similar to that as in the previous sections, thus the discussion is not done here. However, in declination state, VUT experiences downhill road load condition, which causes the torque of the DC machine to decrease, the inertia of VUT is decreased but its speed is increased. From Table 4.12, in buck mode, the power generated by VUT, $P_{VUT(e)}$ with 2081.74 W in steady state decreases to 810.15 W in decline state. Also, $P_{VUT(m)}$ with 2073.46 W is greater than $P_{dyno(m)}$ with 2073.22 W. In buck mode and decline state, $P_{dyno(e)}$ supplies PADU with 779.78 W to execute switching and produces output power with 738.51 W, which is P_{SS} at the storage.

Table 4.12 Power during declination test in normal condition.

Power	$P_{VUT(e)}$,(W)	$P_{VUT(m)}$,(W)	$P_{dyno(m)}$,(W)	$P_{dyno(e)}$,(W)	P_{ss},(W)
Buck Mode (steady state)	2081.74	2073.46	2073.22	2070.67	1983.45
Buck Mode (decline)	2081.74 decreasing to 810.15	2073.46 decreasing to 795.20	2073.22 decreasing to 779.93	2070.67 decreasing to 779.78	1983.45 decreasing to 738.51

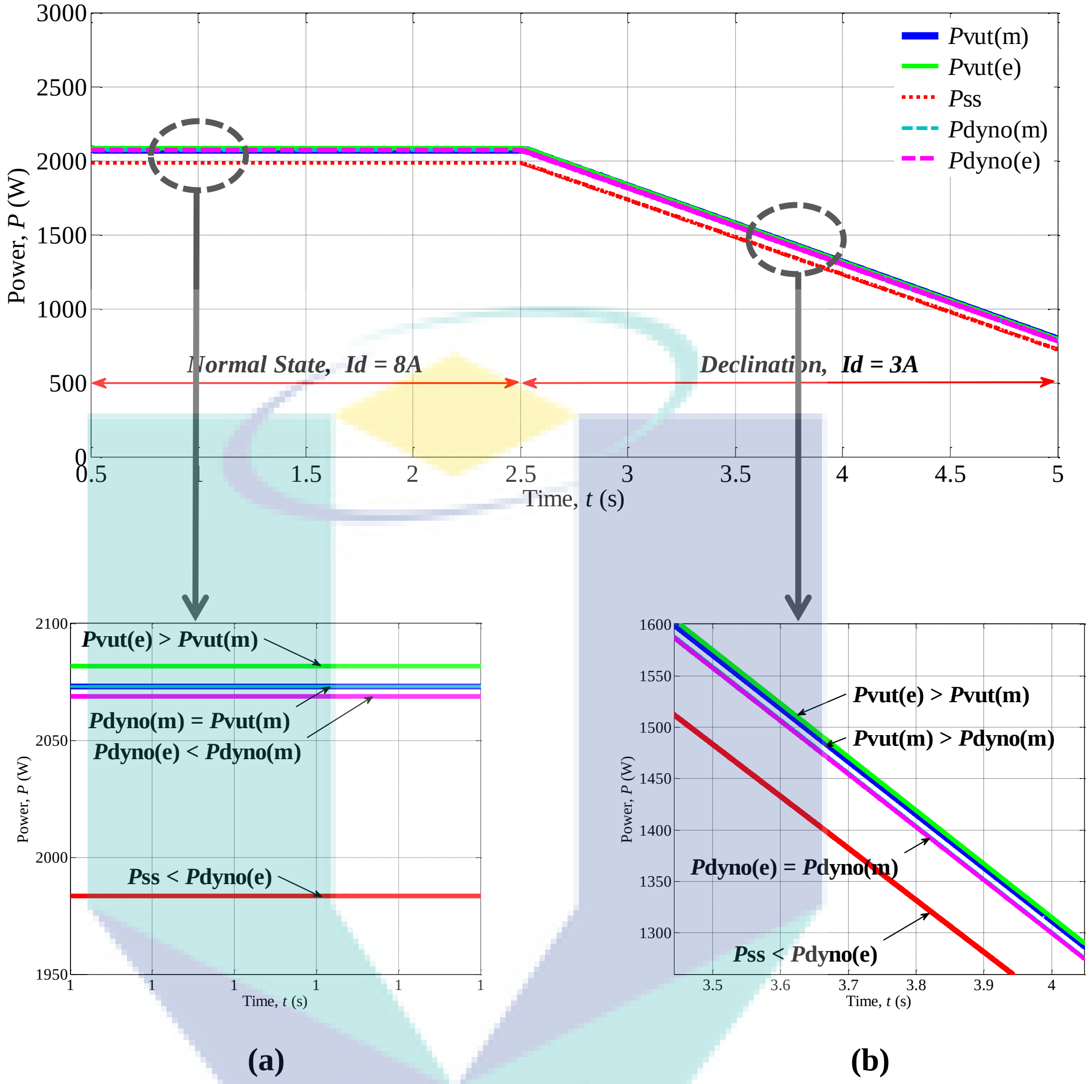

Figure 4.41 Power plots of bidirectional chassis dynamometer in normal condition during buck mode with declination test and magnification of power plots from declination test in normal condition: a) Buck mode (steady state), and b) Boost mode (declination mode).

The overall power transfer that occur during declination test in normal condition is summarized in Table 4.13. In steady state test, $P_{VUT(e)}$ is greater than $P_{VUT(m)}$ because VUT produces energy to be transmitted to the DC machine. However, in declination test, $P_{VUT(m)}$ is greater than $P_{dyno(m)}$ because the internal torque of VUT is greater that of the DC machine. This is so because the mechanical force from the DC machine is imposed onto the mechanical shaft of VUT, hence the DC machine emulates downhill road load to VUT. Meanwhile, the electrical power generated by the DC machine acts as the input power, $P_{dyno(e)}$, for PADU. However, during regenerative braking tests, P_{SS}

supplies power to the systems. Thus the P_{SS} is greater than others power transfer, since P_{SS} is input power.

Table 4.13 Power in normal condition during declination test.

Mode	VUT (Prime Mover)	Dyno (DC machine)	PADU (HBDC)
Buck	$P_{VUT(e)} > P_{VUT(m)}$	$P_{dyno(m)} > P_{dyno(e)}$	$P_{dyno(e)} > P_{ss}$
	$P_{VUT(m)} = P_{dyno(m)}$		
Buck (decline)	$P_{VUT(e)} > P_{VUT(m)}$	$P_{dyno(m)} < P_{dyno(e)}$	$P_{dyno(e)} > P_{ss}$
	$P_{VUT(m)} \neq P_{dyno(m)}$; $P_{VUT(m)} > P_{dyno(m)}$		

4.4.3 Regenerative Braking Test

Power flow that occurs during regenerative braking test is illustrated in Figure 4.42, where the input power to the system begins with P_{SS} at PADU, while the output power is $P_{VUT(e)}$. Since mechanical parameter is not included in bidirectional chassis dynamometer, mechanical power losses that occur in the system is neglected.

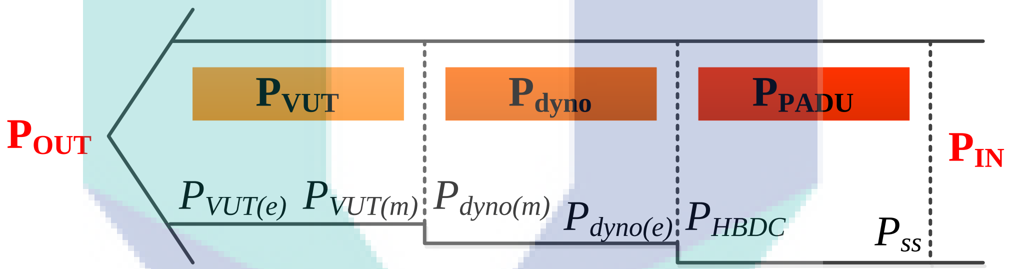

Figure 4.42 Power flow diagram in regenerative braking test.

4.4.3.1 VUT in drive condition

Figure 4.43 shows the steady state step response of bidirectional chassis dynamometer in normal condition and regenerative braking, which is similar to that when the dynamometer is in normal condition. In normal condition, I_d is set to 2.0 A and the power transfer is 500 W; the power transfer in regenerative braking is -750 W with I_d equal to - 3 A, indicating that power is reversed in regenerative braking. Magnification of part of the power plots is shown in Figure 4.43 (a) Buck mode and (b) Boost mode. This section discusses only the results related to regenerative braking as the results for the normal condition has been explained previously.

Generated power is constant as the testing was conducted in steady state. From Table 4.14, power generated by the storage (sink/source), P_{SS}, which acts as the input power to the system, supplies 835.75 W to PADU, from which PADU produces an output power of 784.35W. This power is then transmitted as $P_{dyno(e)}$ to dynamometer, while $P_{dyno(m)}$ is supplied to the DC machine to emulate VUT. Since $P_{VUT(m)}$ and $P_{dyno(m)}$ are mechanically connected to each other, both $P_{VUT(m)}$ and $P_{dyno(m)}$ is 782.34 W. Power generated at PADU $P_{dyno(e)}$ is absorbed by the DC machine, which emulates VUT in regenerative braking condition. At this time, motoring mode occurs at the dynamometer which produces power $P_{dyno(m)}$. Regenerative braking test with VUT in drive position shows that P_{SS} is greater than $P_{dyno(e)}$ because the storage (source/sink) produces energy to be transmitted to PADU. Thus, the electrical power generated from PADU is transformed to mechanical power, $P_{dyno(m)}$, which is attached to the mechanical power at VUT. This situation happens because the mechanical force from the dynamometer is imposed onto the mechanical shaft of VUT. Since PADU causes the shaft of the DC machine to rotate, equal power is produced by the machine. Meanwhile, power $P_{dyno(m)}$ generated at the DC machine acts as the mechanical power to produces input power for VUT. $P_{VUT(m)}$ with 782.32 W is transmitted to $P_{VUT(e)}$ producing 780.65 W of electrical power. The overall power transfer is summarized in Table 4.14 and Table 4.15.

Table 4.14 Power management results during steady state tests in regenerative braking.

Power	$P_{VUT(e)}$,(W)	$P_{VUT(m)}$,(W)	$P_{dyno(m)}$,(W)	$P_{dyno(e)}$,(W)	P_{ss},(W)
Buck Mode (VUT drive)	520.44	519.95	519.85	519.62	464.93
Boost Mode (VUT drive)	780.65	782.32	782.34	784.35	835.75

Table 4.15 Complete power management in regenerative braking with steady state test.

<table>
<tr><th>Mode</th><th>VUT (Prime Mover)</th><th>Dyno (DC machine)</th><th>PADU (HBDC)</th></tr>
<tr><td rowspan="2">Buck</td><td>$P_{VUT(e)} > P_{VUT(m)}$</td><td>$P_{dyno(m)} > P_{dyno(e)}$</td><td rowspan="2">$P_{dyno(e)} > P_{ss}$</td></tr>
<tr><td colspan="2">$P_{VUT(m)} = P_{dyno(m)}$</td></tr>
<tr><td rowspan="2">Boost</td><td>$P_{VUT(e)} < P_{VUT(m)}$</td><td>$P_{dyno(m)} < P_{dyno(e)}$</td><td rowspan="2">$P_{dyno(e)} < P_{ss}$</td></tr>
<tr><td colspan="2">$P_{VUT(m)} = P_{dyno(m)}$</td></tr>
</table>

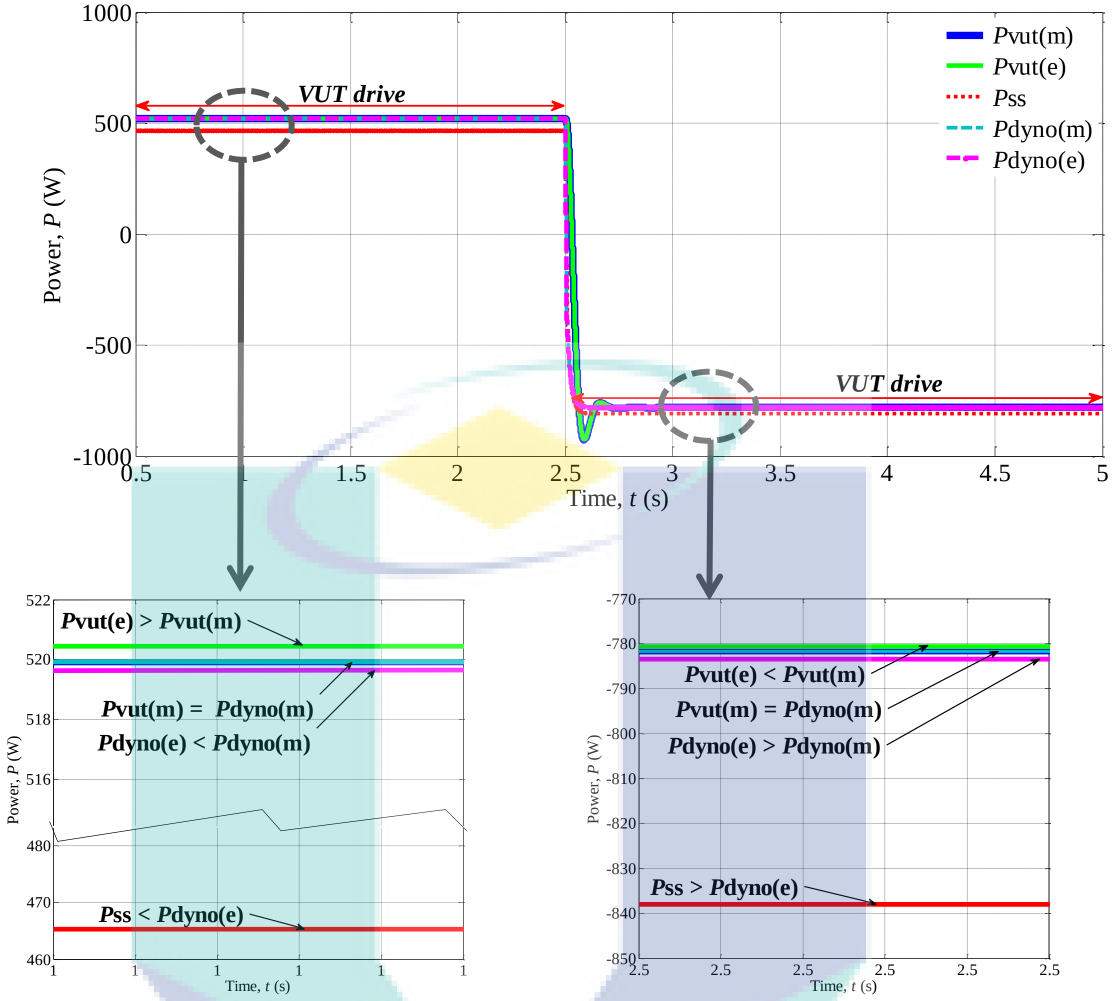

(a) (b)

Figure 4.43 Power in bidirectional chassis dynamometer in buck mode and boost mode during normal condition regenerative braking test with VUT in drive condition with magnification of power plots during regenerative braking with VUT in drive condition: a) Buck mode and b) Boost mode.

4.4.3.2 VUT in stop test

Figure 4.44 shows the step response obtained when VUT is in drive state and stop state during normal regenerative braking, and power transfer is approximately 500 W with I_d set to 2.0 A. However, when VUT in stop condition, power jumps from 0 W to 1000 W, with I_d = - 3.0 A. Magnification of the step response in regenerative braking mode with VUT in stop condition is shown in Figure 4.44.

Generated power is constant as the testing was conducted in steady state. As noted in Table 4.16, the power generated by the storage (sink/source), P_{SS} is 901.87 W. PADU transmits the power to the dynamometer as $P_{dyno(m)}$, and the dynamometer is directly connected to the DC machine that emulates as the VUT. Since regenerative braking test was performed while VUT is in stop state, $P_{VUT(m)}$ with 0 W is less than $P_{dyno(m)}$ with 875.97 W. The power generated at PADU is absorbed by the DC machine as $P_{dyno(e)}$ to emulate VUT in regenerative braking. P_{SS} supplies PADU with 901.87 W of power to execute the switching, which produces an output power of 875.95 W. The DC machine absorbed the output power as $P_{dyno(m)}$, and motoring mode occurs at the dynamometer. Thus $P_{VUT(m)}$ become 0 W since VUT is set in stop condition.

Table 4.16 Power during regenerative braking test with VUT in stop condition.

Power	$P_{VUT(e)}$,**(W)**	$P_{VUT(m)}$,**(W)**	$P_{dyno(m)}$,**(W)**	$P_{dyno(e)}$,**(W)**	P_{ss},**(W)**
Buck Mode (VUT drive)	520.44	519.95	519.85	520.62	438.49
Boost Mode (VUT stop)	0	0	875.97	875.95	901.87

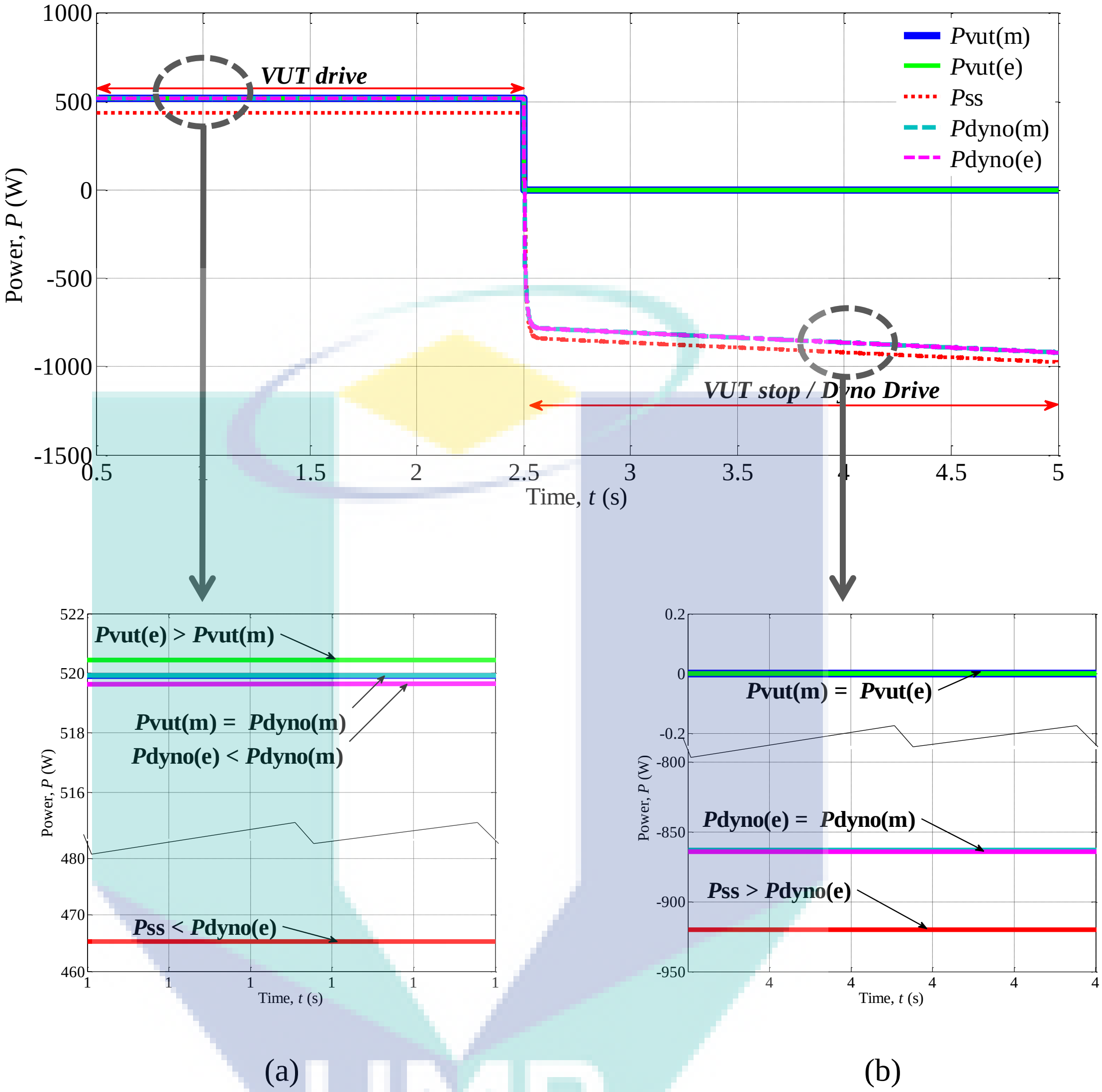

Figure 4.44 Power transfer of bidirectional chassis dynamometer during buck and boost modes in regenerative braking test with VUT in stop condition with magnification of step response during regenerative braking with VUT in stop state: (a) Buck mode, and (b) Boost mode.

In the regenerative braking test with VUT in stop position, P_{SS} is greater than $P_{dyno(e)}$ because the storage (source/sink) produces energy to be transmitted to PADU. The electrical power generated from PADU is transform into mechanical power, $P_{dyno(m)}$, which is associated with the mechanical power at VUT. Also, P_{SS} acts as the input power to the system with 901.87 W is highest power in the system, while power generated by $P_{dyno(m)}$ is 875.97 W, and $P_{VUT(m)}$ is 0 W. This situation happens because the mechanical force from dynamometer is imposed onto the mechanical shaft of VUT. Power is considered to be produced by PADU since it helps rotate the shaft of the DC machine. The power generated at the DC machine $P_{dyno(m)}$ acts as the input power the VUT, while both $P_{VUT(m)}$ and $P_{VUT(e)}$ are 0 W. Besides, during regenerative braking tests, P_{SS} changed to supplied power to the systems. The overall power transfer is summarized at Table 4.17.

Table 4.17 Power management in regenerative braking mode with VUT in stop condition.

Mode	VUT (Prime Mover)	Dyno (DC machine)	PADU (HBDC)
Buck (VUT drive)	$P_{VUT(e)} > P_{VUT(m)}$	$P_{dyno(m)} > P_{dyno(e)}$	$P_{dyno(e)} > P_{ss}$
	$P_{VUT(m)} = P_{dyno(m)}$		
Boost Mode (VUT stop)	$P_{VUT(e)} = P_{VUT(m)}$	$P_{dyno(m)} = P_{dyno(e)}$	$P_{dyno(e)} < P_{ss}$
	$P_{VUT(m)} < P_{dyno(m)}$		

4.4.3.3 VUT in brake condition

Figure 4.45 shows the step response obtained during a regenerative braking test with VUT in drive state, brake state and stop state. The I_d is set from 3.0 A to 0 A and power transfer is 700 W. This section will only evaluate VUT in brake state as VUT in drive state and stop state have been discussed previously. A magnification of part of the figure is shown in Figure 4.46.

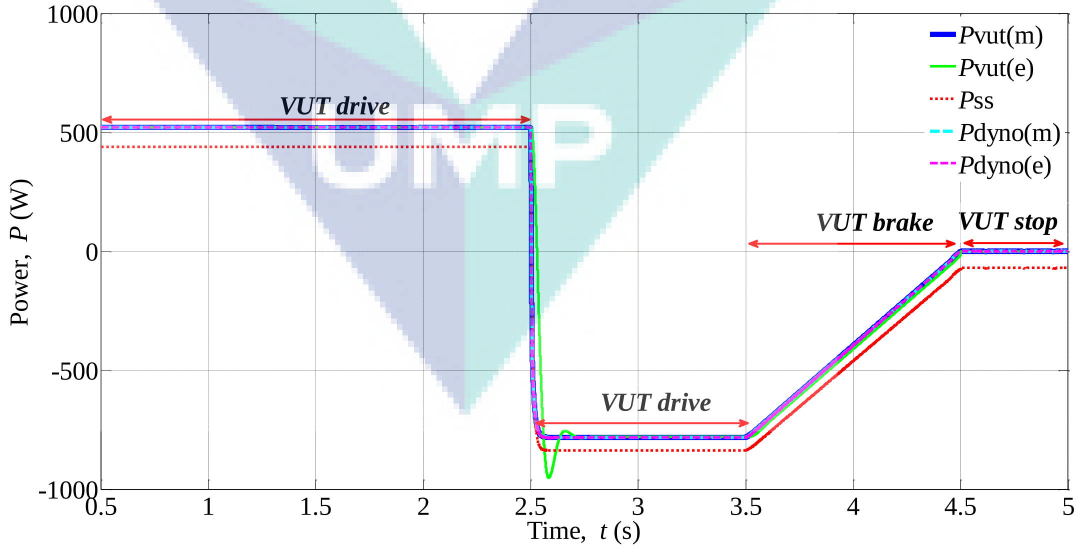

Figure 4.45 Power transfer of bidirectional chassis dynamometer during buck mode and boost mode in regenerative braking test.

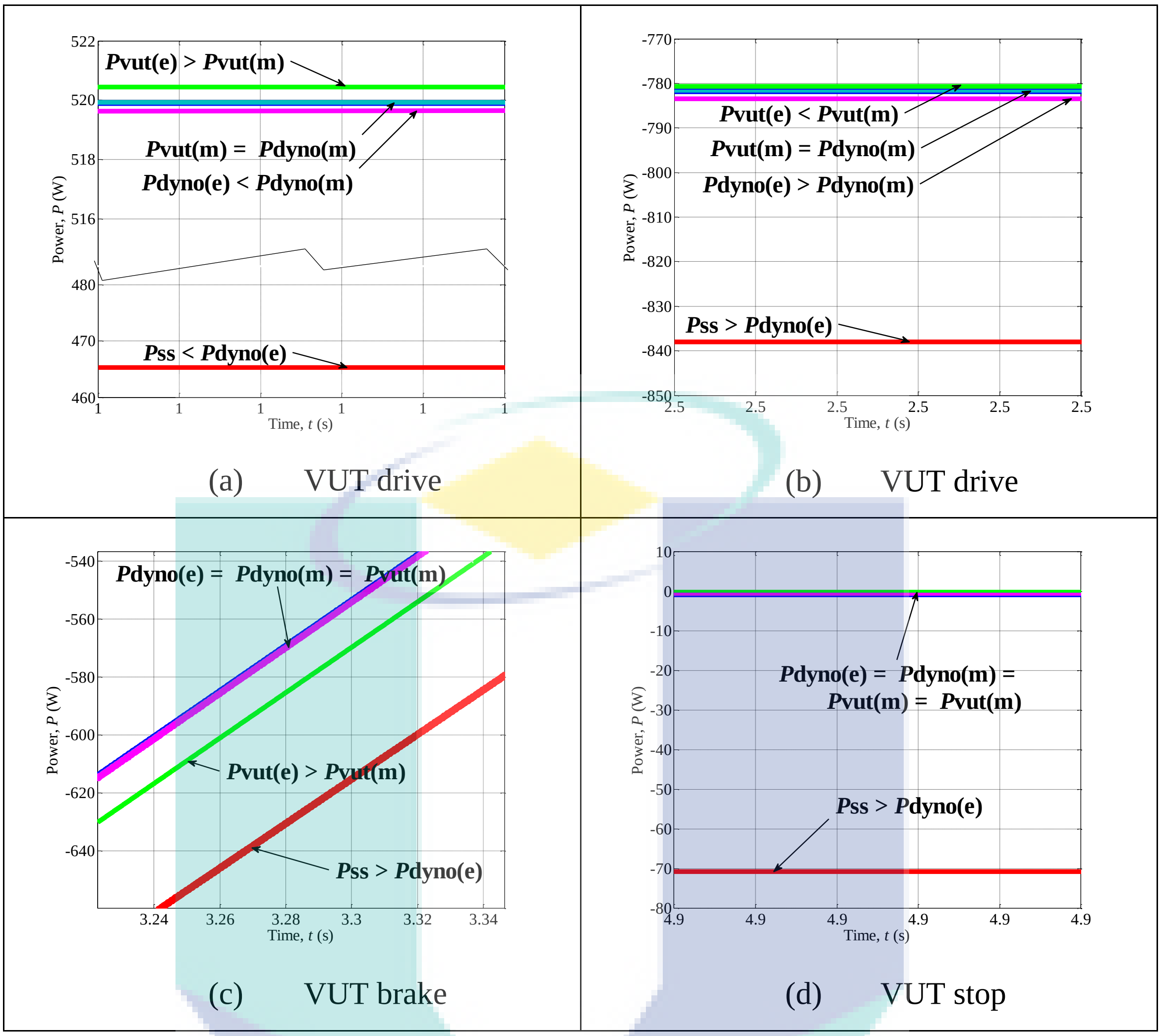

Figure 4.46 Magnification of power plots obtained during regenerative braking test: a) Buck mode (VUT drive condition), b) Boost mode (VUT drive state), c) Boost mode (VUT brake state) and d) Boost Mode (VUT stop state).

Table 4.18 shows the power transfers that occur during the regenerative braking test. The power generated by the storage (sink/source), P_{SS} is 835.75 W, which is transmitted by PADU to dynamometer as $P_{dyno(m)}$. However, $P_{dyno(m)}$ is directly connected with $P_{VUT(m)}$ to emulate VUT with the DC machine. Since regenerative braking test is performed with VUT in brake state, hence $P_{VUT(m)}$, $P_{dyno(m)}$ and $P_{dyno(e)}$ have the same value with 782.34 W. Thus, power generated at PADU is absorbed by the DC machine as $P_{dyno(e)}$ to emulate VUT regenerative braking. P_{SS} supply PADU with 835.75 W to execute switching from buck mode to boost mode and produces output power of 784.35 W. The output power $P_{dyno(m)}$ is absorbed at the DC machine causing motoring mode to occur in the dynamometer. $P_{VUT(m)}$ is used to set up the brake state, and since DC machine is set up to emulate VUT braking, $P_{dyno(m)}$ and $P_{VUT(m)}$ have the same value.

Table 4.18 Power measured during complete tests in regenerative braking.

Power	$P_{VUT(e)}$,(W)	$P_{VUT(m)}$,(W)	$P_{dyno(m)}$,(W)	$P_{dyno(e)}$,(W)	P_{ss},(W)
Buck Mode (VUT drive)	520.44	519.95	519.85	519.62	438.22
Boost Mode (VUT drive)	780.65	782.32	782.34	784.35	835.75
Boost Mode (VUT brake)	780.65 decreasing to 0	782.32 decreasing to 0	782.34 decreasing to 0	784.35 decreasing to 0	835.75 decreasing to 70.91
Boost Mode (VUT stop)	0	0	0	0	70.91

The overall power transfer is summarized in Table 4.19. Regenerative braking test conducted with VUT in brake position shows that P_{SS} is greater than $P_{dyno(e)}$ because storage (source/sink) produces energy to be transmitted to PADU. The electrical power generated from PADU is transformed to mechanical power, $P_{dyno(m)}$ and attached with mechanical power at VUT. Thus, the highest power is P_{SS} with 835.75 W, being the input power to the system. Also, power generated by $P_{dyno(m)}$ is equal to $P_{VUT(m)}$ with 782.34 W because the mechanical force from dynamometer is imposed to the shaft of VUT. The power produced by PADU helps the shaft of the DC machine to revolve. Meanwhile, the power absorbed by the DC machine act as a mechanical power to produce the input power, $P_{dyno(m)}$ for VUT. $P_{VUT(m)}$ with 782.32 W is then transmitted to $P_{VUT(e)}$, and the power transfer ends at $P_{VUT(e)}$ with 0 W when VUT completed the braking and finally stopped. Besides, during regenerative braking tests, P_{SS} becomes the input power to the system.

Table 4.19 Complete power management in regenerative braking test

Mode	**VUT (Prime Mover)**	**Dyno (DC machine)**	**PADU (HBDC)**
Buck (VUT drive)	$P_{VUT(e)} > P_{VUT(m)}$	$P_{dyno(m)} > P_{dyno(e)}$	$P_{dyno(e)} > P_{ss}$
	$P_{VUT(m)} = P_{dyno(m)}$		
Boost (VUT drive)	$P_{VUT(e)} < P_{VUT(m)}$	$P_{dyno(m)} < P_{dyno(e)}$	$P_{dyno(e)} < P_{ss}$
	$P_{VUT(m)} = P_{dyno(m)}$		
Boost (VUT brake)	$P_{VUT(e)} > P_{VUT(m)}$	$P_{dyno(m)} = P_{dyno(e)}$	$P_{dyno(e)} < P_{ss}$
	$P_{VUT(m)} = P_{dyno(m)} = P_{dyno(e)}$		
Boost (VUT stop)	$P_{VUT(e)} = P_{VUT(m)} = P_{dyno(m)} = P_{dyno(e)}$		$P_{dyno(e)} < P_{ss}$

4.4.4 Discussion

Power transfer obtained from normal condition test and regenerative braking test have shown that the bidirectional power flow in the dynamometer can be applied to chassis dynamometer as the VUT is affected by the performance of the dynamometer. When the chassis dynamometer is in regenerative braking mode, the dynamometer emulates braking condition of VUT. Also, the DC machine is affected by the different states of VUT, whether in drive state, braking state or stop state.

4.5 Summary

In buck mode, the DC machine acts as generator, whereas in boost mode it acts as a motor to perform regenerative braking test. Modified Hysteresis Current Control (HCC) together with PID is design in bidirectional chassis dynamometer. From the controller, the new control technique has been introduced in half-bridge bidirectional DC-DC converter to reduces switching loss and conduction loss. Therefore, to emulate road load test, the desired current is executed in PID to control torque performance at DC machine. According to the torque performance, limitation at power produced and power demanded by the PADU system is occurred. From modified HCC, bidirectional power flow is executed, and together with PID controller as outer loop, the controller regulates the performance of the DC machine. Thus, bidirectional power flow tests can be performed on the chassis dynamometer using PADU. From the results collected, objective one has been achieved.

The DC machine is controlled by PID to emulate road load condition, and the road load conditions performed on the machine are normal condition and regenerative braking. In emulating the required road load condition, the value of the desired current controls the actual current in the DC machine. Using half-bridge bidirectional DC-DC converter, a new chassis dynamometer is designed since limited power electronics usage in traditional chassis dynamometer. At the same time, both testing (1) normal condition and (2) regenerative braking for EV is applicable with HBDC topology. From the results gathered, it is observed that the power flow goes from DC machine to VUT during normal condition tests. On the other hand, regenerative braking tests occurs when power is demanded by DC machine, forcing Power Source/Sink, P_{SS} to supply power to HBDC system. From the explanations, objective two in this research has been achieved.

The capability of the bidirectional chassis dynamometer is determined by analysing and evaluating its power transfer during buck mode and boost mode. In buck mode, it is found that power that originated from VUT (P_{VUT}) is finally transmitted to the storage (sink/source) as Pss, during which P_{VUT} is greater than Pss. Meanwhile, during boost mode, P_{VUT} is less than P_{SS} because P_{SS} now supplies power to the system. The power is then absorbed by the dynamometer as P_{dyno} to perform regenerative braking. The simulation of the bidirectional flow of current can be used to predict the system of bidirectional chassis dynamometer features. End of analysis shows the objective three has been achieved.

CHAPTER 5

CONCLUSION

5.1 Conclusions

This research introduces the modified hysteresis current control (HCC) in half-bridge bidirectional DC-DC converter (HBDC) to be applied in chassis dynamometer. The following conclusions are drawn from achieved results.

(1) The modified HCC together with PID controller has been designed as a new current control technique for HBDC topology. The advantage of this control technique is reduction in conduction losses and switching losses at zero crossing between buck mode and boost mode. It happens every time the current's direction changes. To regulate the machine's torque, PID controller is designed as outer loop control. PID determine torque at DC machine (dynamometer) based on the power transfer for normal condition test and the power demands for regenerative braking.

(2) An improved method for testing vehicle performance mainly for EV has been introduced. With the implementation of HBDC, conventional chassis dynamometer with Power Absorption Unit (PAU) has been enhanced to Power Absorption and Delivery Unit (PADU). HBDC can control bidirectional power transfer; deliver power to sink/source during normal condition tests and demand power from sink/source during regenerative braking tests. In simulation, normal condition tests consist of steady state, uphill and downhill conditions. Simultaneously, VUT operation has been recorded by DC machine according to torque performance. As the torque produced from VUT is identical to the torque at DC machine, power delivered by VUT is calculated and recorded to assess power transfer performance. The main difference between conventional chassis dynamometer and bidirectional chassis dynamometer is the latter

can perform regenerative braking test. In normal condition, the bidirectional chassis dynamometer performs similarly with the conventional dynamometer. Whereas, in regenerative braking condition, the power transfer changed from power storage to the DC machine. The current's direction changed due to the power required by DC machine to evaluate regenerative braking. In this research, the regenerative braking test has been applied in three conditions; driving, braking and stopping.

With the implementation of PADU, the power transfer is now bidirectional. To ensure the correct power transfer, the powers at each stage of conversion are measured. For normal condition test, power generated by DC machine is recorded as $P_{dyno\ (e)}$ and the power loss is calculated from the discrepancy between $P_{dyno\ (e)}$ and P_{SS}. P_{SS} is defined as the power at the storage element. Power transfers during normal condition test for inclination test and declination test have also been analysed. From the results, it is evident that, at regenerative braking tests, P_{SS} supply power to the DC machine because power is demanded to perform the regenerative braking test. It is also being observed that the bidirectional power transfer happens in this chassis dynamometer system.

5.2 Recommendations

(1) The modified hysteresis current can be extended to real experimental study to estimate the efficiency of the switching and conduction process.

(2) The application of bidirectional chassis dynamometer can be developed in real prototype to evaluate the efficiency of regenerative braking tests.

(3) The control of modified hysteresis current controller of half bridge bidirectional DC-DC converter can be applied to other applications.

REFERENCES

Al-sheikh, H., Bennouna, O., Hoblos, G., & Moubayed, N. (2014). Modeling , Design and Fault Analysis of Bidirectional DC-DC Converter for Hybrid Electric Vehicles. In *IEEE 23rd International Symposium on Industrial Electronics (ISIE)* (pp. 1689–1695).

Ananth, D. V. N., Nagesh Kumar, G. V, Ramana, K. V, Sai Kiran, S., & Rajesh, B. (2013). Analysis of Three Phases Four Wire Hysteresis Current Controller for Unbalanced Loads Like DC Motor and Diode Rectifier on Different Phases Using DSTATCOM. In *IEEE India Conference INDICON*.

Babu, R. S. R., & Henry, J. (2011). A Comparison of Half Bridge & Full Bridge Isolated DC-DC Converters for Electrolysis Application. *International Journal of Soft Computing and Engineering (IJSCE)*, *1*(4), 37–42.

Baburaja, C., & Jayakumar, J. (2013). Transformer less Soft Switching Bidirectional DC-DC Chopper. *International Journal of Engineering and Advanced Technology (IJEAT)*, *2*(3), 391–395.

Bennetts, C. D. (2002a). *Chassis Dynamometer Software , Inertia Determination and Recalibration*.

Bennetts, C. D. (2002b). *Chassis Dynamometer Software , Inertia Determination and Recalibration*. University of Canterbury.

Buvana, D., & Jayashree, R. (2012). Bidirectional DC to DC Converter, *4*(2), 21–30.

Caricchi, F., Crescimbini, F., Noia, G., & Pirolo, D. (1994). Experimental study of a bidirectional DC-DC converter for the DC link voltage control and the regenerative braking in PM motor drives devoted to electrical vehicles. In *Proceedings of 1994 IEEE Applied Power Electronics Conference and Exposition - ASPEC'94* (pp. 381–386).

Dotelli, G., Ferrero, R., Stampino, P. G., Latorrata, S., & Toscani, S. (2015). Low-Cost PEM Fuel Cell Diagnosis Based on Power Converter Ripple With Hysteresis Control. *IEEE Transactions on Instrumentation and Measurement*, *64*(11), 2900–2907.

Du, Y., Zhou, X., Bai, S., Lukic, S., & Huang, A. (2010). Review of non-isolated bi-directional DC-DC converters for plug-in hybrid electric vehicle charge station application at municipal parking decks. In *25th Annual IEEE Applied Power Electronics Conference and Exposition (APEC)* (pp. 1145–1151).

Duan, Q., & Zeng, Y. (2010). Adaptive torque control using RBF neural networks for nonlinear DC chassis dynamometer drive. *2010 8th World Congress on Intelligent Control and Automation*, (1), 5093–5098.

Ebin, J. T., & Sreethumol, M. V. (2015). Speed Control of BLDC Motor Drive under Direct Torque Control Scheme with Modified Integrator. *IEEE*, *9*(2).

Elankurisil, S. A., & Dash, S. S. (2012). Compare the Performance of Non-isolated DC – DC converter with SEPIC converter for DC Motor. *Journal of Electrical and Control Engineering*, *2*(6), 25–32.

Fardoun, A. A., Ismail, E. H., Sabzali, A. J., & Al-Saffar, M. A. (2014). Bidirectional converter for high-efficiency fuel cell powertrain. *Journal of Power Sources*, *249*, 470–482.

Ghasem HosseinI Aghdam, M., Fathi, S. H., & Ghasemi, a. (2005). The Analysis of Conduction and Switching Losses in Three-Phase OHSW Multilevel Inverter Using Switching Functions. *2005 International Conference on Power Electronics and Drives Systems*, *1*, 209–218.

Hardy, T., Member, S., & Jewell, W. (2011). Emulation of a 1 . 5MW Wind Turbine with a DC Motor, 1–8.

Hasan, K. N., Haque, M. E., Negnevitsky, M., & Muttaqi, K. M. (2008). Control of Energy Storage Interface with a Bidirectional Converter for Photovoltaic Systems. In *Australasian Universities Power Engineering Conference (AUPEC)* (pp. 1–6).

Hong, S.-K., Lee, J.-S., Byeon, N.-H., & Kim, K.-S. (2014). A study on realization of hysteresis current regulator for reducing switching loss using the slope of reference current. *2014 17th International Conference on Electrical Machines and Systems (ICEMS)*, 1472–1475.

Jeongwoo, L., & Douglas J., N. (2005). Rotating Inertia Impact on Propulsion and Regenerative Braking for Electric Motor Driven Vehicles. In *2005 IEEE Vehicle Power and Propulsion Conference* (pp. 308–314).

Jiang, J., Bao, Y., & Wang, L. (2014). Topology of a Bidirectional Converter for Energy Interaction between Electric Vehicles and the Grid. *Energies*, *7*(8), 4858–4894.

Jiaqiang Yang, Jin Huang, J. M. (2005). Research on a Novel AC Variable-Frequency Dynamic Power Dynamometer. In *Electrical Machines and Systems, 2005. ICEMS 2005. Proceedings of the Eighth International Conference* (pp. 1687–1691).

Jirawattanasomkul, J., & Koetniyom, S. (2000). Design and Development of Road Load Conditions for Chassis Dynamometer. In *International Conference on Production, Materials and Automobile Engineering (ICPMAE'2012)* (pp. 153–157).

Joshi, M. C. (2013). *Modeling and Control of Bidirectional DC DC Converter Fed PMDC Motor Master of Technology Modeling and Control of Bidirectional DC DC Converter Fed PMDC Motor*.

Joshi, M. C., & Samanta, S. (2013). Modeling and control of bidirectional DC-DC converter fed PMDC motor for electric vehicles. In *2013 Annual IEEE India Conference (INDICON)* (pp. 1–6).

Jun, L., & Dazhi, W. (2009). Study and Simulation of a Novel Hysteresis Current Control Strategy. In *2009 Second International Conference on Intelligent Computation Technology and Automation* (pp. 306–309).

Kanojiya, R. G., & Meshram, P. M. (2012). Optimal tuning of PI controller for speed control of DC motor drive using particle swarm optimization. *2012 International Conference on Advances in Power Conversion and Energy Technologies (APCET)*, (Dc), 1–6.

Karshenas, H. R., Daneshpajooh, H., & Safaee, A. (2011). Bidirectional DC-DC Converters for Energy Storage Systems.

Kelly, K. J., Mihalie, M., & Zolot, M. (2002). Battery Usage and Thermal Performance of the Toyota Prius and Honda Insight during Chassis Dynamometer Testing. In *The Seventeenth Annual Battery Conference on Applications and Advances* (pp. 247–252).

Kim, Y., Kim, J., Ji, Y. H., Won, C. Y., & Jung, Y. C. (2010). Photovoltaic Parallel Resonant DC-link Soft Switching Inverter using Hysteresis Current Control, 2275–2280.

Kolmakov, N. M., & Bakhovtsev, I. A. (2015). Three-Phase Current Source Inverter with Hysteresis Control in Voltage Source Mode. In *EDM 16th International Conference on Micro/Nanotechnologies and Electron Devices* (pp. 429–432).

Komurcugil, H., Ozdemir, S., Sefa, I., Altin, N., & Kukrer, O. (2015). Sliding Mode Control for Single-Phase Grid-Connected LCL-Filtered VSI with Double-Band Hysteresis Scheme. In *IEEE Transactions on Industrial Electronics* (Vol. 46).

Lin, C.-C., Wu, G. W., & Yang, L.-S. (2013). Study of a non-isolated bidirectional DC–DC converter. *IET Power Electronics*, *6*(1), 30–37.

Manoharan, S., & Swarnalatha, A. (2013). Closed Loop Control of Non-Isolated Bidirectional Dc / Dc Converter. *IOSR Journal of Engineering (IOSRJEN)*, *3*(6), 37–43.

Maodong, F., Lei, P., & Weigao, Q. (2010). Study on resistance setting method for chassis dynamometer test of Hybrid Electric Bus. *2010 IEEE Vehicle Power and Propulsion Conference*, 1–4.

Marthanda, A. V. G. ., & Marutheswar, G. . (2015). Analysis of Performance of the Induction Motor under Hysteresis Current Controlled DTC. *International Conference on Electrical, Electronics, Signlas, Communication and Optimization (EESCO)*, (2).

Matthews, C., Dickinson, P. B., & Shenton, A. T. (2009). Chassis Dynamometer Torque Control: A Robust Control Methodology. *SAE International*, *2*(1), 263–270.

Mayyas, A., Prucka, R., Pisu, P., & Haque, I. (2013). Chassis Dynamometer as a Development Platform for Vehicle Hardware In-the-Loop “VHiL.” *SAE International*, *6*(1), 257–267.

Mingjie, C., Zhenhua, J., Qingchun, L., Xiao, Y., Maodong, F., & Kongjian, Q. (2010). A chassis dynamometer laboratory for fuel cell hybrid vehicles and the hydrogen consumption measurement system. *HAq2010 IEEE Vehicle Power and Propulsion Conference*, 1–5.

Mohammadi, M. R., & Farzanehfard, H. (2015). A New Family of Zero-Voltage-Transition Non-Isolated Bidirectional Converters With Simple Auxiliary Circuit. In *IEEE Transactions on Industrial Electronics* (Vol. 46, pp. 1–9).

Molavi, N., Esteki, M., Adib, E., & Farzanehfard, H. (2015). High Step-Up / Down DC-DC Bidirectional Converter with Low Switch Voltage Stress. In *6th International Power Electronics Drive Systems and Technologies Conference (PEDSTC2015)*.

Moon, S., Lee, K., Kim, J., & Koo, D. (2012). Closed-Loop Regenerative Efficiency Testing with Electric Vehicle Bidirectional Dc-dc Converter. *IEEE*, 2461–2466.

Muñoz, J., Rohten, J., Espinoza, J., Melín, P., Baier, C., & Rivera, M. (2015). Review of Current Control Techniques for a Cascaded H-Bridge STATCOM. In *IEEE* (pp. 3085–3090).

Mustapa Mohamed. (2014). Sidang Media Dasar Automotif Nasional (NAP) 2014. In *National Automotive Principle*.

NAP. (2014). Summary for Policymakers.

Öberg, P., Nyberg, P., & Nielsen, L. (2013). A New Chassis Dynamometer Laboratory for Vehicle Research. *SAE International Journal of Passenger Cars-Electronic and Electrical Systems*, *6*(2013-01–0402), 152–161.

Park, S., & Song, Y. (2011). An interleaved half-bridge bidirectional dc-dc converter for energy storage system applications. In *8th International Conference on Power Electronics - ECCE Asia* (pp. 2029–2034).

Patil, D., Rathore, A. K., & Srinivasan, D. (2015). A Non-Isolated Bidirectional Soft Switching Current fed LCL Resonant dc / dc Converter to Interface Energy Storage in DC Microgrid. In *IEEE* (pp. 709–716).

Peter, J., & Ramchand, R. (2015). Constant Switching Frequency Hysteresis Controller for VSI fed Induction Motor Drive Using Current Error Space Phasor Approach. In *IEEE International Conference on Technological Advancements in Power & Energy* (pp. 217–221).

Piris-Botalla, L., Oggier, G. G., Airabella, A. M., & García, G. O. (2014). Power losses evaluation of a bidirectional three-port DC–DC converter for hybrid electric system. *International Journal of Electrical Power & Energy Systems*, *58*(2014), 1–8.

Rahman, M. M., Uddin, M. N., & Islam, M. K. (2015). Integration of Bi-Directional DC-DC Converter and Highly Efficient Boost Converter for Electric Vehicles Applications. In *IEEE PEDS* (pp. 687–691).

Ribeiro, E., Marques Cardoso, A. ., & Boccalatti, C. (2014). Fault Diagnosis in Non-Isolated Bidirectional Half-Bridge DC-DC Converters. *IEEE*, 4458–4463.

Rishma, A. A., Rajarajeswari, P., & Sasikumar, M. (2012). High Efficiency Modified Pulse-Width Modulation Bidirectional Converter for. *International Journal of Application or Innovation in Engineering & Management*, *1*(2), 94–100.

Samedaei, E., Vahedi, H., Sheikholeslami, A., & Lesan, S. (2010). Using “ STF-PQ ” Algorithm and Hysteresis Current Control in Hybrid Active Power Filter to Eliminate Source Current Harmonic. In *IEEE 2010 Power Quality Conference (PQC)* (pp. 1–6).

Seki, H., Ishihara, K., & Tadakuma, S. (2008). Novel regenerative braking control of electric power assisted wheelchair for optimal velocity driving on downhill road. *International Workshop on Advanced Motion Control, AMC*, *1*, 510–515.

Sonavane, S. R., & Jadhav, H. T. (2015). Stand-Alone Wind Energy Generation System using Hysteresis Current Control Method for SCIM. In *IEEE* (p. 4799).

Sun, L., & Zhang, N. (2015). Design, implementation and characterization of a novel bi-directional energy conversion system on DC motor drive using super-capacitors. *Applied Energy*, *153*(2015), 101–111.

Tech, P. (2014). PSIM Tutorial. In *PSIM Tutorial* (pp. 1–8).

Vijay, A. D., & Scaria, R. (2013). Closed Loop Control of Non-isolated Bidirectional ZVS-PWM Active Clamped DC – DC Converter. *IJEIT International Journal of Engineering and Innovative Technology*, *3*(1), 242–245.

Wu, F., Li, X., & Duan, J. (2015). Improved Elimination Scheme of Current Zero-Crossing Distortion in Unipolar Hysteresis Current Controlled Grid-Connected Inverter. *IEEE Transactions on Industrial Informatics*, *11*(5), 1111–1118.

Yao, Z., Xiao, L., & Yan, Y. (2009). Dual-Buck Full-Bridge Inverter With Hysteresis Current Control. *IEEE Transactions on Industrial Electronics*, *56*(8), 3153–3160.

Yinding, L., Wenhua, H., Mingyang, H., Jiansong, Y., Zhu, Q. Z., & Xiong, Z. (2011). Emulation and Experimental Study of Drum Dynamometer for Simulating the Vehicle’s Road Braking. *2011 Third International Conference on Measuring Technology and Mechatronics Automation*, *1*, 37–40.

Zhang, J. (2008). *Bidirectional DC-DC Power Converter Design Optimization , Modeling and Control by Junhong Zhang Dissertation submitted to the faculty of the Virginia Polytechnic Institute and State University.*

APPENDIX A
LITERATURE MAP